



Laser-based directed energy deposition (DED-LB) of advanced materials



David Svetlizky^a, Baolong Zheng^b, Alexandra Vyatskikh^b, Mitun Das^{a,1}, Susmita Bose^c, Amit Bandyopadhyay^c, Julie M. Schoenung^b, Enrique J. Lavernia^b, Noam Eliaz^{a,*}

^a Department of Materials Science and Engineering, Tel-Aviv University, Ramat Aviv, Tel Aviv, 6997801, Israel

^b Department of Materials Science and Engineering, University of California, Irvine, CA92697-2575, USA

^c School of Mechanical and Materials Engineering, Washington State University, Pullman, WA, 99164-2920, USA

ARTICLE INFO

Keywords:

Additive manufacturing
Directed energy deposition (DED)
Laser engineered net shaping (LENS™)
Laser methods
Powder methods
Microstructure
Mechanical properties
Alloy design
Alloys
Ceramics
Composites
Functionally graded materials (FGMs)

ABSTRACT

Directed energy deposition (DED) has matured into an essential additive manufacturing (AM) branch. DED has been broadly implemented in the design and fabrication of novel materials. These include metals, ceramics, and composites. Successful DED operation requires a good understanding of many critical phenomena, including laser-material interactions, fundamentals of casting and solidification of alloys, welding metallurgy and joining interfaces, along with microstructure-mechanical properties relations. Also critical are powder flowability, heat transfer, and various machine-related parameters. Several review articles have been published in recent years on metal AM via powder bed fusion (PBF) and DED, focusing on either a specific material system, mapping the recent technologies for AM, or issues related to the deposition process or material properties. Yet, no recent review is dedicated to a comprehensive presentation of material systems, design, fabrication, challenges, and the relationship between microstructures and mechanical properties of various DED-ed material families. Since the DED-based approach is becoming popular to manufacture bimetallic and multi-material structures, repair high-value structures, and alloy design, this comprehensive review focuses on materials design via DED, including a survey of a variety of monolithic and multi-material compositions. Finally, the critical challenges and opportunities in this area are highlighted.

1. Introduction

Additive manufacturing (AM), often called three-dimensional (3D) printing, allows for the rapid, on-demand fabrication of near-net-shape components directly from a computer-aided design (CAD) file without any part-specific tooling. Recently, it was identified among the twelve disruptive technologies driving the fourth industrial revolution [1]. Although AM started as a rapid prototyping tool for “touch and feel” parts, it is mainstream manufacturing now for various industries [2]. AM machines make 3D parts from a digital model by progressively depositing materials in a ‘layer-by-layer’ approach [3]. Subsequent innovations in AM technologies have expanded the variety of printed materials from polymers to metals, ceramics, composites, and even living tissues [4–6]. The integration of advanced automation and robotics in AM has helped reduce manufacturing variance, fabricating large and complex structures with high quality and repeatability. The unique features of AM, such as the ability to form complex geometries

with topological optimization, enable innovative product design and freeform fabrication of lightweight components. A low “buy-to-fly” ratio, i.e., the mass of the input raw material divided by the output part, reduces the production cost and time. These inherent advantages of AM have attracted the attention of the aerospace, biomedical, automotive, and consumer product industries [7,8].

From 2010 onwards, the US Food and Drug Administration (FDA) has been approving AM processed parts for human use, and in 2013 the US Federal Aviation Administration (FAA) approved a fuel nozzle, the first metal AM part for a critical jet engine application, manufactured by the General Electric Company [9]. In 2013, the National Aeronautics and Space Administration (NASA) installed the first polymers AM machine at the International Space Station (ISS). These events boosted the confidence of AM processed products in various industrial sectors, and enhanced the growth of this field. Not surprisingly, over the last 15 years, there has been a rapid increase in the intensity of research and development (R&D) activities related to metal AM, both in academia

* Corresponding author.

E-mail address: neliaz@tau.ac.il (N. Eliaz).

¹ Permanent address: Bioceramics and Coating Division, CSIR – Central Glass & Ceramic Research Institute, Kolkata 700032, India.

and industry, as evidenced by the remarkable growth of the annual number of patents and scientific publications (Fig. 1).

Metal AM was boosted in 1994 when Electro Optical Systems (EOS) printed a metal part in a direct metal laser sintering (DMLS) machine [5]. The laser powder-based directed energy deposition (DED) technique was invented at the Sandia National Laboratories in the US and is called laser engineered net shaping (LENS™). In 1997, the LENS™ technology was licensed to Optomec®, Inc. (Albuquerque, NM) [10]. Over the years, other companies also started selling laser powder-based DED machines worldwide due to limited patent protection in the core technology. Hybrid AM machines with DED technology and wire and arc additive manufacturing (WAAM, also known as DED-arc) machines with filament feeding also add new dimensions to this market segment.

DED processes generally use powder or wire as the feedstock and laser/electron beam/arc as the energy source. The concentrated energy source melts the feedstock at a particular point and creates a melt pool, generally shielded with an inert atmosphere. Like any other AM process, DED also uses a computer-aided design (CAD) model to deposit the

feedstock material (e.g., powder or wire) in a layer-by-layer fashion [11]. The most frequently used metal AM processes are PBF and DED (Fig. 2a and b, respectively). While PBF commonly has higher dimensional accuracy and yields parts with lower surface roughness [11,12], DED has multiple unique advantages over PBF (Fig. 2c–f): (1) DED enables higher deposition rates (up to 2.5 kg/h for DED versus 0.25 kg/h for PBF [13]); (2) DED has an inherent capability for multi-material deposition (e.g., *in situ* alloying [14]) and fabrication of functionally graded structures with location-specific properties [15,16]; (3) DED systems can be adapted to the processing of coatings/cladding [17,18] and repair of damaged parts [19,20]; (4) DED enables processing of large (>1000 mm 3) part volumes [21]; and (5) 5+ axes in DED systems allow layers to deposit in any direction.

Among different metal DED processes, powder-based feedstock with laser beam as the energy source is the most commonly studied process. Fig. 3 shows schematic diagrams of laser-based DED for powder and wire-based feedstock, whose characteristics have recently been compared [12]. Commercially available metal wires are cheaper than

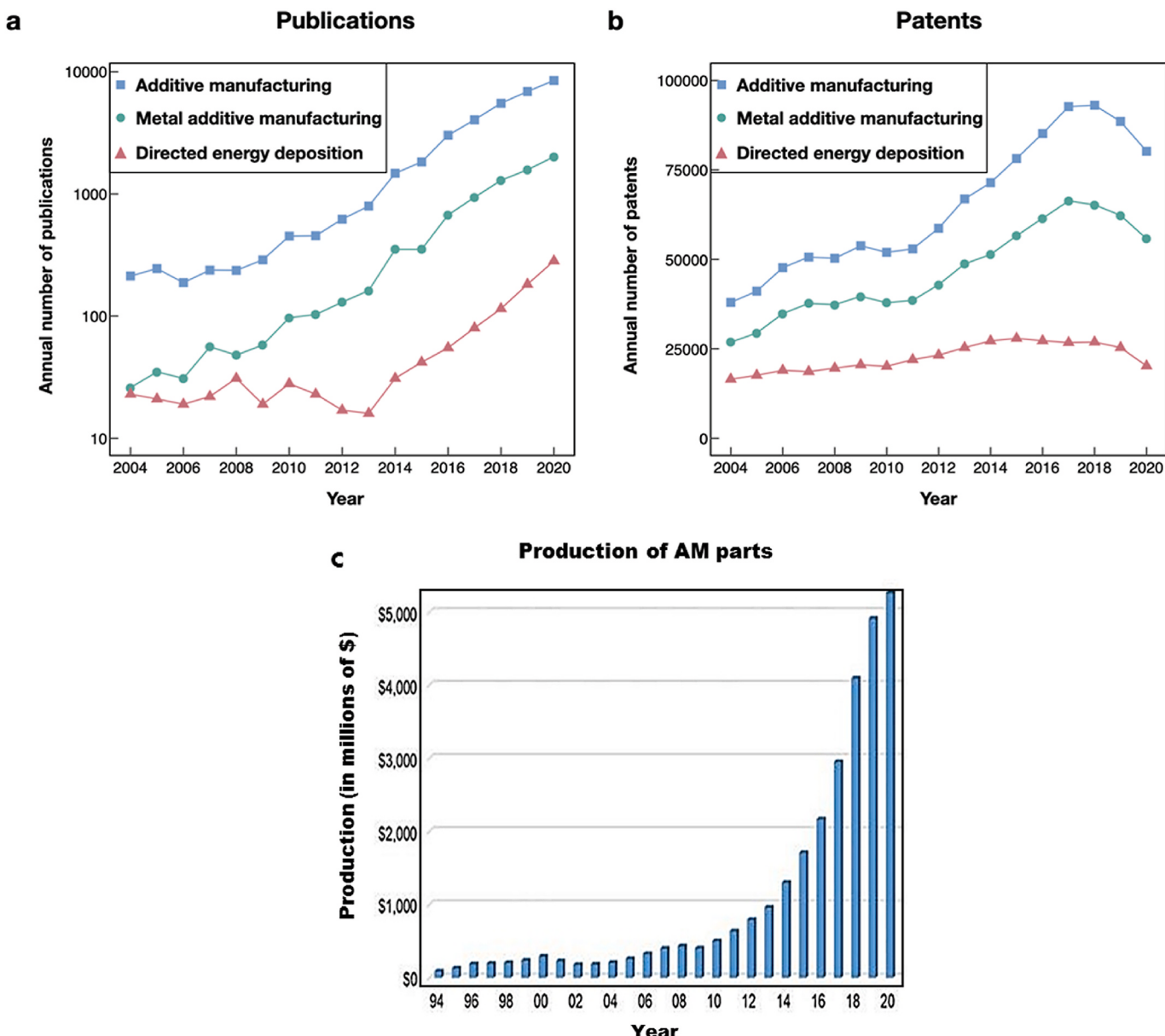


Fig. 1. Trends in metal AM research and intellectual property. Annual number of (a) publications (note the logarithmic scale of the y-axis), (b) published patents, and (c) production of AM parts (in millions of dollars) from independent service providers (source: Wohlers Report 2021).

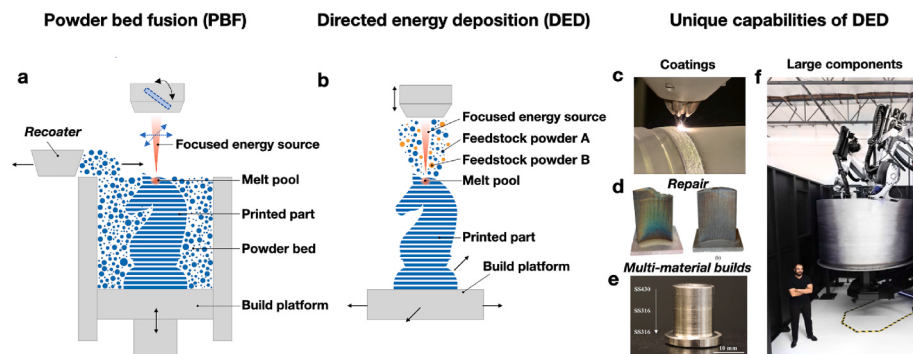


Fig. 2. Metal AM technologies. (a) A schematic of the powder bed fusion (PBF) process. (b) A schematic of the directed energy deposition (DED) process (needed support structures are not shown here). (c) Application of DED in cladding and repair (image courtesy Optomec). (d) Repair of a DED-fabricated 316L stainless steel turbine blade. Reprinted from Ref. [19], with permission from Elsevier. (e) A functionally graded magnetic-nonmagnetic bimetallic structure fabricated via DED. Reprinted from Ref. [15], with permission from Elsevier. (f) A large aerospace component fabricated by a custom DED-based process (image courtesy Relativity Space).

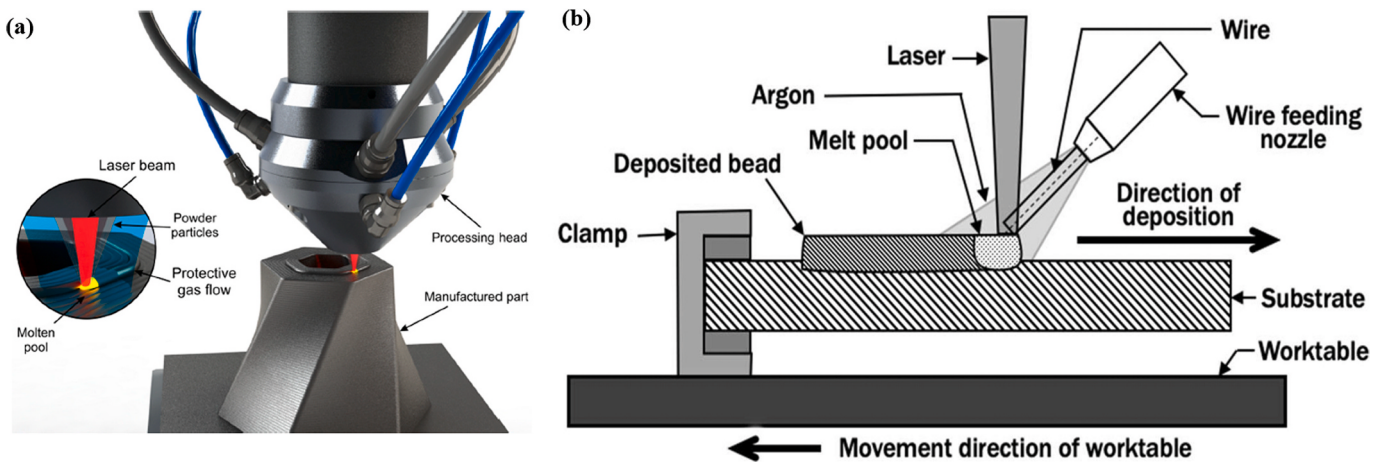


Fig. 3. Schematic illustration of DED processes. (a) Powder-feed system with coaxial particle injection set-up. The inset shows the interaction zone, with a convergence of the laser beam and powder particles into the molten pool under an inert protective atmosphere. Reprinted from Ref. [22], with permission from MDPI. (b) Wire-feed system. The deposition head type defines the applied thermal energy source. A protective atmosphere in the form of shielding gas or high vacuum is utilized to protect the melt pool. Electric arc could be TIG (tungsten inert gas), GMAW (gas metal arc welding), or plasma. This figure is a modification of Fig. 1 in Ref. [23].

metal powders. Metal wires are also safer and easier to store than powders. However, increased laser power is required to melt the metal wires, thus leading to the higher price of wire-feed laser DED systems.

While DED in its core principles is like welding, it presents various unique technical and scientific challenges [24]. Thus, the knowledge established based on welding metallurgy could be helpful to improve the DED processes with controlled microstructure and process repeatability [25]. Combining different welding methods with AM broadens the potential of AM technology for large-scale manufacturing. Welding-based AM processes such as laser metal deposition with wire (LMD-W), electron beam AM (EBAM), and WAAM are capable of depositing large-scale components at low production cost [24]. Specifically, the WAAM process has attracted more interest in the aerospace industry for fabricating high-strength aluminum structures due to its high deposition rate and flexibility in producing large structures [26]. High cooling rates of up to 10^5 K/s [27] combined with the layer-by-layer deposition of DED processing that subjects the material to unique thermal cycles can lead to both complex phase transformations [28] and the formation of detrimental residual stresses [29]. The macrostructure and microstructure of the as-deposited material are controlled by the thermal history in the DED process. These may influence the mechanical and physical properties of the as-deposited parts [12]. *In situ* monitoring, process optimization, and feedback control are reported to minimize defects associated with the DED process and improve part quality [12]. Commercial DED systems are available from various vendors worldwide. Most DED machines are still open-loop systems. Although the basic operation principle remains the same, each vendor adds special features

for its unit. The free-axis or six-axis of freedom deposition heads are becoming common to print on any surface and add-on features on existing parts as well as printing of large freestanding parts. For powder deposition, nozzle coaxial feed improves deposition efficiency and has become popular in many systems. Finally, melt-pool sensors (MPS) are also helpful to understand and control metal deposition.

Several review articles have been published in recent years on metal AM via PBF and DED [12,27,30–35]. Yet, it appears that no recent comprehensive review has been dedicated to a broad presentation of material systems, material design, fabrication, challenges, and the relationship between microstructures and mechanical properties of a variety of material families. The objective of this review is thus to provide a comprehensive analysis of materials deposited via DED, including monolithic-, bimetallic-, and multi-material systems. These materials include titanium alloys, steels, aluminum alloys, nickel alloys, cobalt alloys, intermetallics, shape memory alloys (SMAs), high-entropy alloys (HEAs), ceramics, composites, FGMs, and multilayered materials. Emphasis is placed on the relationships between DED process parameters, microstructures, and resulting mechanical properties of the printed components. Alloy design, freedom structure deposition, material cladding and repair by DED are also discussed. Finally, the critical challenges and opportunities in this area are highlighted.

2. Material systems deposited by DED, their microstructures, and mechanical properties

There is a rapidly growing interest in developing functional and

structural materials for AM. Such interest by leading industries, including the automotive, aerospace, military, and biomedical, leads to significant investments in studying various materials for AM. This section reviews materials that were recently reported to be processed via DED technology. The effect of processing parameters on microstructure and mechanical properties of the processed materials are discussed, emphasizing the current scientific and technological gaps for designing industry-reliable engineering components. To date, various materials have been processed via DED technology, with varying levels of success. This list of materials may be divided into two main groups: (1) commonly studied AM materials, such as titanium-based alloys, alloy steels, stainless steels, tool steels, nickel-based alloys, and aluminum-based alloys; and (2) novel AM materials, such as cobalt-based alloys, intermetallics, SMAs, HEAs, ceramics, composites, and FGMs. Relevant references, only some of which will be further discussed in this review article, are listed in Table 1. Naturally, no single review can cover every materials system, as this would fall outside the scope of covering significant findings and align them with results for important structural alloys. Thus, some material systems, e.g. Mg- and Cu-based alloys, will not be discussed herein.

2.1. Alloy steels

Alloy steels contain between 1.0 and 50 wt% alloying elements and are widely used as structural materials in the automotive, marine, petroleum, and chemical industries. They offer high strength and good ductility, along with excellent wear and corrosion resistance [31]. Alloy steels can be formed via various forming and joining operations [542, 543]. Manufacturing in a low oxygen environment can improve the mechanical properties of alloy steel parts [543]. Naturally, AM of alloy steels is being practiced at different industries, and is a rapidly growing research field.

Most commonly, the phrase “alloy steel” is used regarding low-alloy steels, which are generally defined as iron-carbon alloys with the sum of alloying elements between 1.0 and 4.0 wt%. The addition of alloying elements improves the mechanical properties and corrosion resistance compared to conventional carbon steels [543]. To date, various low-alloy steels have been successfully processed by DED [544]. Guan et al. [36] studied the effect of energy density on the resulting microstructure, deposit density, and mechanical properties (Fig. 4a) of DED'ed 12CrNi2Y steel. A local maximum of relative density of 98.95% was achieved within the used set of energy densities. DED-processed parts transformed from polygonal ferrite at lower energy densities to granular bainite at higher energy densities. The increase in energy density at a threshold value resulted in a reduced cooling rate and grain coarsening (Fig. 4a). Fang et al. [68] studied the microstructure, mechanical, and corrosion properties of DED'ed FeCrNiMnMoNbSi steel. It was shown that the microstructure consisted of homogeneously distributed elements with nano-scale lath spacing of martensitic phase and

minor amounts of nano-polycrystalline precipitates (Fig. 4b). Concerning yield strength and elongation, the as-deposited material met the standard of the wrought precipitation-hardened (PH) stainless steel base material (Fig. 4b). The additions of Cr resulted in enhanced corrosion resistance of the as-deposited alloy compared to the FV520B stainless steel.

Liu et al. [42] studied the DED of ultrahigh-strength 300M steel. Ultrahigh-strength steels are commonly defined as steels with yield strength higher than 1380 MPa (200 ksi). The high Si content in the 300M steel provides higher hardenability depth, higher solid-solution hardening, and higher resistance to softening at elevated temperatures compared to the AISI 4340 steel. The microstructure of the as-deposited steel consisted of tempered martensite, retained austenite, and finely dispersed carbides. Microstructure evolution at the heat-affected zone (HAZ) and its dependence on the thermal cycling associated with the DED process were also reported, see Fig. 4c. DED was also utilized to deposit 24CrNiMo steel [57]. Experimental observations and simulations were employed to study the microstructural transformation mechanism corresponding to the simulated cooling rate and temperature distribution at the melt pool area (Fig. 4d). Grain morphology analysis revealed columnar grains with a strong <100> texture along the deposit's surface, and random crystal orientation in the bulk of the deposit. This difference between the surface and the bulk microstructure was ascribed to the inherent thermal cycling during DED, which resulted in tempering effects.

2.2. Tool steels

Tool steels are used to fabricate tools for cutting, forming, or shaping materials. The material should withstand high loads at high speeds without fracture or undergoing substantial deformation. These steels typically contain relatively high concentrations of carbide formers such as Cr, Mn, V, Mo, and W, and C concentration in the range of 0.6–1.3 wt % [542, 543].

The inherent rapid solidification process and high thermal gradients associated with the DED-LB process were reported to affect the as-deposited material's microstructure and mechanical properties, particularly notable in the case of wrought tool steels [545]. Park et al. [545] studied the effect of laser energy density on the properties of as-deposited AISI H13 and D2 tool steels. A reduction in the average microhardness with increased energy density was reported for both steels. This phenomenon was explained by the apparent increase in secondary dendrite arm spacing and reduced carbon content due to CO formation. Baek et al. [69] reported the DED-LB processing of AISI H13 and M2 alloys. A refined microstructure with a fine cellular dendritic structure was observed, enhancing microhardness. The M2 deposited sample exhibited superior wear properties than the commercial heat-treated D2 steel with Cr-rich carbides (see Ref. [69] for heat-treatment specification). This was explained by the high content of carbides in the as-deposited M2 alloy. Rahman et al. [546] studied the microstructure and mechanical properties of two novel DED-LB high-carbon, high-speed steels (HC HSS) – Fe_{bal}-C-Cr-Mo-V and Fe_{bal-x}C-Cr-Mo-V-W_x. The microstructure of both steels consisted of a martensite matrix with retained austenite and inter-dendritic networks of primary, secondary, and eutectic metal carbides (Fig. 5a). A formation of an oxide layer on the surface and higher carbide density was observed in the steel alloyed with W, which resulted in enhanced wear resistance (Fig. 5a). Tensile tests after tempering treatment showed a brittle nature of the fracture surfaces.

Baek et al. [83] studied the effect of substrate preheating on the microstructure and mechanical properties of AISI M4 tool steel. It was shown that by increasing the substrate preheating temperature, the cooling rate decreased, resulting in reduced residual stress, increased hardness, but decreased tensile and impact strengths. Zhao et al. [79] studied the effect of the deposition methodology on the microstructure and mechanical properties of H13 tool steel. It was shown that the

Table 1
Selected publications on different material systems deposited by DED.

Material	References
Carbon and alloy steels	[36–68]
Tool steels	[69–87]
Stainless steels	[62,67,88–150]
Titanium-based alloys	[22,145,151–218]
Aluminum-based alloys	[145,219–245]
Nickel-based alloys	[29,246–299]
Cobalt-based alloys	[300–312]
Intermetallics	[291,313–323]
Shape memory alloys (SMAs)	[324–353]
High-entropy alloys (HEAs)	[354–374]
Copper and its alloys	[696–704]
Ceramics	[375–411]
Composites	[98,200,412–473]
FGMs and multilayered materials	[287,418,436,474–541]

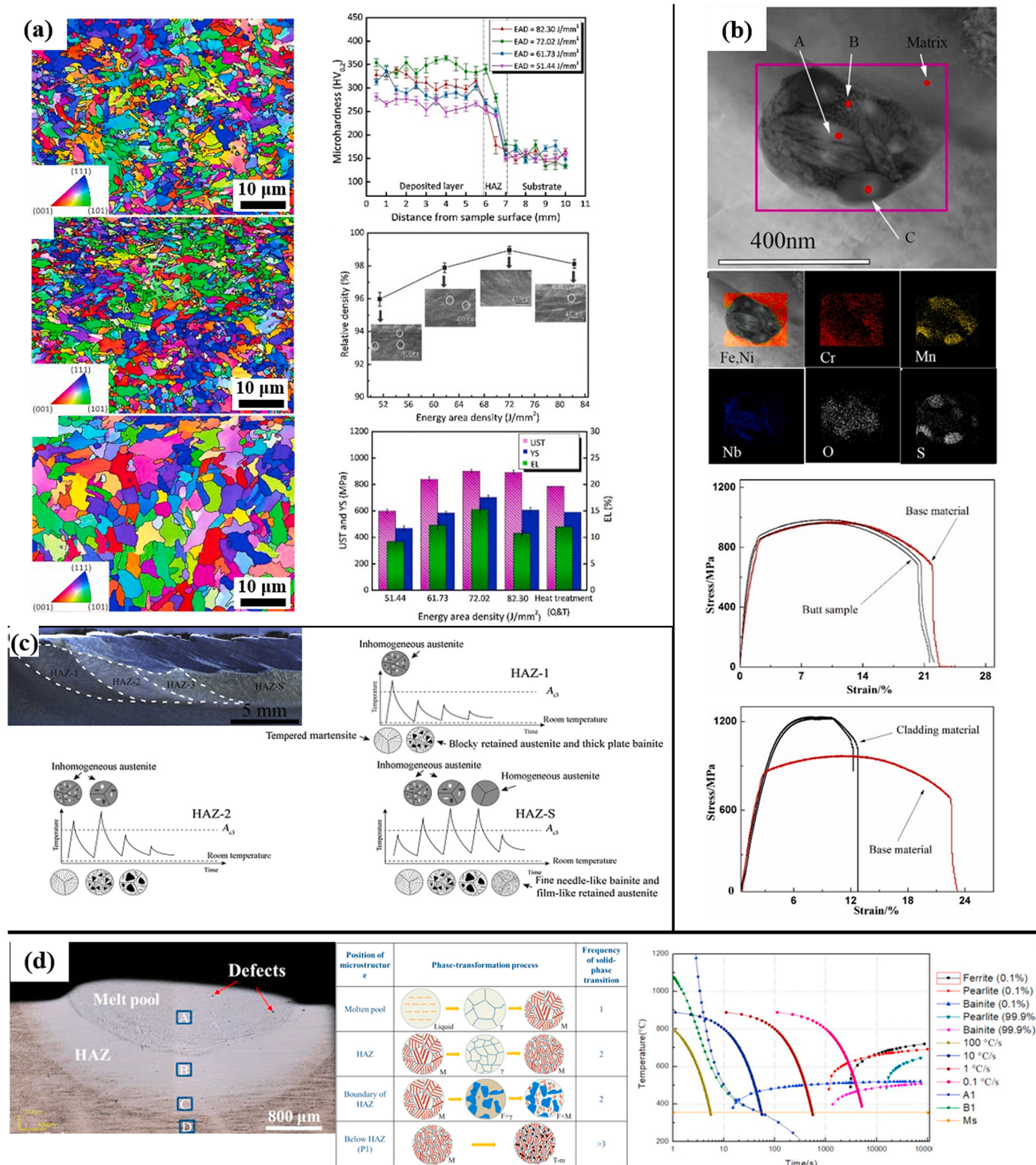


Fig. 4. (a) The effect of applied laser energy density on the microstructure, relative density, and mechanical properties of DED-LB 12CrNi2Y alloy steel. Reprinted from Ref. [36], with permission from Elsevier. EAD = energy area density, DED-LB = laser-based DED. (b) Precipitation evolution and mechanical properties of as-deposited FeCrNiMnMoNbSi steel for repair applications. Reprinted from Ref. [68], with permission from Elsevier. (c) Macrostructure and phase transformation of AerMet100 steel cladding on 300M alloy steel substrate at various regions, along with the formed HAZ, corresponding to the thermal history during deposition. Reprinted from Ref. [42], with permission from Elsevier. (d) Microstructure evolution and cooling rate analysis during DED-LB of 24CrNiMo steel. Reprinted from Ref. [57], with permission from Elsevier.

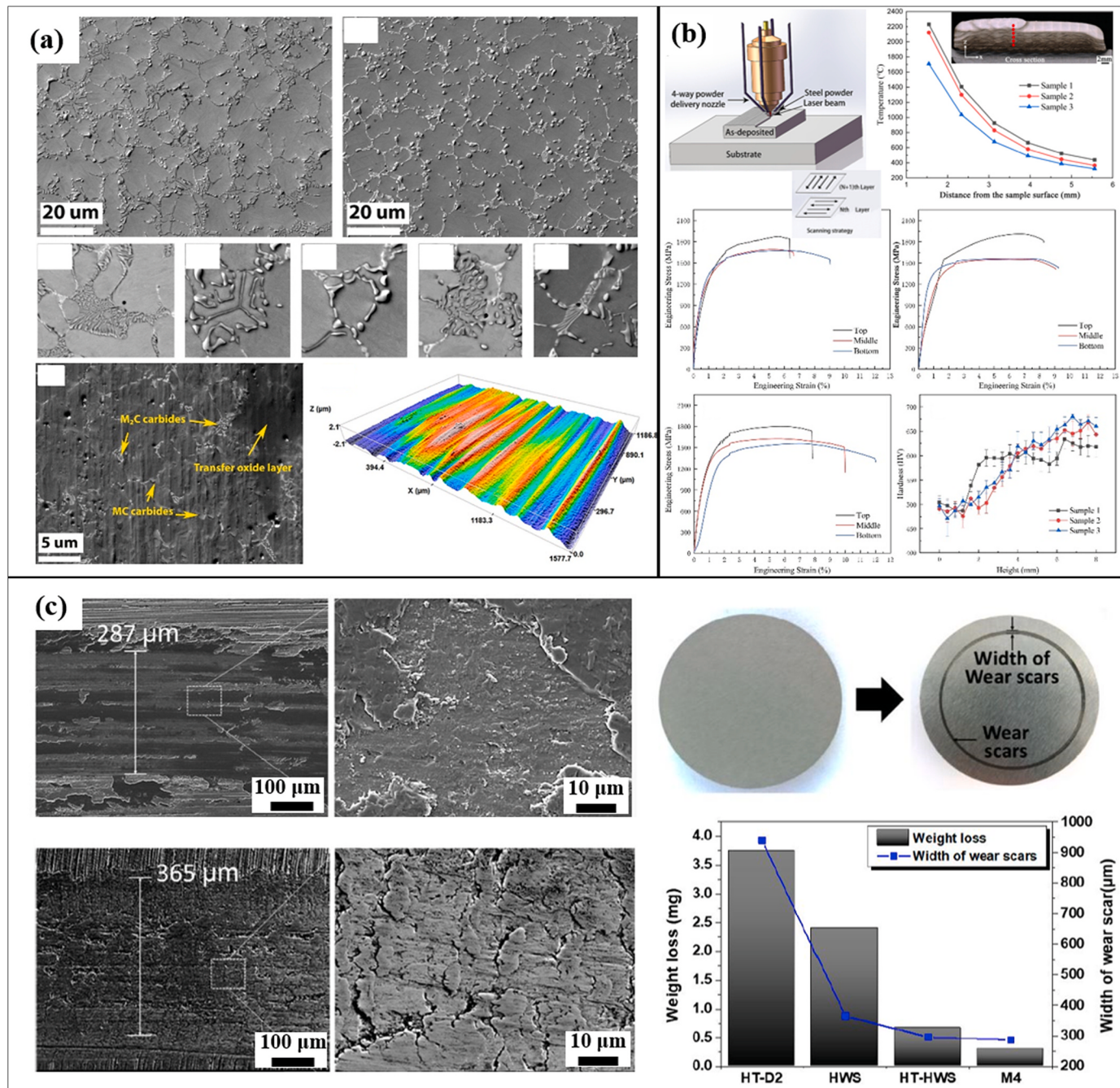


Fig. 5. (a) DED-LB Fe_{bal}-C-Cr-Mo-V (top left) and Fe_{bal-x}-C-Cr-Mo-V-W_x (top right) and the effect of the addition of W on the microstructure and wear resistance. Reprinted from Ref. [546], with permission from Elsevier. (b) The effect of deposition methodology on the thermal history and mechanical properties, with heterogeneous microstructure and mechanical properties along the build direction of DED-LB H13 tool steel. Reprinted from Ref. [79], with permission from Elsevier. Samples 1, 2, and 3 correspond to the applied scanning strategy (see Ref. [79] for scanning strategies specifications). (c) Wear scar morphology and characteristics of as-deposited M4 and high-wear resistance steel (HWS). Reprinted from Ref. [75], with permission of MDPI.

resulting thermal cycle is directly affected by the deposition methodology. The addition of time intervals in between successively deposited layers and a change in applied laser power or a combination of the two resulted in distinct thermal histories, which caused variations in microstructure and mechanical properties along with the deposit height (Fig. 5b). DED-LB of high carbon AISI M4 steel and high-wear-resistant steel (HWS) were also demonstrated [75]. The influence of post-heat treatment (quenching followed by tempering, see Ref. [75] for heat treatment specifications) on the microstructure and mechanical properties, including hardness, impact, and wear characteristics, were also reported. Fig. 5c shows the results of the wear analysis of the wear scars

on as-deposited M4 and HWS steels and the wear characteristics before and after heat treatment. To sum up, it is clear that DED-LB is a viable option to manufacture tool steels; however, processing parameters significantly influence the microstructures and mechanical properties of the components. Moreover, post-process heat treatments are highly recommended to minimize residual stresses.

2.3. Stainless steels

Stainless steels are iron-based alloys typically containing at least 10.5 wt% Cr to form a passive surface layer that provides excellent

corrosion resistance [542,543,547,548]. Such alloys are widely used in structural applications requiring a combination of corrosion resistance, strength, and ductility [543]. In this section, only few austenitic and precipitation-hardened stainless steels shall be discussed. Information on DED of ferritic and martensitic stainless steels is available in many references, some of which are listed in Table 1. In general, AM processing of stainless steels is challenging due to their high Cr content. The high oxygen affinity of Cr results in significant oxidation during laser-based deposition [549]. However, controlling the oxygen concentration to a few ppm in the deposition chamber during the DED process can overcome this challenge. Several studies have shown strong influence of processing parameters on the stainless steel microstructure evolution during DED [88,89,92,93,95,99–106,108,110,111,116,117,124,125,131,149]. The high thermal gradients, dynamic melt pool flow, and the rapid solidification associated with the non-uniform repetitive layer-by-layer deposition process result in a unique hierarchical and heterogeneous microstructure. Such microstructure is characterized by

epitaxial growth of columnar grains in various orientations through the prior deposited layer boundaries (Fig. 6a) [125]. The influence of build height was also studied. It was shown that as the build height increases, the thermal gradient and cooling rate decrease. This results in the coarsening of the grain structure [99,101,149].

Yang et al. [103] measured the microhardness of as-deposited 316L austenitic stainless steel (the "L" designation in stainless steels stands for low carbon, i.e., less than 0.03 wt%, to prevent sensitization and increase the corrosion resistance). An increase of around 35% in microhardness compared to the wrought counterpart was observed. This increase was related to the fine microstructure of the DED-LB steel compared to the wrought steel. However, large variations in the measured microhardness were reported. These variations were related to the heterogeneous microstructure of the as-deposited steel, which included interpass deposition cells, inclusion pores, and HAZ, all of which are characterized by distinct microhardness values. The tensile properties of DED stainless steels have been extensively studied [88,89,

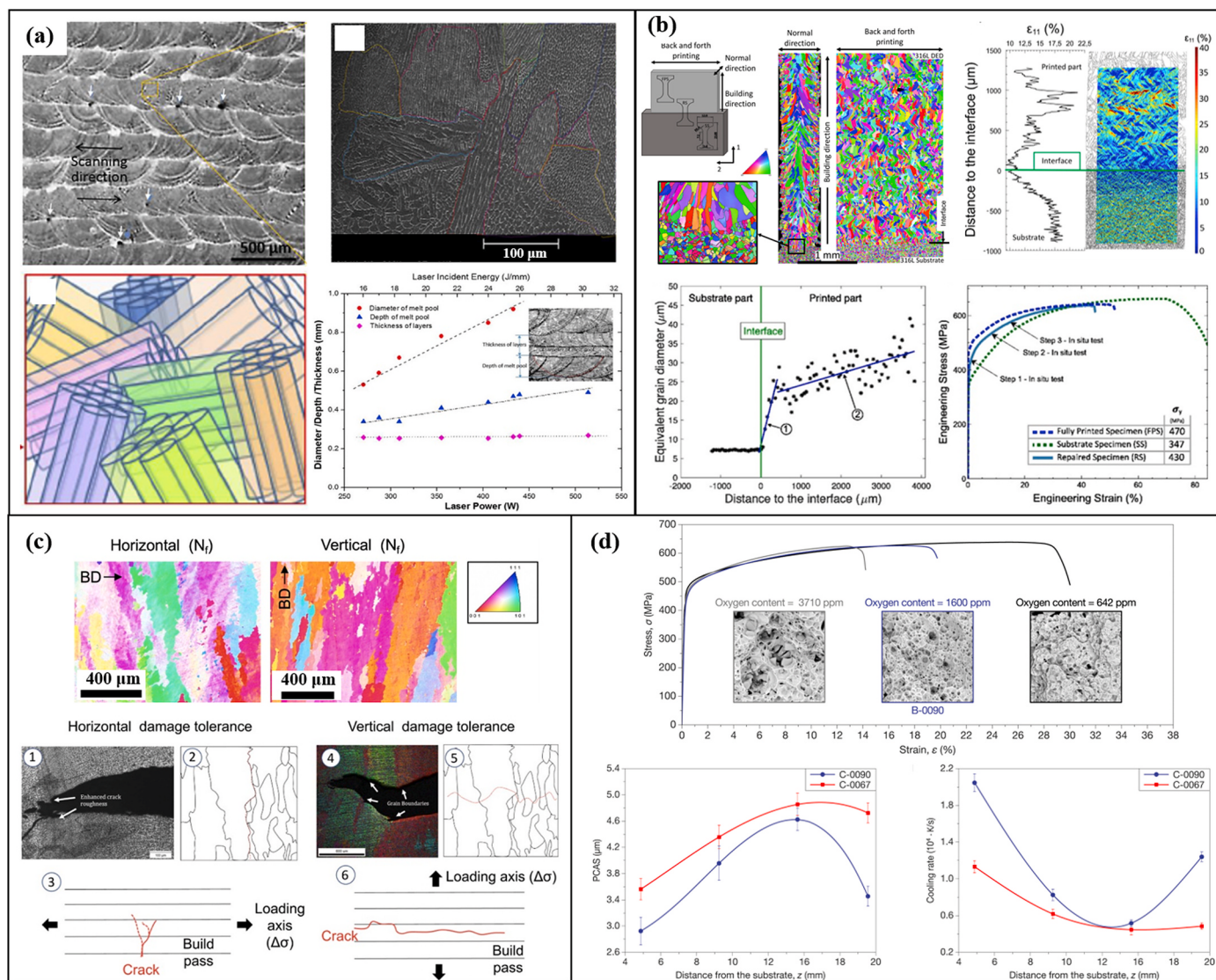


Fig. 6. (a) Microstructure evolution and melt pool geometrical characteristics and dependence on the applied laser energy in DED-LB of 316L SS. Reprinted from Ref. [125], with permission from Elsevier. (b) Utilization of DED-LB for repair application using 316L. A good fit between the obtained grain size and the build height and the developed uniaxial strains is evident. Reprinted from Ref. [138], with permission from Elsevier. (c) Grain morphology and orientation after N_f cycles for horizontal and vertical build orientations with corresponding crack propagation mechanisms in 304L deposited by DED-arc. Reprinted from Refs. [131,550], with permission from Elsevier. (d) The effect of the DED-LB deposition pattern on the cooling rate along with the vertical build height and the PACS, and the effect of oxygen content on the tensile properties of DED-LB 316L SS. Reprinted from Ref. [139], with permission from Elsevier. C-0090 and C-0067 correspond to 0–90° and 0–67° deposition patterns, respectively.

[92,93,99,100,103–105,108,110,117,119,125–127,149,150]. It was shown that there is a strong influence of the deposition orientation on the tensile properties [89,93,99,117,119]. The variations in tensile properties of samples with distinct orientations are associated with variations in thermal history during the deposition process, as the cooling rate is highly affected by the thermal gradient, and consequently – by deposition height. It was shown that hot isostatic pressing (HIP) enhances the tensile properties due to reduced porosity and residual stresses [119]. Balit et al. [138] studied the microstructure and tensile properties of as-deposited thin-wall DED-LB 316L for repair applications. A good correlation was found between the measured grain size and the analyzed mean axial strains using an *in situ* digital image correlation (DIC) combined with electron backscatter diffraction (EBSD) analysis, Fig. 6b. Gordon et al. [131] studied the fatigue properties of as-deposited 304L SS (stainless steel) fabricated by gas metal arc welding, DED-arc, in the high-cycle fatigue (HCF) loading regime. It was shown that fatigue life is highly governed by the inherent anisotropy, preferred grain growth orientation, and porosity in the as-deposited steel. The study showed that the fatigue properties are similar or superior to those of wrought 304L SS. This is in good agreement with other studies of the fatigue properties of stainless steels fabricated by DED-LB [126,127].

The damage tolerance and crack propagation mechanisms of as-deposited stainless steels in the horizontal and vertical orientations were studied [131,550]. In vertical samples, the crack propagation path was transgranular. In samples with horizontal orientation, crack branching and propagation along grain boundaries were evident (Fig. 6c). Smith et al. [127] reported that the fatigue performance of as-deposited 304L SS was highly dependent on defects in the as-deposited steel. It was shown that superior fatigue properties were achieved when the number of defects was minimized. The fatigue cracks' origin was characterized by areas of irregular shape lack-of-fusion (LoF) defects with partly melted trapped powder particles. Fig. 6d illustrates the effect of oxygen content on the elongation of as-deposited 316L. It is evident that the deposition pattern (either 67° or 90° in between successive layers) directly affects the resulting thermal history and the distance from the substrate, which in turn results in variations in the primary cellular arm spacing (PCAS).

Precipitation hardened (PH) steels are Fe–Cr–Ni alloys with low carbon content (less than 0.1 wt%) containing precipitate-forming elements such as Cu, Al, Ti, Nb, and Ta. They can be either austenitic or martensitic in their annealed condition. PH steel parts require a unique set of properties. Among others, such attributes include high strength, high corrosion resistance, oxidation resistance, as well as excellent heat and fire resistance. PH steel parts are utilized as structural materials in various applications, including marine structures, gas turbines for aircraft, fuel tanks, hydraulic systems, fasteners, and nuclear power plants. To date, relatively little work has been carried out on the DED-LB of 17–4 PH (AISI 630) by LENST™ [120,145,551]. It has been shown that the inherent raw powder porosity has a more significant effect on the resulted intralayer porosity than the applied deposition conditions [120]. Utilizing ultrasonic vibration during the deposition process improved the hardness and tensile properties of the as-deposited parts. These were ascribed to the effect of ultrasonic vibration in increasing the powder catchment efficiency, reducing the surface roughness, increasing the melt pool dimensions, porosity, reducing micro-cracking, and refining the grain size [551].

2.4. Titanium alloys

Titanium (Ti) alloys are of interest in aerospace, automotive, naval, and biomedical applications [542,543,552–555] due to their high specific strength, exceptional corrosion resistance, high fracture toughness, excellent fatigue resistance, good mechanical properties at elevated temperatures (up to 450 °C), low coefficient of thermal expansion (CTE), and good biocompatibility. However, Ti and its alloys have poor

machinability, low thermal conductivity [556] and are more challenging to cold work than other alloys due to their low Young's modulus and high yield strength. Moreover, Ti alloys show poor machinability and have a very high affinity towards oxygen; naturally, Ti alloys are challenging to manufacture via traditional techniques, such as machining and casting [542,557]. Therefore, AM of Ti-based alloys has been extensively studied and implemented, producing complex, intricate geometries and small dimensions with high precision, which is impossible in casting or milling. The properties of Ti-based alloys can be tailored by percentage, shape, size, and distribution of the α (HCP) and β (BCC) phases at room temperature [542,556,557], as well as by the interstitial oxygen content. The dual ($\alpha+\beta$) phase Ti6Al4V alloy is the most widely used Ti alloy. This is mainly due to its abundant use in high-impact industries such as aerospace and biomedical. Several published papers have reviewed the AM of Ti6Al4V in general, and specifically by DED [205,496,510,558–560].

For AM of Ti6Al4V, it has been reported that a fine acicular martensitic α -phase (i.e., α') arranged in a Widmanstätten microstructure provides high tensile strength [11] and fatigue strength [561], with a tradeoff of reduced ductility [11]. Thus, to improve the ductility of the as-deposited part, a post-processing heat treatment is necessary. Some comparisons between the mechanical properties of DED-LB, PBF-EB, cast, and wrought Ti6Al4V alloys have been reported and explained in terms of their different microstructures. Compared to the wrought alloy, the shorter fatigue life of the DED-LB-processed alloy has been associated with microstructure and porosity [213]. DED-LB processing parameters optimization was suggested to reduce defects and improve mechanical properties. Furthermore, there is a relationship between the obtained microstructure characteristics and the fatigue life performance of the as-deposited part. It was suggested that due to the increased density of grain boundaries, fine microstructures lead to an increase of the fatigue life at lower strain amplitudes, while at higher strain amplitudes, they lower the fatigue life of the as-deposited part [213]. High laser power was utilized to DED-LB-process Ti6Al4V, resulting in lower ductility, comparable tensile strength, and fracture toughness, with similar fatigue crack growth (FCG) threshold values for the PBF-EB-processed alloy [164,167]. Higher laser power resulted in an alloy with higher FCG threshold values for the DED-LB process. DED-LB-processed Ti6Al4V alloy displayed improved low-cycle fatigue (LCF) performance, reduced high-cycle fatigue (HCF), reduced FCG threshold values, and superior fracture toughness than mill-annealed alloy. These differences were ascribed to the unique lamellar microstructure obtained in the DED-LB alloy. It was suggested that the α -phase morphology controls the FCG threshold value of DED-LB alloy. This was attributed to the fact that utilizing high laser power resulted in coarser α morphology, which in turn resulted in increased FCG thresholds, with lower intermediate regime FCG rates [164]. Porosity was claimed to be responsible for the reduced fatigue life of the DED-LB-processed Ti6Al4V alloy compared to the wrought alloy [215].

Kobryn and Semiatin [562] studied the effect of stress relief and HIP post-processing on the fatigue properties of DED-LB-deposited Ti6Al4V alloy. It was shown that the fatigue strength, ductility, fracture toughness, and tensile strength of HIP'ed (at 900 °C and 100 MPa for 2 h) Ti6Al4V is favorably comparable to wrought Ti6Al4V alloy. It was also shown that the LoF porosity significantly affects anisotropy and mechanical properties [562]. Yield strength anisotropy was observed in the stress-relieved (at 700–730 °C for 2 h in a vacuum environment) sample and ascribed to the residual porosity in the DED-LB part. Mechanical and crystallographic anisotropies were also observed in the HIP'ed and stress-relieved conditions [562]. HIP was shown to be effective in closing LoF porosity. Prabhu et al. [177] showed that DED-LB-deposited Ti6Al4V in the as-deposited state had a comparable fatigue life to the wrought alloy, although residual partly melted powder particles present at the as-deposited part surface would trigger crack initiation, thus resulting in a significant reduction in the observed fatigue life. Razavi and Berto [214] observed higher fatigue life and fatigue strength of

DED-LB-processed Ti6Al4V (annealed for 1 h at 600 °C for residual stress relief) than the wrought alloy. This phenomenon was ascribed to the finer grain size of DED-LB-processed alloy, which leads to higher fatigue crack nucleation time, and the basket-weave and columnar prior β grains in its microstructure, which leads to a higher degree of tortuosity and, accordingly, more roughness-induced closure effects during crack propagation [214]. The reader is referred to Refs. [205,496,552, 558–560] for a more comprehensive description of the relations between processing parameters, defects, microstructure, heat treatment, and mechanical properties of DED Ti6Al4V.

Examples of some other Ti-alloys are presented in Fig. 7. Byun et al. [181] studied the effects of Cr and Fe additions to pre-alloyed Ti6Al4V on the microstructure and mechanical properties. It was shown that increasing the concentrations of Fe and Cr resulted in grain refinement of the prior- β grains and the martensite grains, with alterations in the grain morphology from columnar to equiaxed. The increased Fe and Cr concentrations also enhanced strength, hardness, and reduced the ductility. Dargusch et al. [198] studied the microstructure, corrosion, and biocompatibility properties of near- β Ti25Nb3Zr3Mo2Sn alloy. It was shown that the resultant microstructure was composed of a mixture

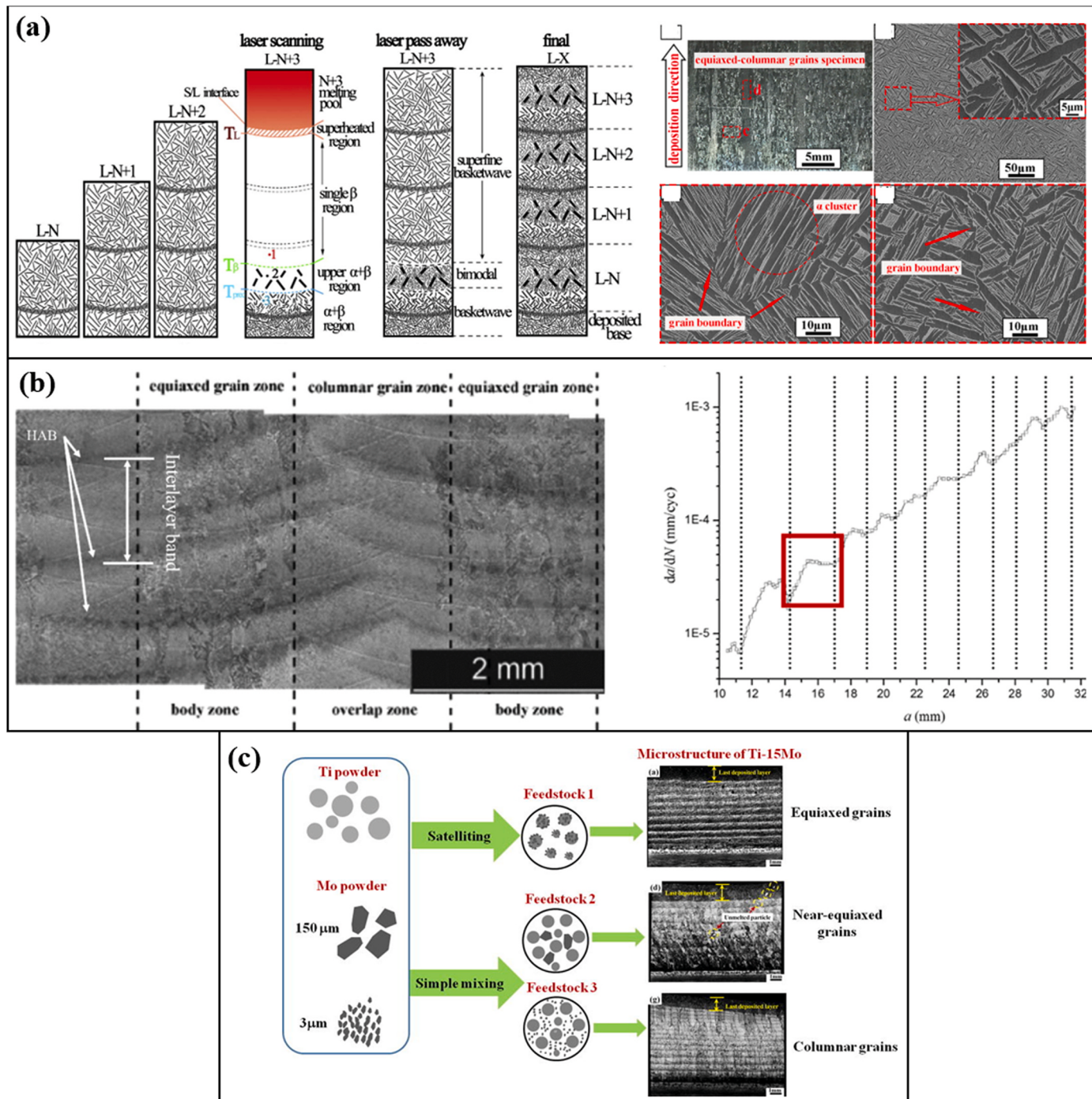


Fig. 7. Ti-based alloys deposited by DED. (a) Microstructure evolution in DED-LB Ti6.5Al3.5Mo1.5Zr0.3Si alloy. Reprinted from Refs. [190,204], with permission from Elsevier. (b) The effect of the microstructure of as-deposited Ti6.5Al3.5Mo1.5Zr0.3Si alloy on the fatigue and crack growth characteristics. Reprinted from Ref. [186], with permission from Elsevier. (c) Nucleating mechanisms through satellitelling in DED-LB Ti15Mo. Reprinted from Ref. [187], with permission from Elsevier.

of 91% β and 9% α . The nucleation of the α -phase was explained by the repetitive heating cycles during deposition, which caused a reduced heat extraction during solidification. Compared to commercially pure (CP) Ti, the DED-LB near- β alloy exhibited reduced corrosion resistance, which was strongly affected by the addition of alloying elements, the applied manufacturing processes, variations in the resulting microstructure, and the quality of the native oxide layer. The microstructure of DED-LB Ti6.5Al2Zr1Mo1V was also studied [185]. The macrostructure of the as-deposited material consisted of large columnar β grains that grew across several layers in the build direction. A basket-weave microstructure was evident, with rod-like shaped α -phase (volume fraction of $76.0 \pm 3.6\%$) in the β -phase matrix. The thermal expansion of the as-deposited material was irreversible and anisotropic. After annealing at 960°C for 1 h, an increase in α -phase was observed along with expansion in the x and y transverse directions, whereas a contraction was observed in the deposition, z -direction.

Fig. 7a shows the microstructure evolution mechanism and characteristics of the mixed equiaxed and columnar grain morphology of DED-LB bimodal Ti6.5Al3.5Mo1.5Zr0.3Si alloy [190,204]. The relationship between the DED-LB processing parameters, microstructure, and fatigue properties of this $\alpha+\beta$ alloy was also reported [186]. The deposition process resulted in a mixed grain morphology of large columnar and equiaxed grains alternately distributed. Periodic fluctuations in fatigue crack growth rates were observed because of the heat-affected bands (HABs), Fig. 7b. The crack growth rate decelerated at the HABs, accelerated immediately after it passed the HABs, and decreased again. The suggested mechanisms for the deceleration and acceleration were based on the differences in fracture characteristics in the HAB and its adjacent area and the changes in microstructure between the two adjacent HABs. Cracks mostly grew in the equiaxed grain zone and near the edge of the two zones, although some of them propagated across the columnar grain zone and finally in the equiaxed grain zone.

β -Ti alloys are known for their attractive biocompatibility and a good combination of low Young's modulus and high strength. Such attributes triggered the design of β -Ti alloys, which do not contain toxic elements. Bhardwaj et al. [207] utilized DED-LB to deposit Ti15Mo alloy as a prospective alloy for bone implant applications. The deposition orientation was found to directly affect the corrosion resistance of the alloy. An increased corrosion resistance (by ca. 75%) was reported for the vertically deposited alloy compared to the horizontally deposited alloy. The surfaces of the as-deposited materials were hydrophilic in both cases, enhancing apatite formation *in vitro*. Zhang et al. [187] introduced a method for microstructural control of DED-LB Ti15Mo alloy using a "satellitizing" technique (Fig. 7c). This powder feedstock preparation technique resulted in a controlled attachment between two distinct elemental powders that varied in size and chemical composition, forming a Ti powder covered with Mo satellites. A comparison between conventional elemental mixing of Ti and Mo powders and the powder feedstock prepared by the satellite technique revealed that the latter resulted in refined equiaxed grain morphology, while the former yielded a mixture of large equiaxed and columnar microstructure.

2.5. Aluminum alloys

Conventionally processed aluminum and its alloys second only to steel in industrial use owing to their low density, high specific strength, high ductility, high toughness at subzero temperatures, high corrosion resistance, high thermal and electrical conductivities, high reflectivity, good processability, good recyclability, and cost-effectiveness [542]. They play a significant role in various applications, including plane airframes, wings, airfoils, forged engine pistons, fuel cells, fuselages, satellite and automobile parts, construction, cookware, etc. [145].

Combining the favorable characteristics of Al alloys with part design freedom in AM has attracted great interest in AM of Al alloys. Unfortunately, laser-based AM of most Al alloys raises some significant challenges due to high surface reflectivity and thermal conductivity

combined with the high cooling rate associated with AM, causing pore formation and hot cracking in Al alloys [35,563,564]. The inherently high surface reflectivity of Al requires the application of increased laser power to allow sufficient energy absorbance and to promote complete melting of the deposited Al powder [565]. This increased laser power might lead to gas porosity in the as-deposited alloy due to the vaporization of low-boiling-temperature alloying elements [35,228,438]. Svetlizky et al. [228,238] have recently addressed the abovementioned challenge. They utilized DED-LB to deposit a pre-alloyed gas-atomized Al 5083 powder and characterized the microstructure and mechanical properties of the as-deposited alloy. The 5xxx series is Al-Mg-based and is not age-hardenable. It combines medium-to-high strength with good weldability and good corrosion resistance in a naval environment. Svetlizky et al. reported a reduction of 35% in the Mg concentration due to elemental vaporization. The as-deposited alloy's chemical composition and mechanical properties were compared with wrought Al 5754 in the annealed (O) condition, with a maximal relative density of 99.26% (Fig. 8a).

Wang et al. [233] studied the influence of alloying AlMg alloy with Sc and Zr during the DED-LB process and aging post-treatment at 325°C for 4 h on the precipitation mechanism of $\text{Al}_3(\text{Sc}, \text{Zr})$ and the resulting mechanical properties. The microstructure of the deposited AlMgScZr alloy was governed by the distinct thermal history and cooling rate during air and water cooling. Homogenous equiaxed grain and heterogeneous grain structures were reported for air and water cooling, respectively. The water-cooled samples showed a twofold increase in the yield strength following aging compared to the air-cooled alloy. This increase was due to severe precipitation of an $\text{Al}_3(\text{Sc}, \text{Zr})$ phase in the water-cooled alloy. The increase in the precipitated secondary phase also affected the microhardness. It was shown that the higher microhardness of the water-cooled alloy and the addition of the precipitated phase increased the effect of the aging heat treatment (Fig. 8b).

Residual stresses are also a challenge when dealing with laser-based deposition of Al. The high CTE of Al makes it highly susceptible to shrinkage, crack formation, and possible material deformation during the inherent repetitive thermal cycles [35]. The poor powder flowability of Al due to its low density affects the stability of the blown powder mass flow rate (PMFR) and, consequently, the deposit's quality [564]. The high moisture absorption and surface oxidation of Al are additional properties hindering good laser-based deposition of Al alloys [35,566]. Due to the above-listed challenges, only limited Al alloy compositions have been deposited using DED, mainly focusing on AlSi and AlSi10Mg alloys. This is due to their unique properties, such as excellent laser absorption, high corrosion resistance, good weldability, and good static and dynamic mechanical properties [564,567]. An additional reason for their extensive study is their high content of Si. The addition of Si enhances the melt pool wettability, lowers the melting temperature, reduces the shrinkage and cracking susceptibility during solidification, and improves the corrosion resistance [564,567]. Javidani et al. [242] studied the microstructure evolution and mechanical properties of as-deposited DED-LB AlSi10Mg. The microstructure morphology was reported to vary with the vertical deposition distance from the substrate. It was shown that the microstructure of the as-deposited Al alloy consisted of three distinct morphologies along the build direction (Fig. 8c), changing from cellular near the substrate to columnar dendritic at the center, and finally equiaxed near the top edge. This phenomenon was attributed to the decrease in cooling rate as the build height increased.

Some studies investigated the effect of the dominant processing parameters on the microstructure and properties of DED AlSi10Mg alloy [222–224,243]. España et al. [239] showed that process parameters in DED-LB of as-deposited Al12Si could significantly influence the microstructure, hardness, and thermal properties. Liu et al. [223] utilized the Taguchi methodology and analysis of variance (ANOVA) to study the variable processing parameters (laser power, laser scanning speed, PMFR, and argon shielding gas flow rate) and any synergistic interactions to optimize the density of the as-deposited AlSi10Mg alloy,

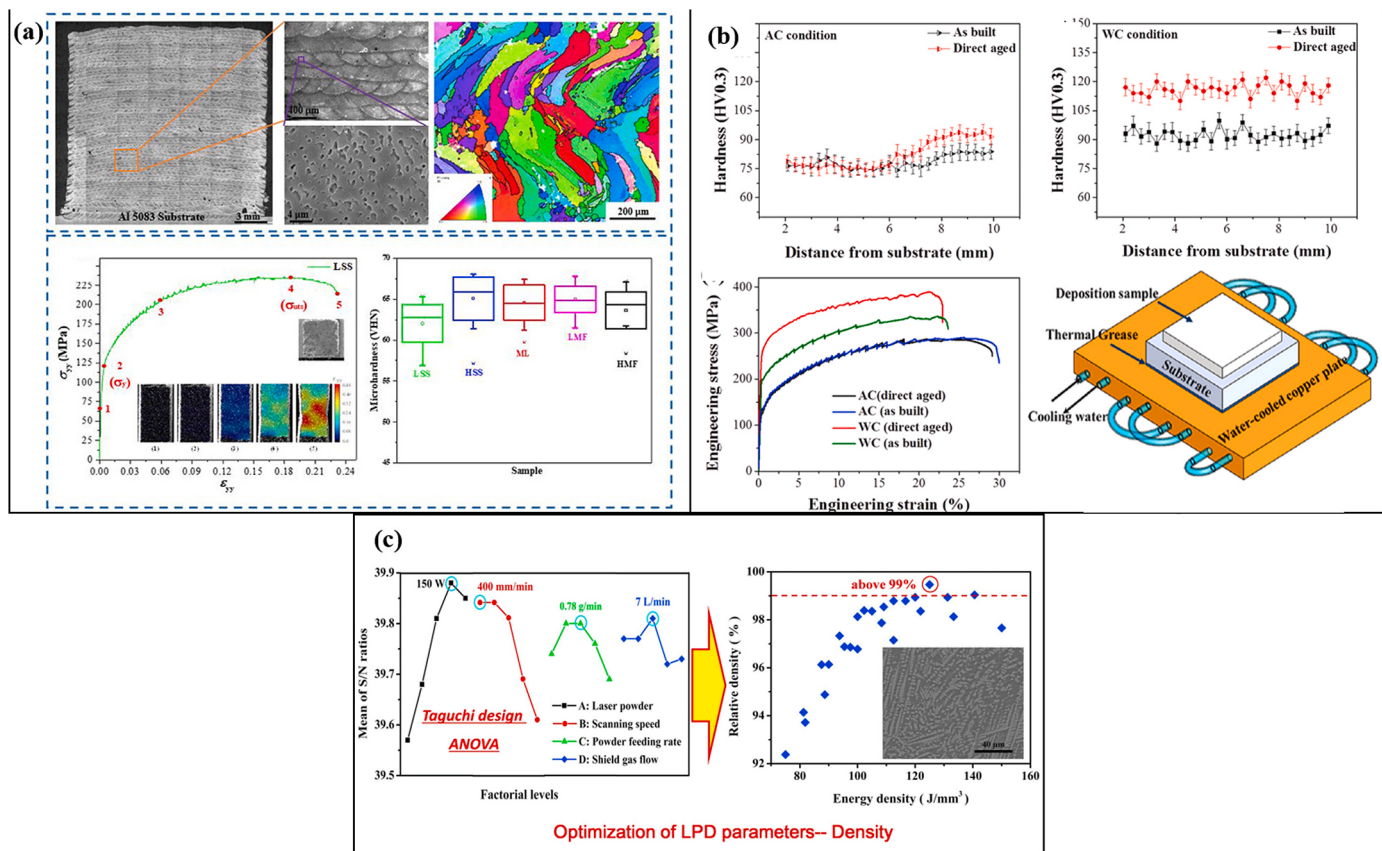


Fig. 8. (a) DED-LB high-density (above 99%) Al5xxx alloy showing selective elemental evaporation of Mg and Zn and mechanical properties comparable to those of wrought Al 5754-O. Reprinted from Ref. [228], with permission from Elsevier. LSS = low scan speed, HSS = high scan speed, ML = middle level, LMF = low powder mass flow rate, HMF = high powder mass flow rate. (b) The effect of active substrate cooling (air and water) on the microstructure and mechanical properties of AlMgScZr alloy. Reprinted from Ref. [233], with permission from Elsevier. AC = air-cooled, WC = water-cooled. (c) Process parameters optimization of DED-LB AlSi10Mg alloy using the Taguchi method. Reprinted from Ref. [223], with permission from Elsevier. LPD = laser powder deposition.

Fig. 8d. An optimal set of processing parameters was adequate for high-density (above 99% relative density) AlSi10Mg alloy deposition. Gao et al. [222] showed the importance of laser scan speed on pore formation, microstructure evolution, and microhardness of AlSi10Mg. It was concluded that, under similar processing parameters, the increase in the laser scan speed resulted in increased deposit density, microstructure refinement, and increased microhardness and tensile properties. This conclusion is consistent with other studies on the DED of AlSi10Mg alloy [223,225,243].

Outstanding mechanical properties characterize the Al 7xxx series compared to the AlSi and AlSi10Mg alloys. Unfortunately, AM of the Al 7xxx series is still a challenge [245]. Selective evaporation of low boiling point elements such as Zn, Cu, and Mg, the principal alloying elements in these alloys, might induce gas porosity and consequently degrade the mechanical properties of the as-deposited alloy [228]. Singh et al. [220, 226,245] evaluated the potential of DED-LB of Al 7050. It was shown that after its deposition, a significant reduction in Mg and Zn occurred and resulted in porosity and LoF in the as-deposited alloy [220,245]. To address this challenge, Singh et al. [245] used a surface modified Al 7050 pre-alloyed powder coated with Ni to allow improved laser energy absorbance during laser processing and, by that, reduce the applied laser energy [226]. Although the Ni-modified Al 7050 powder was found beneficial in reducing porosity, degradation in mechanical properties was still observed due to segregation of Ni to the inter-dendritic boundaries and formation of a brittle Al₃Ni intermetallic phase.

The microstructure of DED-LB Al4047 has been reported to consist of both equiaxed and columnar dendrites, resulting from the melt pool's rapid solidification [145,226]. Eliaz et al. [145] suggested applying high

laser power (higher than 380 W) as a means for avoiding LoF or cracking in the outer deposited layers, which determine the surface roughness of the as-deposited part.

2.6. Nickel-based alloys

Nickel-based alloys are conventionally processed as wrought, cast (polycrystalline, directionally solidified, or single crystal), or powder metallurgy (P/M) alloys. They combine excellent tensile and creep strengths at high homologous temperatures, high aqueous corrosion resistance, high-temperature oxidation resistance, high hardness and toughness, low CTE, high strength and ductility at cryogenic temperatures, and excellent solution ability of alloying elements, good weldability and formability [568–570]. The abovementioned properties make Ni-based superalloys suitable for jet engine, steam turbine, space, petrochemical, energy conversion, and cryogenic applications [568, 570–572]. However, Ni-based alloys have poor machinability. Their machining might induce residual stresses and various types of defects, which might promote catastrophic failure during the part's service life [569–571]. Addressing these challenges, AM can serve as a potential alternative to the traditional manufacturing processes of Ni-based alloys. In addition, the inherent design flexibility of AM parts may have a beneficial role in innovative turbine designs with enhanced performance by incorporating internal cooling micro-channels for improved heat transfer [292,573,574].

Previous studies have shown the potential of the DED processes to fabricate and repair Ni-based alloys. Inconel 718 in particular has been processed by DED and other AM processes [247,248,254,256,258–267,

275,277,278,280,281,283,285,286,290,296–299] due to its versatility and abundant use in applications that require excellent performance at high temperatures and corrosive environments [569,570]. The effect of applied DED processing parameters on the as-deposited Inconel 718 was studied by many research groups [258,262,267,299]. Zhong et al. [267] studied the effects of processing parameters, such as laser power, laser scan speed, and PMFR, on single-track deposition's geometrical characteristics, porosity, and powder catch efficiency at high deposition rates (i.e., higher than 0.3 kg/h). A strong influence of the deposition path and laser power on the microstructure and texture of as-deposited Inconel 718 was observed (Fig. 9a) [254]. The variations in dendritic growth morphology and crystallographic orientation were ascribed to the influence of the vertical and horizontal heat fluxes along with the melt pool as the scanning paths and applied laser energy sequence during deposition were changed. The increase in laser power resulted in an elongated, aligned columnar grain structure that resulted in epitaxial grain growth. This phenomenon was explained by the increased laser power affecting the thermal gradient and the melt pool, which resulted in nearly vertical heat flux. Based on experimental results, Liu et al. [299] reported a nonlinear melt pool temperature profile with an increase in the single wall deposit's height. Furthermore, the influence of

the applied laser power and scanning speed on the temperature profile in the melt pool was shown. Johnson et al. [264] reported comparable tensile properties of DED-LB and heat-treated versus wrought Inconel 718 (see Ref. [264] for heat-treatment specifications). However, the DED-LB alloy had a considerably shorter fatigue life than the wrought alloy. Fractographic analysis revealed that the fatigue crack was initiated from apparent porosity near the surface and LoF defects. In a later study [277], the same group investigated the fatigue properties of heat treated (according to AMS 5596C specifications) Inconel 718 at elevated temperatures (650 °C). The HCF life of the DED-LB alloy was found comparable to that of the wrought alloy. However, the LCF life of the DED-LB alloy was shorter than that of the wrought alloy. This was ascribed to cracking of the brittle δ and Laves phases at high strains promoted by elevated temperatures (Fig. 9b). Fig. 9d shows the influence of heat treatments (direct aging, homogenization, solution treatment, or combination of them) on the tensile properties and fracture toughness properties compared to either the as-deposited condition or wrought alloy (see Fig. 9d). Li et al. [280] studied the microstructure evolution

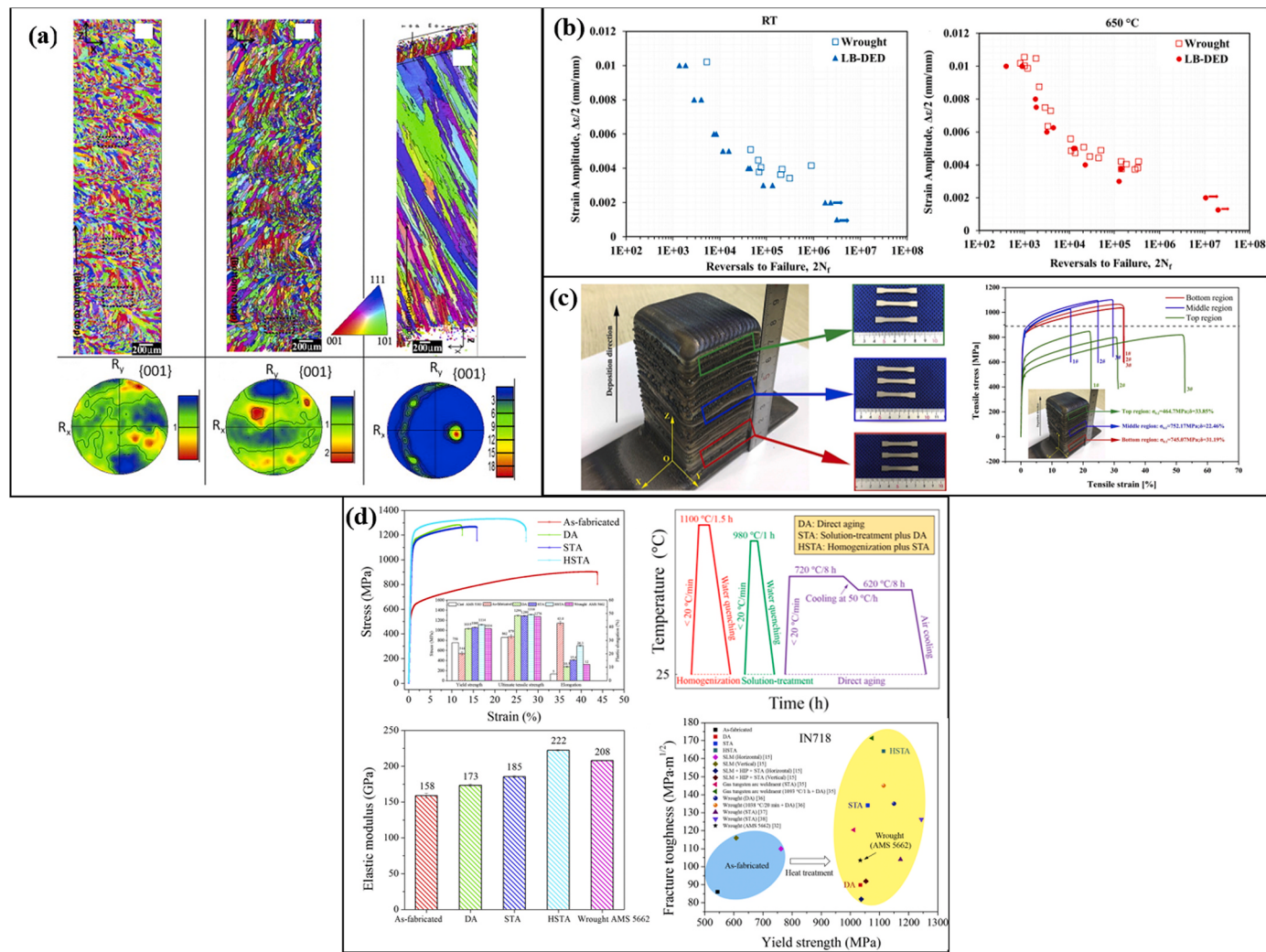


Fig. 9. (a) The effect of applied deposition strategies (unidirectional, bidirectional, and bidirectional at increased laser power) on the grain morphology and texture of as-deposited Inconel 718 alloy. Reprinted from Ref. [254], with permission from Elsevier. (b) Comparison between the fatigue properties of wrought and as-deposited Inconel 718 alloy at both room and elevated (650 °C) temperatures. Reprinted from Ref. [277], with permission from Elsevier. (c) The influence of high deposition rate (2.2 kg/h) of Inconel 718 alloy and thermal history on the precipitation-strengthening and tensile properties along the build direction. Reprinted from Ref. [280], with permission from Elsevier. (d) The influence of various thermal treatments on the mechanical properties of DED-LB Inconel 718 alloy. Reprinted from Ref. [278], with permission from Elsevier. DA = direct aging, STA = solution treatment + aging, HSTA = homogenization + STA.

and mechanical properties of as-deposited Inconel 718 DED-LB at a high deposition rate (2.2 kg/h). It was shown that a unique thermal history was involved under these conditions. This thermal history influenced the microstructure evolution and precipitation of δ , γ' , and γ'' phases along the build direction. While γ' and γ'' phases precipitated at the bottom and middle zones, the short holding time within the temperature range required for precipitation was not sufficient at the top zone. Consequently, the tensile strengths and microhardness were inferior at the top zone compared to the bottom and middle zones, affirming the necessity of post-processing heat treatment of DED-LB Inconel 718 (Fig. 9c).

The study of DED Ni-based alloys has not been limited to Inconel 718. The effects of processing parameters on the deposit's quality and porosity in Inconel 625 were also studied [271]. Variation in microhardness as a function of the layer's distance from the substrate was reported. This was mainly ascribed to variations in the melt pool's cooling rates and thermal history between deposited layers. It was suggested that one could achieve even hardness along the deposited material by controlling the cooling rates during the deposition process. Zhong et al. [296] studied the melt pool characteristics and deposit properties of as-deposited Inconel 625 and 718 using a high-speed camera. While Inconel 718 showed reduced microhardness compared to its wrought alloy's standard, Inconel 625 showed superior hardness compared to its standard requirement. Such differences in microhardness between the two alloys and their wrought counterparts were attributed to the differences in the melt pool's cooling rates. Higher cooling rates result in refined grain size and an increase in the density of grain boundaries, which resist dislocation motion during deformation, and the apparent microhardness is increased. The reduced microhardness of Inconel 718 was also ascribed to its strengthening mechanism, which is dominated mainly by precipitation hardening, unlike that of Inconel 625, which is mainly strengthened by solid solution of Nb and Mo [273]. Jinoop et al. [249] utilized DED-LB to study the deposition process and properties of defect-free Hastelloy X (NiCrMoCoW) alloy at high deposition rates (between 8.25 and 13.2 kJ/g). It was shown that, far from the deposition substrate, fine columnar dendrites grew in the direction of heat flow and across adjacent deposition layers, thus suggesting epitaxial grain growth. In contrast, such secondary dendrites were not observed close to the substrate. It was shown that the mechanical properties, such as microhardness, tensile strength, yield strength, and ductility, of as-deposited DED-LB Hastelloy X were comparable to those of either its wrought or PBF-LB counterparts.

2.7. Cobalt-based alloys

Co-based alloys exhibit high hardness, exceptional wear resistance, biocompatibility, and good corrosion resistance [301,302,309,542], but suffer from poor machinability, casting ability, and forgeability. Co-based alloys are better than Ni-based alloys in service conditions that require high resistance against hot corrosion [572] and thermal fatigue (due to their lower CTE). However, unlike Ni-based alloys, Co-based alloys are usually not strengthened by coherent precipitates. The final part requires complex geometries and complex mold preparation. This makes AM a potentially attractive alternative for manufacturing Co-based parts requiring substantial design flexibility and minimal post-processing. Applications of Co-based alloys include jet engines, petrochemical, oil and gas, load-bearing knee, dental and other implants, magnetic devices, etc. [303,308,309].

To date, relatively limited work has been carried out on DED of Co-based alloys, focusing on CoCrMo [300,301,305–308,310,575] and CoCrW [302,303,309,311,312] alloys. The properties of CoCrMo alloys are controlled by the applied heat treatment and the presence, size, and distribution of carbide precipitates [301,576]. The effect of heat treatment and processing parameters of DED-LB-processed CoCrMo alloy was studied using the design of experiments (DOE) approach [300,695]. The group has shown that the aging time has the most predominant effect on

microhardness. DED-LB CoCrMo had uniform microhardness comparable to the wrought alloy in the as-deposited state. However, heat treatment (see Ref. [300] for heat-treatment specifications) showed non-uniform surface microhardness, although the hardness was higher than in the non-heat-treated condition. Mallik et al. [301,575] reported the effects of deposition conditions and heat treatment on the corrosion resistance of DED-LB CoCrMo alloy. Corrosion appeared mainly at grain boundaries due to carbide precipitation and a local decrease in Cr concentration. The effect of heat treatment was also studied [300]. It was shown that both solution and aging treatments had no significant effect on the measured grain size. It was reported that by increasing the duration of the solution heat treatment, one could reduce the concentration of precipitates, as it allowed more time for carbides to dissolve in the cobalt matrix. In contrast, an increase in the aging duration resulted in increased carbide precipitation. This phenomenon was ascribed to the decrease in carbide solubility in the matrix. The wear resistance of DED-LB-deposited CoCrMo was also studied [308,575]. It was concluded that the as-deposited samples processed under conditions that yield finer microstructure exhibited enhanced wear resistance [575]. Ram et al. [308] reported reduced wear resistance of the as-deposited CoCrMo alloy compared to its wrought counterpart. This was mainly due to irregular, continuous interconnected carbide morphology, which provided reduced wear protection than the optimal case where the precipitated carbides are regularly shaped and uniformly distributed in the cobalt matrix. The effect of the dominant processing parameters on the microstructure and wear properties of CoCrW deposited by DED-LB was studied by Suresh et al. [311]. It was shown that carbide precipitation was mainly along dendritic grain boundaries, with two distinct morphologies and compositions – lamellar (Co-rich) and particulates (Cr-rich). Wear analysis of the as-deposited CoCrW alloy showed comparable results to its wrought counterpart. The effect of different heat treatment conditions (see Ref. [302] for heat-treatment specifications) on the microstructure and microhardness of DED-LB CoCrW alloy was also studied [302]. The microhardness highly correlated with the change in carbide's fraction, morphology, and distribution in the cobalt matrix, which were associated with the specific heat treatment.

2.8. Intermetallics

Intermetallic compounds, particularly metal aluminides such as iron, titanium, or nickel aluminides, combine high melting temperature, high strength at high temperatures, low density, and good oxidation resistance [313,318,577]. Traditionally, intermetallics are processed by casting, P/M, or hot extrusion. However, these manufacturing processes are costly and might yield brittle parts with high shrinkage and coarse microstructures, which do not allow post-processing such as cold working or subtractive processing, thus limiting their applications [313, 318, 323]. Recent studies have demonstrated the potential use of DED to fabricate high-quality intermetallics, particularly iron aluminides [313–315,318,319,321,323]. Karczewski et al. [313] studied the microstructure and mechanical properties of annealed (at 400 °C for 10 h) thin-walled parts made of FeAl with 16 wt% Al and fabricated by DED-LB. Variations in wall thickness directly affected the apparent melt pool cooling rates, resulting in distinct crystalline structures in the as-deposited material. Despite the high cooling rates, the microstructure was characterized by elongated columnar grains of the order of magnitude of several hundreds of micrometers along the build direction. This result was consistent with other studies of DED-LB of Fe-(28 at%)Al [315]. High brittleness with substantial cracking in the as-deposited material after EDM cutting was also observed. Rolink et al. [315] showed that preheating the substrate to 200 °C hinders the cracking upon rapid cooling. Other studies showed that modifying the binary Fe-Al compound by alloying elements such as (Cr, Nb, B) [319], Ti [323], (Zr, B) [314,318], and Cr [321] may result in enhanced tensile and compression strengths, microhardness, ductility, and corrosion

resistance. Nickel aluminides [291,317,320] and titanium aluminides [316,322] for high-temperature applications were also processed by DED-LB. Tlotteng [316] studied the effect of heat treatment (at 1400 °C for 2 h in argon environment) of binary DED-LB TiAl by utilizing elemental Ti and Al powder feedstock. It was shown that heat treatment strongly affected the microstructure in terms of grain size, phase, and lamellae. A strong dependence of microhardness on the grain size and type of lamellae at three distinct regions along the build direction was reported. No apparent influence of heat treatment on the microhardness was observed when compared to the as-deposited condition. Balla et al. [322] demonstrated strong effects of the DED-LB processing parameters, such as laser scan speed and applied laser power, on defects appearance, wear and corrosion characteristics of as-deposited TiAlCrNb (γ -TiAl), and defined acceptable windows for different processing parameters.

2.9. Shape memory alloys (SMAs)

SMAs are metallic materials that undergo solid-to-solid phase transformations [327,547], which are induced by proper temperature or stress changes and during which they can recover permanent strains. Such alloys include, among others, NiTi, NiTiCu, and CuAlNi. SMAs benefit from a combination of shape memory effect (SME), superelasticity, high strength, high fatigue resistance, and good damping properties [547]. The advantages derived from the unique properties of SMAs, which ordinary metals do not display, have resulted in many applications such as medical devices (e.g., cardiovascular, dental, and orthopedic devices as well as surgical tools), aerospace, automotive, construction, robotics, telecommunication, optics, vibration-dampers, release or deployment mechanisms, etc. [326,334,349,547,578–581]. To date, NiTi (Nitinol), at a near Ni/Ti equiatomic ratio, is considered the most used SMA due to its unique combination of functional properties, which allow it to recover relatively large strains (up to 8% [582]) by either heat activation or unloading [326].

Although the applicability of SMAs is promising in a broad aspect of industries, it is still considered in its infancy as several critical aspects are yet to be addressed [578]. Traditional NiTi manufacturing processes such as casting and P/M are common practices but are still considered challenging due to the high reactivity of Ti, its poor machinability, and the high levels of impurities associated with such process [330,338,583,584]. DED has therefore been studied as a potential manufacturing process, which allows the fabrication of near-net-shape NiTi parts from either a mixture of pure Ni and Ti powders [325,327,329,331,334–336,338,347,352,353] or pre-alloyed NiTi [324,326–328,333,334,337,338,348–352,585] with a pre-defined Ti-to-Ni ratio. The functional properties of NiTi are susceptible to composition, grain size, phase fraction, and impurities (such as oxygen and carbon) [330]. Among others, such impurities may form due to the high reactivity of Ti with oxygen at high temperatures, which might result in the formation of undesired secondary phases, and consequently – variations in the phase transformation temperatures and degradation in functional characteristics, including mechanical properties [336,337,348,579]. Lee and Shin [334] studied the chemical composition of as-deposited NiTi on the microstructure, transformation temperatures, and mechanical properties. The desired final chemical composition was controlled by varying the powder ratios during deposition. It was shown that the as-deposited alloy contained less than 10% of Ti₂Ni secondary phase (i.e., considerably less than following conventional manufacturing techniques [334]). All Ni-rich samples showed austenite and martensite phases at room temperature, while the near-equiatomic material contained only the martensite phase. The variations in the chemical composition of the Ni-rich as-deposited NiTi samples had little effect on the mechanical properties under compression. Pure-element powders were suggested as better powder feedstock than pre-alloyed powder because it is easier to control the chemical composition of the as-deposited material and is more cost-effective [334]. However, the use of elemental powder feedstock might result in heterogeneous microstructures that require heat

treatment to achieve microstructural homogenization [327,334].

Wang et al. [335] performed a comparative study using an elemental mixture of Ni and Ti powders in equiatomic ratio and three different AM techniques: DED, PBF-LB, and PBF-EB. It was concluded that the printability of near-net-shaped NiTi alloy using elemental Ni and Ti powders via PBF-LB and PBF-EB is not sustainable due to a strong exothermic reaction between the Ni and Ti constituents, which results in microstructural inhomogeneity, keyhole, and LoF defects. However, DED-LB successfully deposited dense NiTi samples with a good fusion between adjacent deposited layers and proper phase transformation (Fig. 10a). A high amount of unwanted Ti₂Ni brittle intermetallic phases was formed during solidification (Fig. 10a), and Ni evaporation, altering the final alloy chemical composition, was observed. The formation of unwanted secondary phases and the slight Ni evaporation during laser-based deposition of NiTi have been reported elsewhere too [325,347,352,353,586]; this commonly happens near the substrate or in between deposition layers [347,353]. Various research groups studied the effect of the DED processing parameters on the chemical composition, microstructure, physical, mechanical, and functional properties of near-net-shape NiTi [324,327,328,330,331,333–338,350–352,585]. Kumar et al. [337] reported that the microstructure, phase transformation characteristics, density, and mechanical properties of as-deposited NiTi depended on the applied energy density. It was shown that while increasing the laser energy density (by changing the laser power) reduced the as-deposited NiTi porosity, a small amount of Ti₂Ni precipitates and martensite phase were formed at the highest laser energy density. The increase in laser energy density resulted in higher hardness while presenting reduced elastic and pseudoelastic recovery properties. The increase in laser energy density shifted the transformation temperatures of the as-deposited NiTi to higher values. This phenomenon was attributed to the elemental evaporation of Ni at high energy densities, which resulted in a higher concentration of Ti, thus increasing the transformation temperatures [336,337]. Baran and Polanski [330] supported the importance of the applied energy density on the microstructure and transformation temperatures of as-deposited NiTi. In that study, the applied energy density was varied by changing the laser scan speed (between 1 and 30 mm/s). The laser scan speed significantly affected the microstructure of the as-deposited NiTi and the formation of unwanted secondary phases. The grain structure changed its morphology from columnar to equiaxed at lower scan rates. However, no clear trend was observed at lower scan rates in terms of the effect of laser scan speed and the transformation temperatures. In contrast, the transformation temperatures were characterized by a constant value at higher laser scan rates, regardless of the increase in scan rate (Fig. 10b).

Post-processing heat treatment was reported as an additional means for controlling the microstructure, phase transformation characteristics, functional and mechanical properties of DED NiTi [325,326,334–336,347–349,352,353]. The presence of unwanted secondary phases such as NiTi₂ and Ni₃Ti was reported to modify the chemical composition of the as-deposited NiTi alloy and inhibit the SME [348]. Thus, it is common to perform a solid-solution heat treatment within the range of 800 to 1050 °C as a means for achieving increased microstructural homogeneity and reducing residual stresses and microstructural defects in the as-deposited NiTi [336,348,352,579]. Subsequent aging heat treatment is then done at lower temperatures (300–700 °C) to enhance the mechanical properties by the formation of uniform Ni-rich precipitates (Ni₄Ti₃ and Ni₃Ti) within the NiTi matrix [347,587]. Hamilton et al. [347] studied the effect of different heat treatments of DED-LB Ni-rich Ni53.0Ti47.0 (at%) on the microstructural and superelastic compression responses. For this purpose, four thermal conditions of the same NiTi composition were characterized: (1) as-deposited, (2) solution heat-treated (950 °C for 10–24 h), (3) directly aged (550 °C for 3 h), (4) solution heat treated and aged (950 °C for 10–24 h + 550 °C for 3 h). It was shown that in both the as-deposited condition and the 10 h-solution heat-treated condition, Ni₄Ti₃ and Ni₃Ti secondary phases were

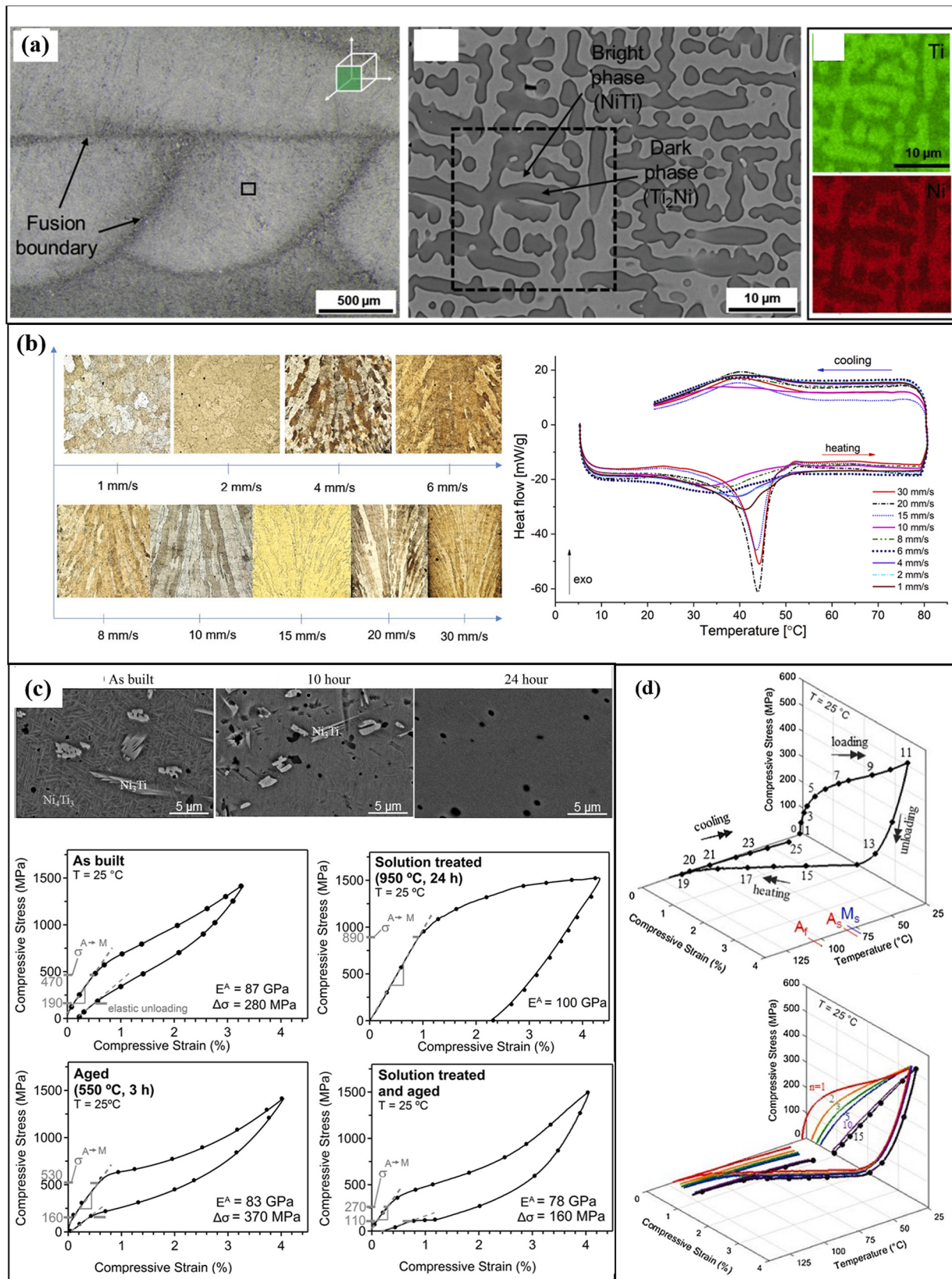


Fig. 10. (a) As-deposited NiTi shows adjacent fusion boundaries, typical microstructures, and corresponding energy-dispersive X-ray spectroscopy (EDS) mapping. Reprinted from Ref. [335], with permission from Elsevier. (b) The influence of applied laser scan speed on the microstructure and transformation temperatures of DED-LB NiTi after the annealing process at 600 °C. Reprinted from Ref. [330], with permission from Elsevier. (c) The effect of the applied thermal treatment on the microstructure and the compressive stress-strain response of DED-LB NiTi. Reprinted from Ref. [347], with permission from Elsevier. (d) Single- and multi-cycle compression stress-strain-temperature curves of DED-LB NiTi. Reprinted from Ref. [327], with permission from Elsevier.

observed. Increasing the solution heat treatment time to 24 h resulted in the full dissolution of these secondary phases and homogenous microstructure (Fig. 10c), leaving the martensitic B19' and R-phases along with austenitic B2 phase predominant. These results agree with the earlier study of the same research group [353]. Chemical composition anisotropy was observed in the as-deposited NiTi along the build direction. This phenomenon was attributed to elemental segregation upon material solidification. The chemical composition anisotropy reduced as the solution heat treatment time increased and upon material homogenization. The group also studied, by a compression test, the superelastic properties in all studied conditions. It was shown that the directly aged sample had a complete strain recovery after compressive load unloading, contrary to the other conditions that exhibited different degrees of residual strains (Fig. 10c). These results are consistent with previous work [353]. Hamilton et al. [327] investigated the SME recovery of DED-LB NiTi. The stress-strain-temperature response showed hardening slope when the critical stress was exceeded, with incomplete strain recovery upon unloading and subsequent heating (Fig. 10d). This was ascribed to the fact that the martensitic phase was permanently deformed beyond the critical stress, not allowing the full strain recovery of the as-deposited NiTi [327]. However, when the applied load did not exceed the critical stress, full recovery of the residual strain was observed (around 3% macroscale strain recovery, see Fig. 10d). The group also performed cyclic stress-strain-temperature experiments (up to 15 cycles). It was shown that the critical stress decreased after the application of five cycles, showing a non-distinguishable transition between elastic linear to nonlinear response, along with the reduction of the elastic modulus from 60 to 10 GPa. No substantial variation in the cyclic response was observed between 10 and 15 cycles, presenting around 2% macro-scale strain recovery (Fig. 10d).

The utilization of DED to fabricate SMAs is not limited to NiTi. In recent years, magnetic SMAs such as Heusler NiMnGa [339,341,342] and CoNiGa [340] have attracted increasing interest due to their ferromagnetic and high-temperature SME [339,341,588]. Such alloys were reported to sustain up to 10% reversible plastic strains upon applying an external magnetic field [588,589], and show promising properties useful in actuators, energy harvesting devices, sensors in biomedical and aerospace applications [341,342,590,591]. However, these alloys are brittle and have poor machinability, making them hard to form and shape [341,589].

Lauhoff et al. [68] successfully utilized DED-LB to deposit crack-free Co49Ni21Ga30 high-temperature SMA. The microstructure of the as-deposited material was characterized by epitaxial growth of columnar grains across adjacent deposition layers along the build direction. The columnar grain growth resulted in a strong microstructural anisotropy. Such microstructural anisotropy enhanced the shape memory and superelastic properties by minimizing grain constraints [340, 592]. A superelastic compressive strain recovery of up to 5.5% was measured for the as-deposited material, with high cyclic reversibility [340].

2.10. High-entropy alloys (HEAs)

HEAs represent a relatively novel alloy design concept introduced in the last decade [593]. Such a design concept involves several alloying elements, usually five or more, in equimolar or near-equimolar ratios [593,594]. It results in a significantly expanded range of alloy design combinations compared to the conventional alloy design concept based on a mixture of one or two main alloying elements with minor additions of specific elements to enhance certain properties [595]. As a result of the multi-compositional alloy design, HEAs offer a distinct combination of properties such as high strength, hardness and fracture toughness, superior wear resistance, good corrosion resistance, and high thermal resistance [593–596].

The combination of the inherent advantages of DED with the superior properties of HEAs has attracted increased interest from various

industries. To date, only limited DED HEA studies have been reported, e.g., ZrTiVCrFeNi [355], TiZrNbMoV [355,374,597], CrMnFeCoNi [356, 358,369,598], LaNiFeVMn [373], AlCoCrCuFeSi_{0.5} [370], CoCrBFeNiSi [599,600], NiCrCoTiV [601], AlCoCrFeNiTi_{0.5} [602], and FeCoCrNiAlB_x [603]. Among the studied HEAs, the equiatomic CrMnFeCoNi alloy has attracted special interest due to its remarkable properties, such as exceptional ductility and high fracture toughness, especially in cryogenic environments [359–361,364,365,596,604]. Guan et al. [354] studied the microstructure and tensile properties of DED-LB CrMnFeCoNi. The microstructure of the as-deposited HEA was characterized by columnar epitaxial grain growth consisting of fine grains of solid-solution FCC phase with an average size of 13 μm along the maximal heat flux direction Fig. 11a. The residual stresses in DED-LB CrMnFeCoNi were measured as ~182 MPa. These high residual stresses were associated with the high dislocation density in the as-deposited HEA. Fig. 11b [360] shows heterogeneous strain distribution with increased tensile strains, where strain concentrations appear mainly at the slip band regions and between slip bands with different grain orientations. It was shown that both transgranular and intergranular cracks are formed at the maximal strain concentration regions.

In a recent study [361], laser shock peening post-treatment was utilized to enhance the tensile properties of DED-LB CrMnFeCoNi alloy. The surface roughness increased because of the increase in shock peening cycles. Interestingly, the shock peening treatment generated sufficient plastic deformation on the surface of the deposited material to effectively enclose pores close to the surface, Fig. 11d. (Al_xCoCrFe)₅₀Ni HEAs with varied Al concentrations (0–16.7 at%) were DED-LB to study the effect of Al concentration on the microstructure and microhardness of the as-processed alloy [363]. An increase in Al concentration resulted in microstructure transformation from FCC single-phase cellular dendritic to lamellar eutectic with L12 nanoprecipitation within a matrix consisting of a mixture of FCC and BCC stable phases (Fig. 11e). The observed nano-precipitation strengthening effect due to the increase in Al concentration substantially increased the microhardness of the as-deposited (Al_xCoCrFe)₅₀Ni HEA, from 132 to 342 VHN.

One of the most comprehensively studied DED HEAs is Al_xCoCrFeNi [357,366,368,371,372,605] due to its unique combination of properties and to the low cost of its elemental constituents [357]. Kunce et al. [366] reported an increase of approximately 13% in the microhardness of DED-LB AlCoCrFeNi alloy compared to its as-cast counterpart due to increased melt pool cooling rate and the increased temperature, resulting in refined grain size. Wang et al. [357] employed atom probe tomography (APT) and observed severe segregation of Ni, Al, and Cr, while Fe and Co were homogeneously dispersed in DED-LB AlCoCrFeNi (Fig. 11c). In addition, reduced corrosion and pitting potential were measured for DED-LB AlCoCrFeNi alloy compared to 304L SS. Chao et al. [605] studied the microstructure of Al_xCoCrFeNi ($x = 0.3, 0.6, \text{ or } 0.85$). It was shown that an increase in the Al concentration in the as-deposited HEA resulted in tailored crystal structure transformation from FCC solid solution to a duplex FCC + BCC and BCC solid solutions. Joseph et al. [371] studied the deformation mechanisms of three distinct crystal structures of Al_xCoCrFeNi ($x = 0.3, 0.6, \text{ or } 0.85$). The alloy with $x = 0.85$ aluminum showed superior yield strength but limited plastic deformation in tension compared to the other two alloys with lower Al concentrations. In contrast, the latter two alloys exhibited relatively low tensile strength and higher ductility [371]. A comparative study between DED-LB and DED-arc Al_xCoCrFeNi ($x = 0.3, 0.6, \text{ or } 0.85$) HEAs yielded similar mechanical properties for both fabrication methods [372].

2.11. Ceramics

Ceramics typically combine excellent resistance to corrosion and oxidation, high melting temperature and creep resistance, high rigidity, low diffusivity, high electrical resistance, low CTE, high compression strength, excellent specific strength, superior hardness, and wear

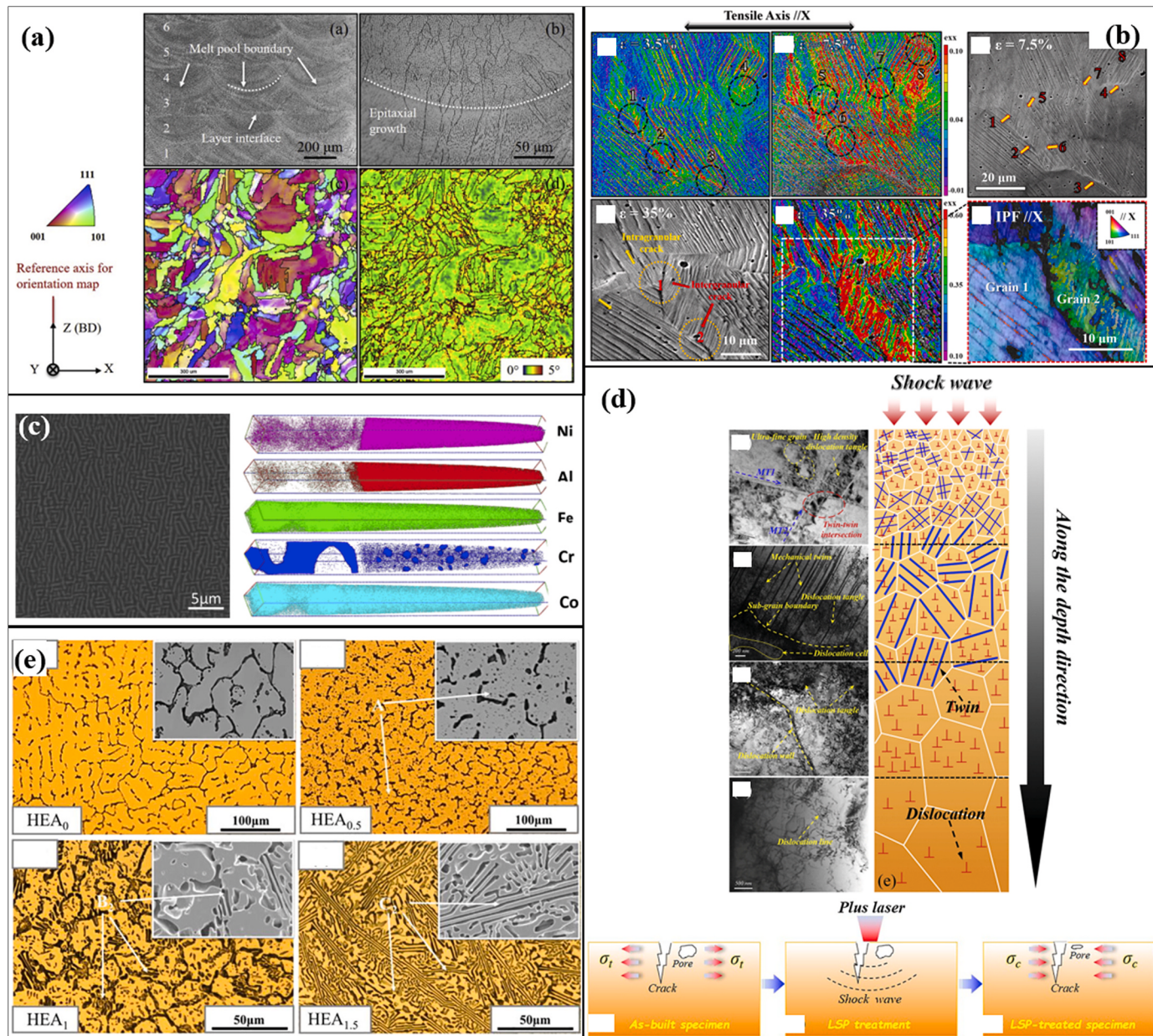


Fig. 11. (a) The microstructure of as-processed CrMnFeCoNi HEA, showing layer-by-layer morphology with epitaxial grain growth. Reprinted from Ref. [354], with permission from Elsevier. (b) High-resolution DIC combined with backscatter electrons (BSE) and EBSD analysis of DED-LB FeCoCrNiMn HEA at increased discrete strains (3.5%, 7.5%, and 35%). Reprinted from Ref. [360], with permission from Elsevier. (c) Microstructure of DED-LB AlCoCrFeNi HEA after aging at 600 °C for 168 h, with the corresponding APT images showing heterogeneous scattering and severe segregation of Al, Ni, and Cr. Reprinted from Ref. [357], with permission from Elsevier. (d) Transmission electron microscopy (TEM) images with the corresponding schematic illustrations showing the effect of laser shock peening treatment on the microstructure along the z-direction of as-deposited CrMnFeCoNi HEA. Reprinted from Ref. [361], with permission from Elsevier. (e) The microstructure of DED-LB (Al_xCoCrFe)₅₀Ni HEAs with varied Al concentrations (0, 6.5, 13.7, and 16.7 at%). Reprinted from Ref. [363], with permission from Elsevier.

resistance. Consequently, they are in high demand in various applications, such as construction, petrochemical, aerospace, and medical devices [542,543]. However, they suffer from poor ductility, low impact resistance, low fracture toughness, limited tensile strength, lack of strain hardening, statistically wide distribution of mechanical properties, and limited manufacturability (poor castability, machinability, plastic formability, non-weldability, and hard to join by fasteners). Consequently, direct fabrication of complex ceramic parts and their processing are highly challenging and often costly [377,379,606,607].

The introduction of AM techniques suitable for processing and manufacturing ceramic parts opened an avenue for fabricating ceramic parts that have been challenging or even impossible using traditional manufacturing processes [379]. Nevertheless, most such AM techniques

are indirect AM processes that use binder materials or plasticizers to form a green part, followed by a sintering process for binder removal and final part densification [608]. Due to residual binder material, these commonly result in high-porosity parts, high crack density, and large organic or inorganic impurities [379]. In contrast, direct AM techniques, such as DED and SLM, show promising results for high purity and functional properties [380,398,406,407,411]. To date, only a limited number of DED ceramics have been reported (see references in Table 1). Balla et al. [398] demonstrated the first-ever direct fabrication of alumina using DED-LB. The as-deposited structures showed strong anisotropy in mechanical properties in directions parallel and perpendicular to the build direction. However, heat treatment at 1000 and 1600 °C for 5 h in air reduced this anisotropy due to sintering effects.

The microstructure was characterized by columnar grain growth parallel to the build direction [398]. Balla et al. [398] also reported that the high cooling rates associated with the DED-LB process resulted in as-deposited Al_2O_3 comprised of thermodynamically stable α - Al_2O_3 phase, without any presence of metastable alumina phases such as γ - Al_2O_3 . Later, Li et al. [379] studied the effect of the DED-LB processing parameters such as input laser power, laser scan speed, and PMFR on alumina quality. It was concluded that the increase in the input laser power had a positive effect on the geometrical properties of the deposit, powder catchment efficiency, surface roughness, flatness, and microhardness. The increase in laser scan speed, however, resulted in opposite effects.

In general, ceramic materials are highly prone to cracking due to their lack of ductility. Therefore, the inherent characteristics of laser-based deposition processes, such as the high cooling rates, high thermal gradient, and high thermal stress, make the deposition of ceramic materials highly challenging. Niu et al. [411] performed a process optimization study on DED-LB Al_2O_3 for effective crack suppression. It was shown that the temperature gradient between two adjacent layers had the most detrimental effect on the crack formation following DED. It was also shown that by increasing the laser scan speed, the resultant thermal stress decreased while the fracture strength increased, consequently resulting in a crack-free deposition. Preheating the substrate was an additional means for effective crack suppression in DED of ceramic-based materials [609]. The preheating process reduced the thermal gradient, resulting in reduced residual stresses and, consequently, reduced cracking in the as-deposited material [248].

Niu et al. [407] utilized DED-LB and studied the effect of second-phase doping of Y_2O_3 in high-purity Al_2O_3 to form an Al_2O_3 -YAG eutectic ceramic. It was shown that the applied laser power strongly affected the geometrical characteristics, such as thickness and height, of the as-deposited ceramic thin wall. Furthermore, it was shown that the as-deposited eutectic ceramic had 98.6% relative density and exhibited comparable microhardness and fracture toughness to those of the counterpart material processed by traditional techniques. Al_2O_3 - ZrO_2 eutectic ceramic is an additional ceramic material that has attracted increased interest in recent years [377,381,387,393,395,406, 408–410], primarily due to its superior thermomechanical properties, which are vital for ultrahigh temperature applications [409]. Yan et al. [393] studied the influence of processing parameters (laser power, laser scan speed, and PMFR) on the density of Al_2O_3 - ZrO_2 . Optimal process parameters yielded a ceramic with minimal porosity of 0.22%. The effect of doping DED-LB Al_2O_3 with ZrO_2 [392,394,406] and Y_2O_3 [406] was studied. Compared to the as-deposited Al_2O_3 sample, which contained numerous vertical cracks due to the thermal stresses developed during deposition, the Al_2O_3 - ZrO_2 and Al_2O_3 - Y_2O_3 samples exhibited less cracking [392,394,406], e.g., with the increase in ZrO_2 concentration [392,394]. It was indicated that the introduction of the second phase resulted in a refined eutectic microstructure with no clear grain growth orientation and with a minimal adverse effect on the microhardness [406]. A unique integration between the LENST™ deposition technique and ultrasonic vibration was applied to deposit Al_2O_3 - ZrO_2 ceramics [377,381,393,409,410]. It was reported that the ultrasonic-assisted LENST™ process resulted in a refined microstructure (Fig. 12c), including a reduction in eutectic spacing (~ 50 nm [393]) and no clear grain boundaries (Fig. 12a). Increased fracture toughness [377, 381] and microhardness [381] were also observed (Fig. 12d).

In recent studies, Pappas et al. [397,399–401] studied DED-LB transparent MgAl_2O_4 spinel ceramics (Fig. 12b). The effects of feedstock powder diameter and applied processing parameters, such as laser power, laser scan speed, and PMFR, on the porosity [399,400], crack length [399], optical properties [397,400,401], and mechanical properties [399], were studied. It was shown that the transmittance of the DED-LB MgAl_2O_4 is mainly influenced by crack density and porosity. The spinel ceramic exhibited a transmittance of up to 82% (at a wavelength of 632.8 nm), planar porosity of 0.2%, hardness (~ 1400 VHN),

and fracture toughness comparable MgAl_2O_4 spinel ceramics produced via conventional sintering processes.

2.12. Composites

The unique ability of DED to utilize a controlled multi-feed powder hopper gives rise to the design and fabrication of novel multi-material systems and engineering components with enhanced properties. Such an attribute allows one to deposit particle-reinforced metal matrix composites (MMCs) with a controlled distribution within the deposited matrix by adjusting the PMFR of the powders introduced to the melt pool [610]. Alternatively, a predetermined mixture of powders can be deposited using a single hopper. This capability results in an increased degree of freedom in designing and fabricating multi-material systems compared to the PBF AM technique, where the powder feedstock or mixture of powders is predetermined and statically placed in a designated vessel. Therefore, over the last years, extensive research has been done to design, fabricate, and characterize DED composite materials with enhanced properties. Such composite materials are designed to have increased strength and stiffness, enhanced wear resistance, and improved thermal properties such as CTE [416,556]. However, the physical, optical, and thermal properties mismatch between the matrix and the reinforcing particulates results in complex interactions and behavior upon the melting and solidification cycles associated with the laser-based DED technique. These play a significant role in achieving high-performance composite materials with high relative densities and good interfacial bonding. Moreover, most reinforcing powders are ceramic-based and are characterized by low density. This results in difficulties in controlling the PMFR during the deposition process. Thus, it is challenging to design a reproducible and optimized deposition process.

Various DED composite systems have been studied, mainly focused on Ti-based MMCs [414–419,426,427,429,434]. Due to the low solubility of boron and carbon in the α and β phases of Ti-based alloys, TiC and TiB are considered suitable particulates for reinforcing the Ti matrix [611]. The introduction of TiB and TiC as reinforcement in Ti-based MMCs results in increased mechanical properties, such as hardness, strength, and wear resistance, and increased thermodynamic stability of the reinforcement particulates in the Ti matrix [556]. Wang et al. [419] studied the effect of the volume fraction of TiC particulates in Ti6Al4V alloy on the microstructure and tensile properties. The effect of subsequent heat treatment (see Ref. [419] for heat-treatment specifications) on the DED-LB MMC was also demonstrated (Fig. 13a). The microstructure of the MMC consisted of a combination of α -Ti and β -Ti phases with primary and eutectic phases of resolidified TiC along with unmelted TiC particles (Fig. 13a). A similar microstructure was also reported by others [416–418,445]. TiC at 5% volume fraction exhibited optimal tensile properties compared to Ti6Al4V base alloy (Fig. 13a). In a related study, Liu et al. [418] studied the melting of the TiC particulates in Ti6Al4V by varying the applied laser energy density at different TiC volume fractions (0–15%). Applying lower energy densities, the least melting of TiC was observed, with a reduced formation of detrimental primary dendritic TiC grains. At low energy densities, the macrostructure of the deposited MMC was characterized by high relative density, defect-free structure, and uniform distribution of the unmelted TiC. It was concluded that the unmelted TiC and solid-solution strengthening by carbon were the primary strengthening mechanisms of the MMC system.

The failure mechanisms, mechanical and physical properties of the deposited MMC are governed by the strength of the interfacial bonding between the particulates and the matrix. To address this issue, several studies [412,416] have successfully deposited Ni-coated TiC reinforcement particulates, which resulted in an enhanced interfacial bonding and considerably increased MMC strength. However, the formation of TiNi intermetallic compounds resulted in a decrease in ductility. Ti-based MMCs reinforced with TiB are also of high interest and have

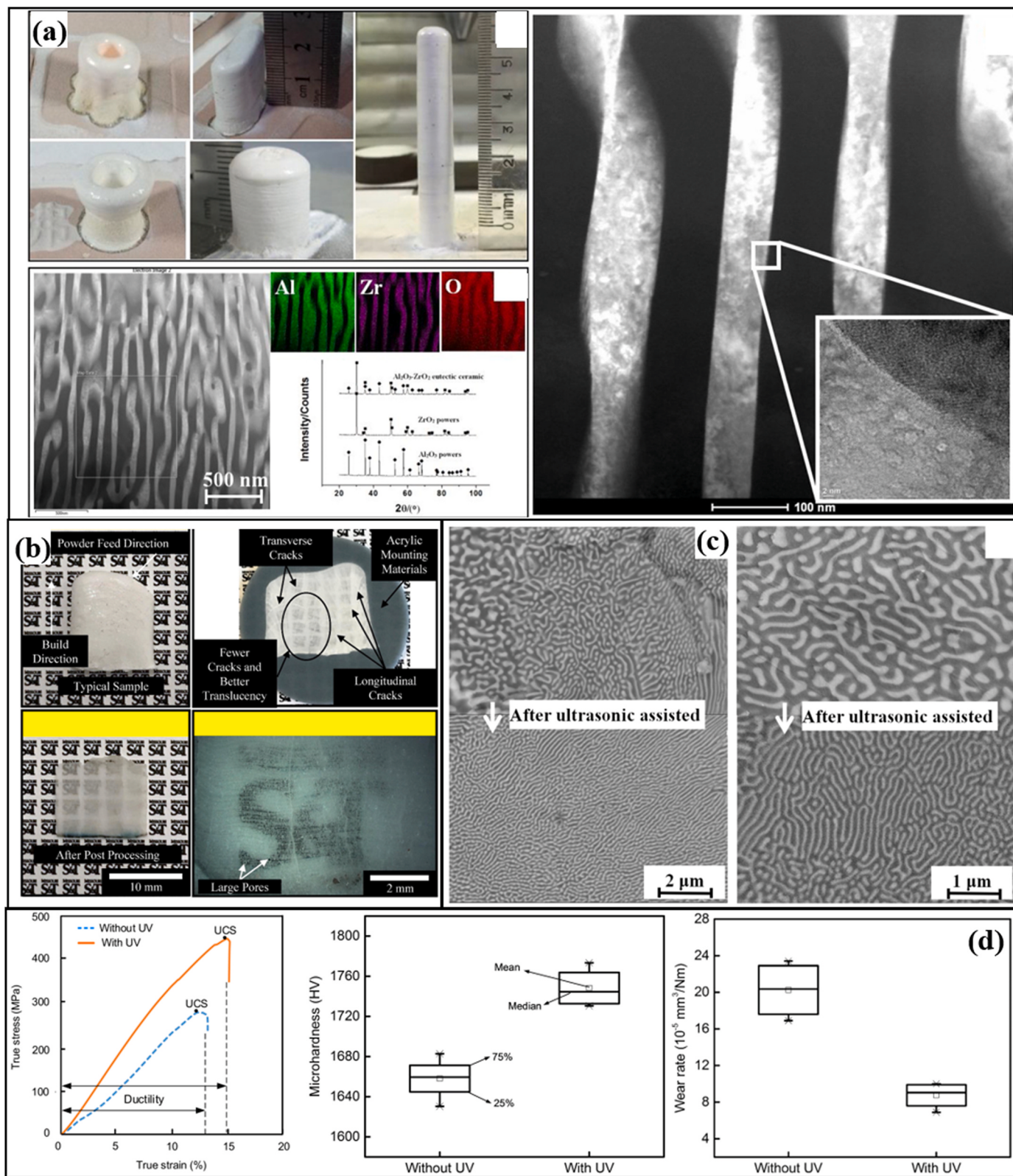


Fig. 12. (a) Ultrasonic-assisted DED-LB Al_2O_3 - ZrO_2 eutectic ceramic showing eutectic spacing at the nano-scale and high density. Reprinted from Ref. [393], with permission from Elsevier. (b) Macrostructure of DED-LB magnesium aluminate (MgAl_2O_4) spinel transparent ceramics before and after post-processing, revealing both transverse and longitudinal cracks. Reprinted from Ref. [401], with permission from Elsevier. Microstructure (c) and mechanical properties (d) of DED-LB Al_2O_3 - ZrO_2 eutectic ceramic, with and without utilizing ultrasonic vibration. UV = ultrasonic vibration. Reprinted from Refs. [377,381], with permission from Elsevier.

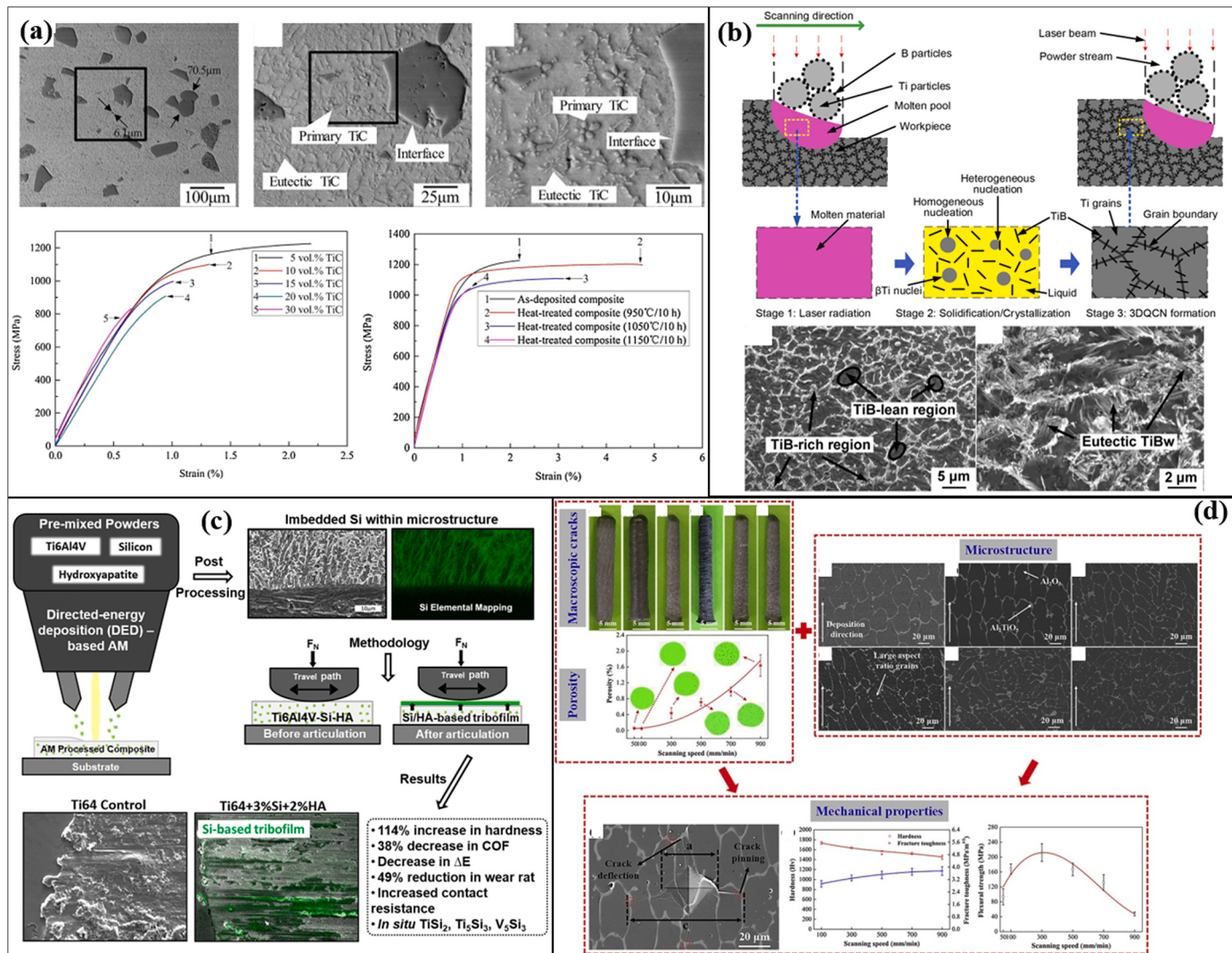


Fig. 13. (a) The microstructure of as-deposited Ti6Al4V-based MMC with 10 vol% TiC and stress-strain curves show the effect of TiC volume fraction and various thermal treatments on the tensile properties of the MMC. Reprinted from Ref. [419], with permission from Elsevier. (b) The microstructure of DED TiB-reinforced CP-Ti MMC with a schematic illustration of the formation mechanism of quasi-continuous network microstructure. Reprinted from Refs. [426,427], respectively, with permission from Elsevier. (c) DED-LB Ti6Al4V-Si-HAp MMC shows enhanced hardness, wear resistance, and bio-tribocorrosion properties promoted by forming Ti_3Si_3 , V_5Si_3 , and Ti_2Si_2 phases. Reprinted from Ref. [448], with permission from Elsevier. (d) The influence of applied laser scan speed on the microstructure, hardness, flexural strength, and porosity of alumina/aluminum titanate CMC fabricated using DED-LB. Reprinted from Ref. [449], with permission from Elsevier.

been successfully DED-LB. Hu et al. [426,427,429] studied the effect of the laser-based deposition process of CP-Ti/TiB powders on the microstructure evolution and mechanical properties. The composite powders were prepared via ball milling, which yielded boron (1.6 wt%) covering the surface of the CP-Ti powder (98.4 wt%). The microstructure of the as-deposited MMC revealed a unique ultrafine 3D quasi-continuous network of TiB aggregates at the Ti grain boundaries (Fig. 13b). The formation of nano-sized eutectic TiB microstructure depended on the applied laser power and provided better mechanical properties, such as hardness and tensile properties, compared to the as-deposited CP-Ti. Apart from TiC and TiB, SiC has also been used as a reinforcement in titanium matrix via DED-LB, both as bulk structures and as coatings, to improve the mechanical properties and wear resistance [612,613].

Several recent studies have focused on the DED of particulate-reinforced steel-based MMCs. Wang et al. [466] studied the effect of additions of various concentrations of Cr_3C_2 reinforcing particulates in 316L SS matrix produced via DED-LB on the microstructure evolution and mechanical properties such as microhardness and wear resistance. The monolithic DED-LB 316L steel was characterized by columnar grain growth along the build direction, with dendritic and interdendritic

structures, a low amount of equiaxed grains, and no apparent defects. As the concentration of Cr_3C_2 increased (to 5% and 15%), the dissolution of Cr_3C_2 promoted fine equiaxed and dendritic grains. When the concentration of Cr_3C_2 was further increased to 25%, a non-uniform fine interdendritic microstructure was formed, with non-uniform distribution of hexagonal precipitated carbides (Fig. 13b). The increase in the concentration of Cr_3C_2 was beneficial for the microhardness and wear resistance properties, governed by solid-solution strengthening and grain refinement strengthening mechanisms. A DED-LB TiC-reinforced CrMnFeCoNi HEA was demonstrated recently [473]. The powder feedstock was either 2.5 or 5 wt% TiC nano-size powder uniformly coated over the pre-alloyed CrMnFeCoNi powder. Epitaxial grain growth of the columnar grains parallel to the build direction was observed. Tensile measurements of the as-deposited composite revealed that the increase in TiC concentration resulted in increased yield strength and tensile strength while being harmful to the ductility of the as-deposited MMC. Fractography confirmed that the surface fracture morphology changed from a ductile fracture, characterized by deep dimples and uniform plastic deformation, in the monolithic CrMnFeCoNi to shallow dimples (at 2.5 wt% TiC) and no dimples (at 5 wt% TiC).

As mentioned in section 2.5, Al-based alloys have unique properties, making them an attractive material for AM. However, for some applications, additional enhancement of mechanical properties is required. In the case of heat-treatable alloys, applying heat treatment to enhance the mechanical properties may be sufficient for a specific application or even can be applied as an additional strengthening mechanism in particulate-reinforced MMC. Alternatively, the fabrication of Al-based MMCs can serve as an effective method for improving properties, and at times, be more cost-effective than applying heat treatments [614]. The satelliting method effectively achieved uniform distribution of reinforcing ceramic particulates in the Al-based matrix [431,438] via DED-LB. Zhao et al. [438] investigated the DED-LB of Al 5024 (AlMgScZr alloy) with varying concentrations of TiC (0, 1, 3, and 5 wt %). The effect of heat treatment (aged at 300 °C for 3, 5, and 7 h) on the mechanical properties was also studied. It was found that when compared to the as-deposited Al 5024, the addition of TiC at all studied concentrations yielded reduced or comparable microhardness, tensile strength, and yield strength. The primary strengthening mechanism was precipitation strengthening (by nanometer-sized secondary Al₃Sc particles) rather than TiC particulate strengthening. However, in another study on DED-LB of Al-based MMC, Tan et al. [431] reported beneficial attributes of additions of TiB₂ reinforcement particulates in AlSi10Mg alloy. Among others, the addition of micro/nano TiB₂ particulates to the Al-based matrix resulted in increased strength and microhardness.

DED MMC-based protective coatings also attract increased interest due to desired properties such as exceptional hardness, wear, and corrosion resistance. Recent studies utilized DED-LB for the processing of ceramic matrix composites (CMCs) [421,449,451,615]. Huang et al. [449] successfully deposited dense (up to 99.95%) alumina/aluminum titanate (Al₂O₃/Al_xTi_yO_z) CMC by pre-mixing of Al₂O₃ and TiO₂ powders to enhance the hardness, flexural strength, and fracture toughness (up to 1640 VHN, 212 MPa, and 3.75 MPam^{1/2}, respectively) of the alumina matrix (Fig. 13d). Over recent years, various combinations of DED-LB MMC protective coatings were studied to enhance surface mechanical properties (e.g., wear resistance and hardness [304,430,458, 460]) and corrosion resistance [448]. Avila et al. [448] utilized DED-LB to fabricate Ti6Al4V-Si-hydroxyapatite coating for articulating surfaces in load-bearing applications (Fig. 13c). To isolate the influence of Si addition on the properties of the Ti-based composite, control samples of monolithic Ti6Al4V and Ti6Al4V MMC reinforced with either 5 wt% or 10 wt% Si were also fabricated, in addition to the Ti6Al4V-(3 wt%)Si-(2 wt%) hydroxyapatite (HAp) sample. The addition of Si particles as reinforcing material resulted in the formation of titanium silicides (Ti₅Si₃ and TiSi₂) and vanadium silicides (V₅Si₃), thus promoting an increase of 114% in hardness (for the 10 wt% Si sample) and a reduction of 38.8% in the coefficient of friction for the Ti6Al4V-Si-HAp composite. Furthermore, it was shown that the formation of Ti₅Si₃, V₅Si₃, and TiSi₂ also reduced the wear rate by ~70% in the case of the 10 wt% Si material. Gualtieri et al. [430] successfully utilized DED-LB as a cladding technique to increase the surface hardness and wear resistance of 304L SS by adding either 5 wt% or 10 wt% of NbC reinforcing particulates in the steel matrix. The effect of a post-deposition laser scan with no powder feeding was also studied. It was shown that the laser scan post-treatment had beneficial attributes on the coating's density, hardness, and wear resistance. DED-LB CoCrAlSiY/YSZ composite coatings were reported recently [421]. A correlation between the applied laser energy and properties such as surface roughness, relative density, microhardness, and wear resistance of the as-deposited MMC material was established.

Finally, two case studies of processing MMCs by LENST™ are highlighted. A dual continuous immersed phase (DCIP) is defined as an MMC with two immersed bulk phases continuous in at least one direction. When the ratio of constituent materials approaches 50:50, neither phase is truly the matrix or reinforcement phase. Since DED can eliminate the need for joining, it is ideal for fabricating parts with a DCIP morphology. Policelli [467] fabricated defect-free bulk MMC samples made of

Ti6Al4V ($\alpha+\beta$ alloy) and Ti10V2Fe3Al DCIPs. The DCIP morphology attenuated epitaxial grain growth compared to bulk laser-deposited Ti6Al4V samples. Samuel et al. [461,468,469] processed by DED-LB an MMC composed of Ti35Nb7Zr5Ta matrix and 2% TiB reinforcement, consisting of an elemental mixture of Ti, Nb, Zr, Ta, and titanium diboride (TiB₂) powders. The goal was to improve wear resistance for applications such as femoral heads in hip implants. The microstructure of the MMC consisted of both eutectic boride precipitates and primary TiB precipitates dispersed in a matrix of β -Ti. A significant enhancement of the wear resistance of the boride-reinforced TiNbZrTa alloys was found compared to Ti6Al4V extra-low interstitials (ELI) alloy. Defect-free interfaces were documented between the matrix and the precipitates.

2.13. Functionally graded materials (FGMs) and multilayered materials

The concept of FGMs was first demonstrated in 1987 by a Japanese research group, which proposed a metal/ceramic thermal barrier for extreme environments and aerospace applications [616]. By definition, FGMs are composite materials that present continuous or discrete transitions in composition or microstructure, resulting in a directional or multi-directional functional variation in material properties [32,610, 617]. In addition to the FGMs' main characteristic of tailored properties, FGMs are beneficial in reducing residual stresses [32] and sharp interfaces where delamination and failure usually occurs [618]. Numerous processes were developed for the fabrication of bulk FGMs [32,619]. However, DED provides unprecedented design freedom, a combination of material properties, and a substantial reduction in production time compared to traditional FGM and multi-materials fabrication techniques [620]. DED provides all the advantages of layer-by-layer AM while also utilizing a multi-feed powder system. These allow the design and fabrication of complex part geometries and control of precise chemical composition with pre-defined functional, tailored properties at specific locations within the deposited part. Thus, DED FGMs may play a significant role in various high-impact engineering applications, such as aerospace, biomedical, marine, and automobile [619,621].

The continuous technological developments of DED give rise to an increasing interest in the design and research of novel FGM and multilayered material systems [480]. While various material systems were reported to be deposited via DED, Ti-based FGMs have attracted the most interest due to their unique combination of properties and their wide engineering applications (see section 2.4). Over the years, numerous Ti-based FGMs and multilayered materials with different

Table 2
Selected systems of Ti-based FGMs and multilayered materials.

Material	References
Ti/Ta	[622]
Ti/CoCrMo	[306]
Ti/Mo _x	[476,497,520]
Ti/V _x	[476]
Ti/W _x	[477]
Ti/Nb _x	[513]
Ti6Al4V/304L	[474]
Ti6Al4V/316L	[475,498]
Ti6Al4V/Nb/410 SS	[528]
Ti6Al4V/V _x	[480]
Ti6Al4V/TiC _x	[418,436,485]
Ti6Al4V/WC	[490]
Ti6Al4V/Mo	[491]
Ti6Al4V/Inconel 718	[494]
Ti6Al4V/Inconel 625	[504]
Ti6Al4V/Invar	[541]
Ti6Al4V/Al ₂ O ₃	[502]
Ti6Al4V/Inconel 625/316L SS	[506]
Ti6Al4V/Ti6Al4V-Mo _x /Inconel 718-Mo _x	[507]
Ti6Al4V/TNTZO ^a	[521]

^a TNTZO = Ti36Nb2Ta3Zr0.3O alloy.

constituents were processed via DED; see selected systems with references in Table 2.

Ti-based ceramic-reinforced FGMS attract increasing interest due to their unique properties and high demand in numerous potential structural applications. They offer superior properties when compared to

their monolithic components [490]. Such materials are characterized by high specific strength, good ductility, high hardness, superior wear resistance, biocompatibility, and low density [436]. Due to its thermal and chemical stability, biocompatibility, CTO, and density similar to Ti6Al4V, TiC is considered one of the most popular reinforcing materials

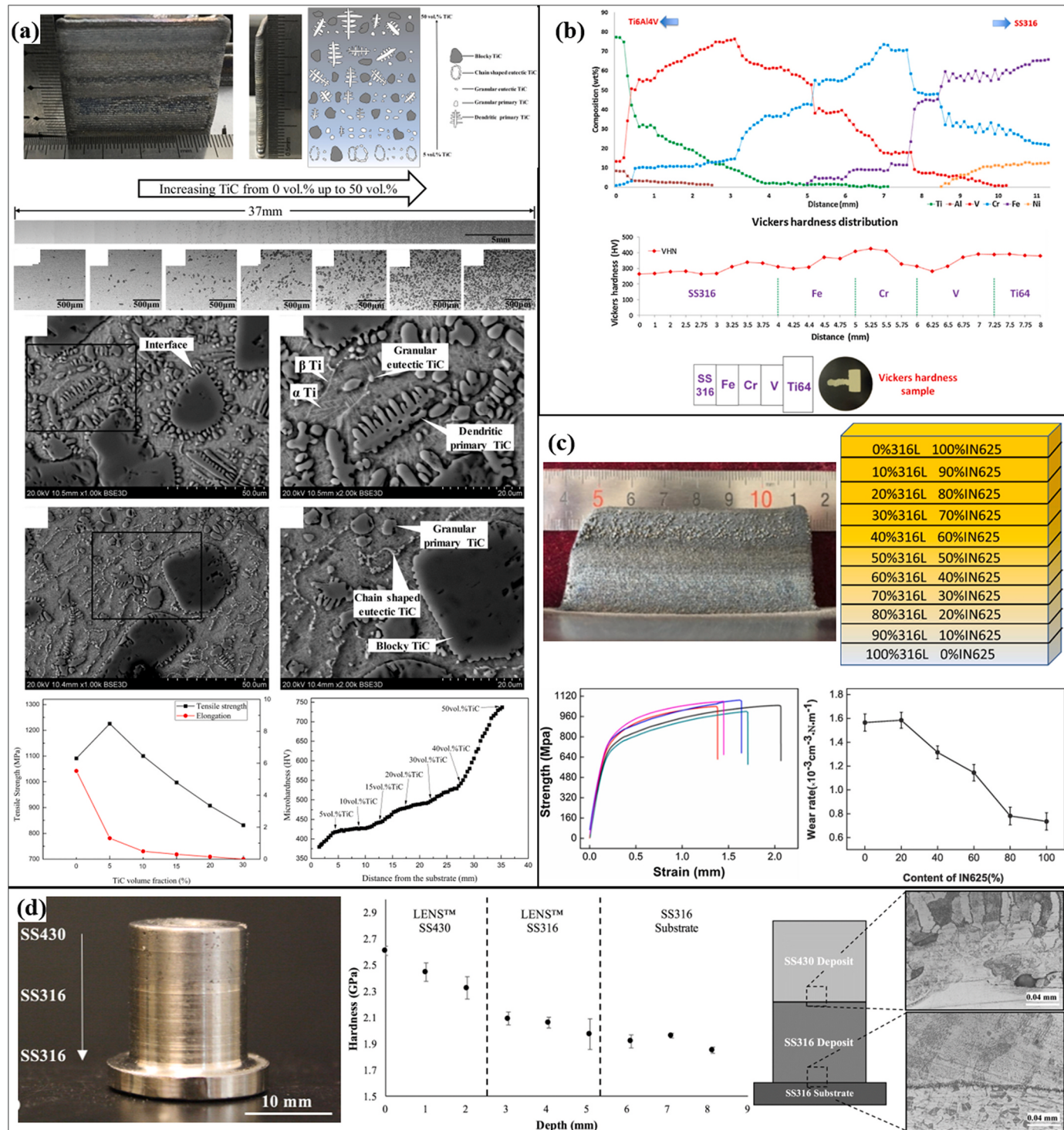


Fig. 14. (a) Microstructure and mechanical properties of DED-LB functionally graded Ti6Al4V/TiC composite with increased fraction ratio (0–50 vol%) of TiC reinforcement particles along the build direction. Reprinted from Ref. [436], with permission from Elsevier. (b) EDS line scan composition analysis and micro-hardness along the build direction in Ti6Al4V to 316 SS FGM with intermediate transition layers (V→Cr→Fe). Reprinted from Ref. [475], with permission from Elsevier. (c) Tensile and wear resistance properties of DED-LB single-wall 316L/Inconel 625 FGM. Reprinted from Ref. [514], with permission from Elsevier. (d) DED-LB austenitic (nonmagnetic) to ferritic (magnetic) stainless steels FGM with tailored magnetic functionality. Reprinted from Ref. [529], with permission from Elsevier.

when embedded in a Ti-based matrix [32,418]. To date, multiple studies utilized DED to deposit functionally graded Ti6Al4V/TiC [418,436,437, 445,485,499–501]. Li et al. [436] successfully deposited a functionally graded Ti6Al4V/TiC composite with different volume fractions (0–50 vol%) of TiC along the build direction (Fig. 14a). It was shown that the TiC particulates were homogeneously distributed in the Ti6Al4V matrix, which exhibited good bonding across deposited layers, with no observed cracks in the as-deposited FGM. In terms of the mechanical properties of the as-deposited FGM, the results revealed opposite trends between microhardness versus tensile strength and elongation with the gradual increase in TiC volume fraction in the Ti-based matrix (Fig. 14a). These results are consistent with related studies [418,437,500]. Interestingly, the measured porosity in the as-deposited FGM increased with the volume fraction of the TiC particulates. This phenomenon was attributed to the inherent rapid solidification associated with DED-LB and the inherent porosity in the TiC powder feedstock.

Ti6Al4V/metal-based alloys also show increasing interest among the FGM systems. Facilitating good metallurgical and mechanical bonding between dissimilar materials is considered a great challenge. Characteristics such as lack of interlayer metallurgical compatibility, the formation of brittle intermetallic phases, hot cracking, residual stresses, and dissimilar CTEs might lead to poor material properties or even material failure [32,474,475]. Due to the above-listed limitations, and mainly the formation of intermetallic phases such as TiCr, TiFe, and TiFe₂, the direct joining of Ti6Al4V and stainless steel is considered highly challenging [475]. Sahasrabudhe et al. [498] were the first to introduce a way to prevent the formation of unwanted intermetallic phases by introducing a diffusion barrier layer between the materials to be joined via DED-LB. NiCr was also an effective intermediate transition layer for joining Ti6Al4V to 410 SS [498]. The results indicated that incorporating NiCr as a transition layer prevented the formation of brittle intermetallic phases and reduced cracking and delamination, which arise due to residual stresses. The selection of such transition material can be based on its ability to form stable solid-solution phases with the joint materials or just act as a diffusion barrier. In the case of joining Ti and Fe, various transition layers were suggested as adequate candidates, including V, Mo, Zr, Nb, and Ta, to allow the formation of stable solid solutions with Ti and, thus, reduce the formation of unwanted intermetallic phases, consequently enhancing the mechanical properties of the joint materials [474,623]. In related work, Reichardt et al. [474] studied the microstructural and microhardness characteristics of functionally graded Ti6Al4V to 304LSS, changing the concentration of V as a transition material along the build direction. It was found that a gradual transition of V along the build direction did not prevent the formation of brittle intermetallic phases such as FeTi, which contributed to cracking during deposition. It was concluded that a few transition layers of 100% V were needed to allow the segregation of 304L SS and Ti6Al4V. A similar formation of brittle intermetallic phases was observed by Bobbio et al. [496]. Significant cracking was observed due to the brittle intermetallic σ -FeV phase in DED-LB Ti6Al4V to 304L with gradual transition vanadium interlayer. In another related work, Bobbio et al. [541] studied the DED of FGM with a gradual transition from Ti6Al4V to Invar. Formation of detrimental intermetallic phases, such as FeTi, Fe₂Ti, Ni₃Ti, and NiTi₂, due to the interaction between Ti6Al4V and Invar alloy during laser processing, was reported. To address this issue, Li et al. [475] studied the DED-LB of Ti6Al4V with 316SS by deposition of three transition layers to avoid the formation of brittle intermetallic phases (Ti6Al4V→V→Cr→Fe→316 SS). The chemical gradient composition (EDS data) of the as-deposited FGM with microhardness values along the FGM build direction are shown in Fig. 14b. It was shown that by applying such a sequence of transition layers, the formation of intermetallic phases and cracking could be prevented. Onuike et al. [528] showed the best Ti6Al4V to 410 SS gradient using Nb as a transition layer. The DED-LB structures were also machined and welded to show the stability of such transition layers. In another study [506], Inconel 625 alloy was used as a transition layer in

316L to Ti6Al4V FGM. Precipitates of Mo-enriched eutectic phase were identified as the major cause of cracking. Laser synchronous preheating made the precipitated phases of the prepared gradient materials fine and uniformly distributed, thus preventing the formation of cracks. A similar beneficial effect of synchronous laser preheating on crack elimination during DED of 316L/Inconel 625 and Inconel 625/Ti6Al4V was also reported elsewhere [504,522]. In a related study [514], the tensile properties and microhardness (up to yield strength of 822 MPa and 346 VHN, respectively, at the region of equal content of 50% between 316L and Inconel 625) of a DED-LB single-wall 316L/Inconel 625 FGM was reported (Fig. 14c). The wear properties along the single-wall graded material were also reported, showing an increase in the wear resistance with the increase in the Inconel 625 relative content (Fig. 14c). Previous studies [476,491,497,507,520] have also demonstrated the feasibility of DED to deposit FGM with tailored composition, from Ti or Ti6Al4V to Mo, for biomedical applications. The gradual transition in chemical composition from Ti and Ti6Al4V allowed adjusting the Young's modulus of the implant material (106–108 GPa for Ti6Al4V) to that of bone (10–30 GPa) as a measure of prevention of stress shielding and osteoporosis associated with modulus mismatch [491]. In related work, Lima et al. [486] successfully deposited compositionally graded Ti35Nb15Zr→Ti25Nb8Zr→CP-Ti→Ti25Nb8Zr→Ti35Nb15Zr for application as fracture fixation plate. The mechanical properties revealed that the Young's modulus was consistent with composition. However, microhardness revealed substantial variation between the Ti35Nb15Zr alloy deposited on the substrate and the top Ti25Nb8Zr region. This change in microhardness was attributed to variations in thermal history between the two regions, resulting in microstructural differences, and thus microhardness.

The development of new combinations of FGMs is not limited to tailoring mechanical properties such as microhardness, tensile properties, and wear properties for structural applications. The ability to tailor other functional properties, such as thermal, electrical, or magnetic, to predefined locations is also of great interest. In a related study [529], DED-LB was successfully utilized to directly fabricate 316 austenitic SS (nonmagnetic) to 430 ferritic SS (magnetic) FGM (Fig. 14d), with tailored magnetic functionality.

3. The construction of DED processing databases and Ashby diagrams

Well-established databases are becoming essential for the development and standardization in AM, including DED. Such databases may allow users to identify optimal processing parameters to achieve a specific set of properties (e.g., physical properties, mechanical properties, thermal properties, electrical properties, etc.) to meet the desired application requirements. Based on these databases, Ashby diagrams can be constructed and help optimize existing DED materials and develop new AM materials. To date, the utilization of Ashby diagrams in DED has been minor (see, for example, Refs. [33,280]). Fig. 15 shows an example of an Ashby diagram that presents the dependence of the relative density of some DED alloy steels on the comparison parameter, S ($S=P/\nu G$, where P is the laser power [J/s], G is the PMFR [g/min], and ν is the laser scan speed [mm/s]) [12]. Both axes are drawn on a linear scale, not a logarithmic one, given the small number of steels included in this diagram and the wish to clarify the value ranges for potential users. All data points were retrieved from references listed in Table 1. The selection of density as the material property to be presented in this diagram was made after retrieving all reported data (processing parameters and material characterization) from all references in Table 1, choosing the property with enough reports to construct such a plot. While there are many publications on each material family, there are many data gaps (e.g., not all processing parameters were reported). Furthermore, not all references characterize the same properties, making it challenging to construct a comprehensive Ashby diagram.

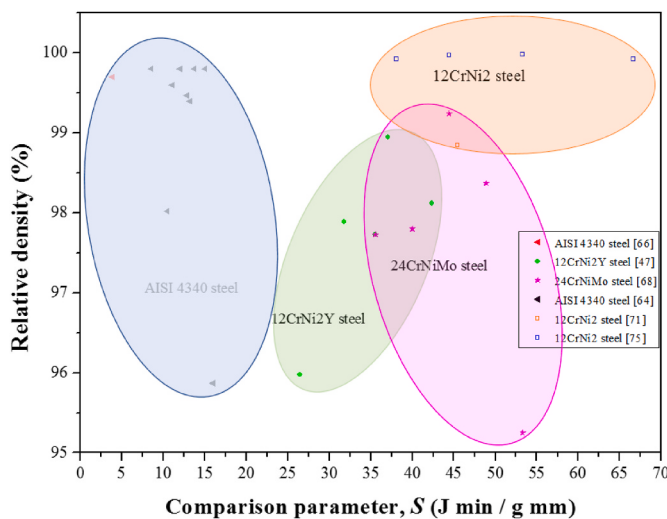


Fig. 15. Ashby-like plot revealing the dependence of the relative density of several DED alloy steels on the comparison parameter.

4. Freeform DED-LB

DED-LB is typically used in industry to fabricate net and near-net-shape freeform structures, clad materials for wear and corrosion resistance, repair, or add features on conventionally processed parts [705]. The paper so far has mainly focused on the freeforming of materials. This section will briefly describe large freeform structures, whereas sections 5 and 6 will describe cladding and repair applications, respectively.

Svetlizky et al. [12] have recently reviewed applications of DED, along with its physical characteristics, challenges and associated defects in the deposited material. Fig. 2f shows a large aerospace component fabricated by Relativity Space by a WAAM process. Fig. 2e [12] shows a large-scale rocket nozzle manufactured for aerospace applications [706]. The manufacturing of liquid rocket engine (channel wall) nozzles by DED has also been demonstrated by NASA [707]. Fig. 13c [12] shows a door handle for the commercial aerospace industry manufactured by FormAlloy using DED-LB [708]. Other examples of freeform fabrication by DED are shown elsewhere [709–714]. It is important to note that the DED is ideally suited for manufacturing large-scale complex structures among all metal AM technologies.

5. The cladding of materials by DED

Laser cladding (LC) is a technique for adding coatings to the surface of metallic components. DED AM is also known as 3D laser cladding since it originally evolved from a robotic multilayer cladding process [27,624]. When implemented as a cladding technique, DED involves feeding powder or wire into a melt pool generated by an energy source (e.g., laser or electron beam) as it scans across the target surface. In this process, thin metallic or composite layers are deposited and fused to a metallic component to improve their wear and corrosion resistance, enhance performance, or replace material worn away.

The DED-based cladding has multiple advantages over other coating techniques [624,625]: (1) a metallurgical bond is created between the substrate and the coating material, which is much stronger than the mechanical bond created using a thermal spray, arc welding, or plating techniques; (2) DED cladding provides a controllable low heat input with minimal dilution and HAZ, minimizing stresses and distortions within the deposited materials; (3) fine microstructures can be achieved in DED cladding due to the high cooling rates; (4) DED instrumentation allows for precise control of coating size, shape, location, and thickness; (5) a wide range of alloys and composites are compatible with DED cladding. Additionally, DED cladding enables the deposition of

multilayer and multi-material (e.g., functionally graded [32]) coatings. Finally, cladding onto curved surfaces and multi-axis cladding are also possible with DED [626,627].

Most materials that have been investigated for LC applications can also be deposited via DED-based cladding. These materials include various alloys [27,624], metallic glasses [412], and MMCs containing ceramics or intermetallic reinforcements [624,628]. The alloys that have been laser cladded include Ni-, Co-, Ti-, Nb-, Al-, Mg-, and Cu-based alloys, stainless steels, and tool steels [629–631]. The general objective of cladding is to enhance wear and corrosion resistance, and materials with these attributes are generally hardfacing alloys for high-temperature applications, making them difficult to process in bulk form but processable by cladding. The high-temperature oxidation resistance of cladding Ni-based alloys can be improved by adding rare-earth elements, such as Hf, Mo, Nb, or Y [629,632]. Intermetallic compounds can precipitate during cooling, and hot and cold cracking can appear in the cladded coating [633]. Pre- or post-heat treatment can help to avoid these problems [634].

Cladding of MMCs containing ceramic or intermetallic reinforcements onto metallic substrates has been the subject of extensive research. MMCs tend to have low ductility and fracture toughness, making them challenge to process by conventional manufacturing processes, such as casting or P/M. Generally, there are two approaches for cladding of MMCs. One approach uses a mixture of metal and ceramic particles projected into the melt pool formed by the laser beam with a limited reaction between the ceramic and metals [635–640] or injecting ceramic particles into the melt pool. In this approach, the ceramic particles are bonded to the surface of the metallic substrate. In general, ceramic particles are not easily wetted by a liquid metal, although the ceramic particles' feeding efficiency and wettability can be improved by using metal-coated ceramic particles [412,416]. One of the main challenges for fabricating high-quality MMC coatings is an inhomogeneous distribution of ceramic particles in the coating, which can be caused by the differences in density and wettability between ceramic and metallic particles. Nevertheless, powder mixtures with ceramic WC [636,639], TiC [637,640], or SiC [638,641] particles have been successfully laser cladded, and some minor reactions between the ceramic particles and metallic matrix were observed. The second approach for cladding of MMC coatings involves *in situ* reactions between the ingredients from the powder or substrate within the melt pool, such as additions of Mo, Si, and C powder in cladding for MoSi₂ and SiC particle formation [642], and TiC, TiN, and SiC reinforced Ti₃Al intermetallic matrix composite coatings *in situ* synthesized on a Ti substrate [643]. The *in situ* formed fine ceramic particles are typically well bonded to the matrix, enhancing the mechanical performance of the cladded MMC coatings [644]. The microstructure evolution, hardness, wear resistance, and corrosion resistance of different laser cladded coatings have been thoroughly investigated in recent years [624]. Results show that both wear and corrosion resistance were significantly improved when compared with those of uncladded materials. Fig. 16 shows the microstructure and properties of some cladded samples using DED processing.

6. Repair using DED

Repair or remanufacturing is restoring worn-out components into their original shape to regain the performance of the component. Remanufacturing or repairing high-value metal parts is of significant interest due to cost savings and minimum downtime for machines. Moreover, repairing parts or remanufacturing from scrap help sustainable manufacturing by efficiently managing natural resources and minimizing waste generation [646]. The high-performance and high-value industrial components that are used in aerospace, naval, automobile, turbine, and machine tools encounter severe thermo-mechanical loadings during operation that cause wear, fatigue cracking, and corrosion-related damage on the surface [647]. For instance, under high temperature and pressure operation, gas turbine

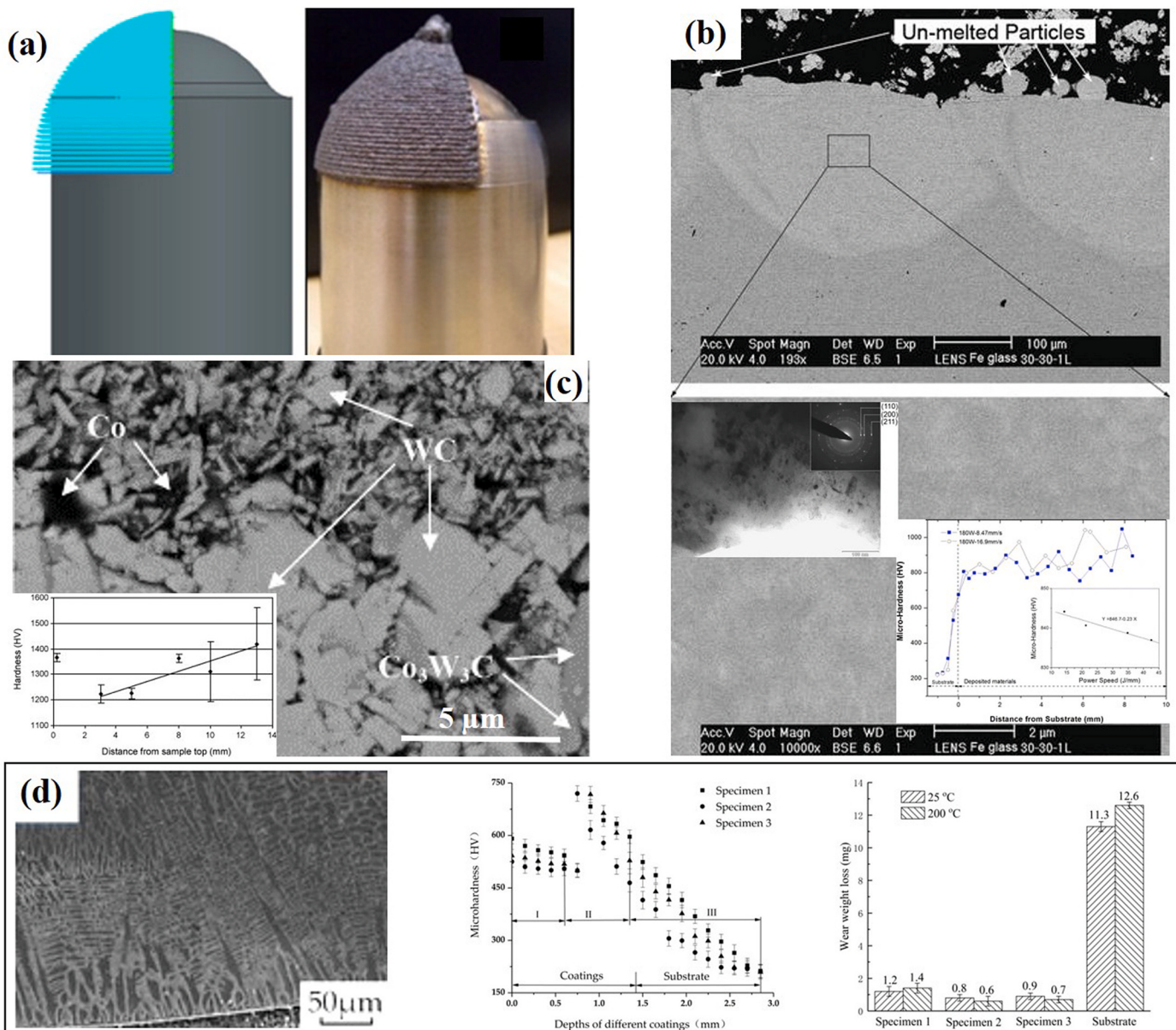


Fig. 16. DED-based cladding. (a) Programmed cladding strategy (left) and coated part (right) with a cladded curve surface of 316L SS on 1045 carbon steel using a five-axis DED-LB. Reprinted from Ref. [627], with permission from Elsevier. (b) SEM and TEM micrographs of the first layer of DED-LB Fe-based metallic glass coating and microhardness variation with distance from the substrate. Reprinted from Ref. [716], with permission from Springer Nature. (c) SEM micrograph of the microstructure of DED-LB WC-Co cermet with the hardness variation related to the position. Reprinted from Ref. [628], with permission from Elsevier. (d) SEM micrograph of cladded Stellite®6-Cr₃C₂-WS₂ self-lubricating composite coating with a variation of the hardness and wear behavior of cladded coatings compared to that of the H13 tool steel substrate. Reprinted from Ref. [645], with permission from MDPI.

blades suffer from hot corrosion, wear, and HCF [20,572]. In addition, the tip of turbine blades is often damaged due to rubbing against the stator liner, which affects the turbine's performance [19]. Conventional techniques, such as welding and thermal spraying, have been used for repairing worn components. However, most of these processes are less precise, ad-hoc, and may require extensive machining. In TIG welding, the high operational temperature (around 5500 °C) negatively affects the repaired components' microstructure. Furthermore, repairing for curved blade and disk is complex, more costly, and less reliable [648]. Therefore, the AM-based automated repairing method has been helpful for complex geometries to maintain tight tolerances for the actual parts.

The Manufacturing Readiness Level (MRL), on a scale of 1–10 (10 being most mature), is a measure developed by the United States Department of Defense (DoD) to assess the maturity of manufacturing

readiness. Accordingly, the repair by LENSTM of an injection mold tool made of H13 tool steel attained MRL 10 already in 2011. LENSTM has also been used to repair the T700 jet engine's disk made from AM355 steel and the leading edge of a Ti6Al4V airfoil, adding a Co-based wear-resistant alloy [649–652]. In addition, the US Army's Anniston Army Depot has been using LENSTM systems to repair some gas turbine engine components for the M1 Abrams Tank, while the US Army has been using LENSTM for its Mobile Parts Hospital (MPH) to provide a real-time battlefield repair capability [653].

6.1. Metallurgical aspects in DED-based repair

DED-based AM processes are getting attention for repairing complex/high-value parts where the damaged section of the component

is rebuilt based on a digital file created from reverse engineering and geometric reconstruction algorithm [5]. The DED-LB process shows minimal distortion due to localized heating with controlled heat input and exhibits good metallurgical bonds, low dilution, and narrow HAZ [654]. Several researchers studied the repaired parts' microstructure, interfacial bonding, and mechanical behavior and compared them with the as-built and conventionally processed components. DED deposits generate finer microstructure due to fast cooling rate, exhibit superior mechanical properties than castings, and are at par with wrought products [654]. DED is the most suitable and widely used method for repairing high-valued components among other metal AM techniques. Its unique characteristics include high material deposition rate, possibility to deposit multi-material, and no need for powder bed. Fig. 17 shows DED-LB repairing a worn anti-rotation bracket of military aircraft [655]. The repairing of such components reduced the lead time, and the post-machining component successfully met the Air Force's re-certification criterion [655].

The development of high-quality DED repaired parts requires precise control of process parameters. The DED technique is susceptible to the process variables, including laser power, laser scanning speed, powder feed rate, hatch spacing, laser beam diameter, laser scanning pattern, etc. [656]. Apart from these measurable parameters, variation in build geometry and heat accumulation can alter the melt-pool temperature, geometry, and layer height that control the quality of the repaired parts in terms of dimensional accuracy, defects, microstructure, and properties [657]. Therefore, real-time monitoring of measurable process variables via advanced sensing technologies and feedback control systems would improve repair quality and integrity [658]. Table 3 lists some high-value components repaired using DED.

6.2. Repair methodology

The maintenance, repair, and overhaul (MRO) sector follow the following basic process chains, shown in Fig. 18, during adaptive repairing or remanufacturing of components: (1) pre-repair examination; (2) pre-repair processing; (3) DED processing; (4) subtractive machining; and (5) repair quality examination [673]. To access the subsurface cracks and considering the inaccessible geometrical defects, pre-repair processing includes pre-repair machining, which is a crucial step that can influence metallurgical bonding [673,674]. Zhang et al. explained that defective material removal around inaccessible defect sites or building steep walls after machining could lead to cracks in turbine blade edges after repair [673]. Fig. 19 shows the pre-repair machining of the defect site to create the optimal contour for AM deposition. Further, the digitization of damaged parts into a 3D CAD model is an important step and carried out using a reverse engineering process. In reverse engineering, several technologies are popularly used for data acquisition, such as coordinate measurement machine (CMM), structured light scanning, laser scanning, stereo scanning, etc., followed

Table 3
DED-based repair of high-value components.

Repaired component	Materials	References
Molds, dies, tools	steel	[659–661]
Railways	steel	[662,663]
Crankshaft, driveshaft, turbocharger, four-stroke piston	steel	[654,664,665]
Centrifugal compressor impeller	FeCrNiCu alloy	[666]
Turbine blade, gas turbine compressor seal, gas turbine burner	Ni-based superalloys	[19, 667–672]

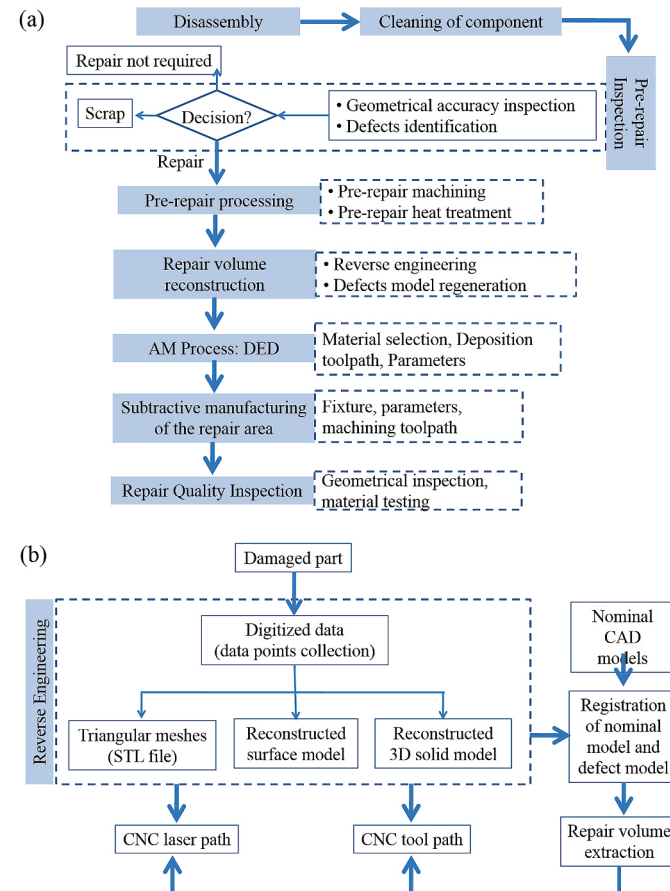


Fig. 18. (a) Process chain for part repair by DED. (b) Process flowchart for tool path generation.

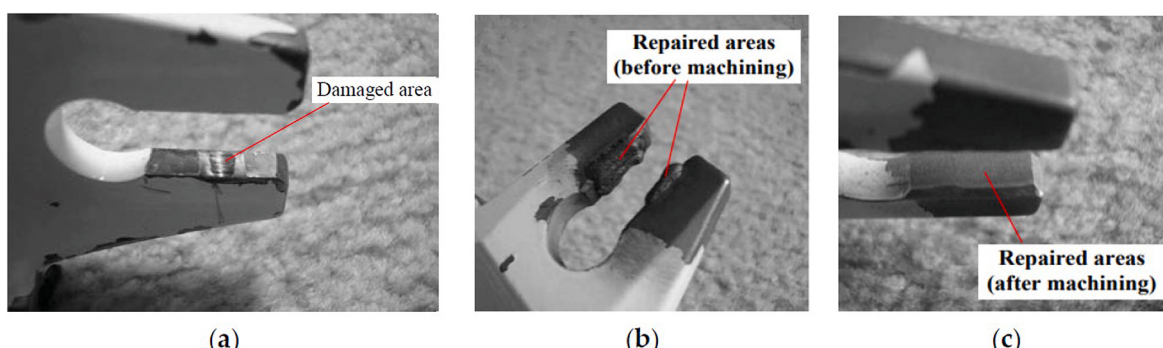


Fig. 17. (a) Damaged anti-rotation bracket, (b) laser cladding, and (c) a component after post-processing. Reprinted from Ref. [655], with permission from the Laser Institute of America.

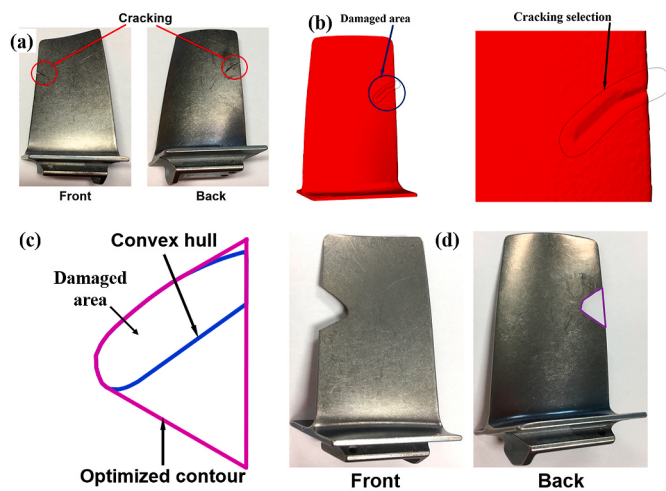


Fig. 19. Pre-repair machining, a part of a repair process chain. (a) A cracked turbine blade. (b) 3D CAD model of the cracked blade area. (c) Contour path for machining. (d) Post-machining blade. Reprinted from Ref. [673], with permission from MDPI.

by reconstructing a geometric representation of a 3D model using those data points [675]. Then, the repaired volume in the damaged part can be achieved through a registration operation by comparing the nominal CAD model with the 3D model of the defective part surface. Generally, the nominal CAD model is compared to the actual digitized model to minimize steps of the computerized numerical control (CNC) tool path for machining and the laser tool path for depositing (Fig. 19b). In the case of no nominal CAD availability, a reverse engineering process is required to reconstruct the original surface model based on the 3D model of the damaged surface. The surface reconstruction algorithm is associated with a parametric representation that enables the manipulation of the surface geometry. Several studies showed adaptive repair of components by the process of digitizing and meshing, and reconstructing the geometry using non-uniform rational b-splines (NURBS) or Prominent Cross-Section (PCS) based algorithm [5,676].

In the next step, the critical challenge for AM process is to deposit materials in the damaged area to restore the missing geometry, maintaining tolerance and surface roughness. The AM process needs to automatically adapt and modify the laser tool path and process parameters for superior repair quality based on orientation, dimension, and shape. For example, thinner sections of the damaged part require less laser power, as less heat input reduces the finished part's HAZ. The coarse surface finish of the DED repaired part requires post-processing machining. CNC machining of the repaired component must achieve the desired surface finish and dimensional accuracy for service. However, machining of complex geometries can be an issue due to limited tool accessibility. Machining also enhances the cost of repair and lead time. Hybrid DED is becoming popular to repair components, where DED-based AM is integrated with CNC machining to overcome these limitations. Several studies showed that combining these two techniques helps to produce parts with desirable accuracy [677,678].

7. Alloy design via DED

AM has changed how new alloys can be designed [11,658,659,679]. Pure metals are rarely used in any application as their properties are not suitable to meet demanding applications. However, a small addition of alloying elements to a pure metal can make a significant difference in the properties of an alloy. Naturally, alloy design has become a new R&D field of AM. Designing new alloys happens with an application requiring extensive experimental capabilities, starting from high-temperature furnaces for melting metals to post-processing heat-treatment set-up and equipment for shaping, such as forging, extrusion, or rolling. For

the past five decades, efforts have been devoted to surface modifications rather than using a new alloy as surface modifications are easy to do and do not compromise bulk properties. Based on AM's unique processing capabilities, new developments in this area are among the most exciting aspects of the next wave of innovation in the field. And among different types of metal AM technologies, DED is the most suitable technology platform for alloy design as different powders in their elemental form can be added at various chemistries and shaped simultaneously. And if a hybrid DED is used, parts can also be machined during AM operation to meet tight dimensional tolerances. The AM technology will revolutionize how different heritage alloy chemistries, such as Ti6Al4V and 316 SS, across numerous industries, can be redesigned for parts with added functionality and increasing complexity, customization, and consolidation for enhanced efficiency [680]. One example is alloy chemistries in biomedical devices. The metallic biomedical devices primarily use three different alloys – commercially pure and Ti6Al4V, 316L SS, and CoCr alloy. For load-bearing implants, Ti6Al4V is the most used alloy. However, the biocompatibility or *in vivo* tissue-material interactions of Ti6Al4V is not optimal. The current solution is to design various coating systems to enhance the biocompatibility and osseointegration of the Ti6Al4V alloy. Some of these coatings include porous tantalum coating, porous titanium coating, or calcium phosphate (CaP) [681] coating. Minimal effort has been devoted to innovating new Ti-based alloys that can show better biocompatibility *in vivo*. It is also important to realize that Ti6Al4V was never initially developed for biomedical devices. This alloy was designed for aerospace applications, keeping high-temperature applications and fatigue resistance in mind. Excellent fatigue and corrosion resistance of Ti6Al4V alloy helped its original transformation in biomedical devices. It is important to note that the challenge is to design a new alloy and find a vendor who can manufacture those compositions on an industrial scale. And the current solution is – keep using the legacy alloys and only make surface modifications. Such an approach is also helpful from the regulatory approval point of view for the biomedical device industries. However, now that most babies born in the 21st century are expected to live 90+ years, new alloys for biomedical devices that can serve longer than a typical 15 years are growing. And it is envisioned that the AM technology platform will be used to accomplish such a goal.

Significant research on additive-based alloy design has been devoted to Fe- and Ni-based systems. Dippo et al. [682] demonstrated a modified Inconel 625 chemistry using DED-LB. Using an industrial alloy development feeder (ADF) from FormAlloy, the solubility of alloying elements in Inconel 625 was experimentally verified after CALPHAD simulations. Hemmati et al. [683] researched the effects of variable Cr–B–Si amounts in Ni-based alloy on the microstructure and properties when processed using laser-based AM. Li et al. [684] investigated compositional effects on NiCrSi alloys using a simulated high-cooling-rate processing setup. Significant work has been done on titanium alloys as well. Zhang et al. [685] demonstrated that Cu addition to titanium reduces the tendency for columnar grain formation due to high constitutional supercooling that causes heterogeneous nucleation. Copper's high diffusion rate in titanium at compositions ranging from 3.5 to 8.5 wt% Cu enables eutectoid microstructures that significantly affect the alloy's strength and ductility. A set of studies from Mitra et al. and Bandyopadhyay et al. [686,687] showed that the incorporation of tantalum into titanium via DED-LB increases its biocompatibility. The authors found that as low as 10 wt% Ta could be incorporated into titanium to significantly increase the biological response of the alloy, like pure tantalum. Overall, alloy design using DED is in its infancy, and it is expected that more research will be done in the future with commonly used alloys to make them more AM friendly, or designing new alloys with superior performance to meet the ever-changing demands for high-efficiency materials in free-standing and coating/repair applications.

8. Summary, current challenges, and future directions

Commercial DED systems have been available since the mid-1990s in the US by Optomec, Inc. (Albuquerque, NM) based on technology developed at the Sandia National Lab. Other leading DED technology providers include DM3D [688], RPM Innovations [689], and Fraunhofer [690], just to name a few. However, as with all metal AM technology platforms, DED's entry into the marketplace was slow due to concerns related to reproducibility of the parts, poor surface finish, and difficulty in manufacturing complex-shaped freestanding parts. Unlike in the PBF process, DED systems usually do not have any support materials available, and naturally, complex-shaped parts were near impossible to make with the first-generation machines that had one powder feeder hopper and a 3-axis control of the build space. Since then, the DED technology has advanced significantly, where commercial machines are now available with more than 10 powder feeders, free axis deposition heads, and CNC machining platform for hybrid systems. Complex parts are easily doable with these new DED machines, although most machines still have only three axes of freedom and two to three powder feeders. As applications in repair, alloy design, surface modifications, and functionally graded structures are realized, DED-based AM is becoming popular in various industrial applications [679,715]. DED has become the primary metal AM technology platform for printing large freestanding parts, a challenging application for PBF systems. In a recent study with NASA, DM3D manufactured a 10-ft tall full-scale RS25 nozzle liner [691]. Any other AM approach cannot manufacture such unique metal structures. While large freestanding parts are uniquely suited for DED, for research machines, the need for a small amount of powder or the ability to deposit multi-material structures have been the most attractive features. Multiple vendors sell commercial DED systems worldwide for reactive and non-reactive powders with or without a hybrid CNC option. DED-based metal AM systems are primarily not competing with the PBF systems but offer a complimentary manufacturing capability. Research and industrial DED systems are used extensively to repair high-value or legacy components, alloy design for optimizing the materials chemistry for AM use or innovating new chemistries, manufacturing large parts, adding a coated layer on existing parts, or creating bimetallic or functionally graded structures. The DED technology platform offers unique strengths to all challenging applications over other metal AM systems. Naturally, sales of commercial DED systems are growing and are expected to continue in the future. Apart from the laser powder-based DED, welding-based systems, such as WAAM, are also becoming popular, particularly for rapid deposition rates for large parts. Applications of DED in different material systems have been discussed throughout this manuscript with specific references to unique compositions, processing histories, and related properties. Among remaining challenges, the cost of the machine is always an issue for any new technology, including the DED, for large-scale acceptance in manufacturing practices. Prices for laser-based DED systems for non-reactive materials have dropped significantly in recent years, and the trend may continue in the future. Coaxial deposition heads have become a standard feature in the most recent DED systems, improving the deposition efficiency and part quality. Incorporating a machine learning-based approach may minimize process optimization requirements in future machines. Although the focus in this article remained on the DED and materials for DED, pre-processing and post-processing issues are also critical. Surface functionalization of metal powders, essentially processing core-shell powders [692,693], for the printing of advanced MMCs is a relatively new direction of R&D. Reusability of metal powders or avoiding mixing metal powders with machining chips or other powder compositions during multi-material builds are still issues that need further R&D. Post-processing treatments are also essential for any critical applications which require a better understanding of the process-property relationships. The introduction of advanced characterization techniques to the AM arena is also evolving. Techniques such as the dynamic pulse-echo technique (for

measurement of the elastic constants) offer higher accuracy, sensitivity, and repeatability and the possibility to use relatively small samples compared to traditional techniques [228,694]. Such techniques are expected to become more common in material design, R&D, and quality control of AM parts. This manuscript provides a comprehensive review on DED of advanced materials which will be a valuable document for engineers and scientists from academia, industry, and national labs worldwide to continue innovating the next generation of materials and structures for various applications.

Originality statement

We declare that this manuscript is original, has not been published before, and is not currently being considered for publication elsewhere. We confirm that the manuscript has been read and approved by all named authors and that there are no other persons who satisfied the criteria for authorship but are not listed. We further confirm that the order of authors listed in the manuscript has been approved by all of us.

Credit author statement

This invited review article is the product of a multi-team work. All authors contributed to it and deserve being listed as authors.

Declaration of competing interest

The authors declare that they have no known competing financial interests or personal relationships that could have appeared to influence the work reported in this paper.

Acknowledgments

DS and NE gratefully acknowledge the financial support from the Israel Ministry of Defense (grant no. 4440783376). ALV, BZ, JMS, and EJL wish to acknowledge financial support from the U.S. Army Research Office under grant W911NF-18-1-0279. BZ, JMS, and EJL are grateful for additional financial support from the Israel Ministry of Defense under P.O. No. 4440873734.

References

- [1] J. Manyika, M. Chui, J. Bughin, R. Dobbs, P. Bisson, A. Marrs, Disruptive Technologies: Advances that Will Transform Life, Business, and the Global Economy, McKinsey Global Institute, May 2013. https://www.mckinsey.com/~media/mckinsey/business%20functions/mckinsey%20digital/our%20insights/disruptive%20technologies/mgi_disruptive_technologies_full_report_may2013.pdf. (Accessed 30 July 2021).
- [2] R. Noorani, *Rapid Prototyping: Principles and Applications*, John Wiley & Sons, NJ, USA, 2006.
- [3] ISO/ASTM 52900:2015(E): Standard Terminology for Additive Manufacturing – General Principles – Terminology, ASTM International, West Conshohocken, PA, 2015.
- [4] M. Jiménez, L. Romero, I.A. Domínguez, M.D.M. Espinosa, M. Domínguez, Additive manufacturing technologies: an overview about 3D printing methods and future prospects, Complexity 2019 (2019) 1–30, <https://doi.org/10.1155/2019/9656938>.
- [5] A. Bandyopadhyay, T. Gualtieri, B. Heer, S. Bose, Introduction to additive manufacturing, in: Additive Manufacturing, second ed., CRC Press, Boca Raton, FL, 2019, pp. 1–23, <https://doi.org/10.1201/9780429466236-1>.
- [6] C. Mota, D. Puppi, F. Chiellini, E. Chiellini, Additive manufacturing techniques for the production of tissue engineering constructs, J. Tissue Eng. Regen. Med. 9 (2015) 174–190, <https://doi.org/10.1002/term.1635>.
- [7] S. Liu, Y.C. Shin, Additive manufacturing of Ti6Al4V alloy: a review, Mater. Des. 164 (2019), 107552, <https://doi.org/10.1016/j.matdes.2018.107552>.
- [8] R. Huang, M. Riddle, D. Graziano, J. Warren, S. Das, S. Nimbalkar, J. Cresko, E. Masanet, Energy and emissions saving potential of additive manufacturing: the case of lightweight aircraft components, J. Clean. Prod. 135 (2016) 1559–1570, <https://doi.org/10.1016/j.jclepro.2015.04.109>.
- [9] G. Warwick, Adding power, Aviat Week Space Technol. 176 (11) (2014) 43–44.
- [10] Optomec Overview. <https://optomec.com/optomec-overview>. (Accessed 30 July 2021).
- [11] T. DebRoy, H.L. Wei, J.S. Zuback, T. Mukherjee, J.W. Elmer, J.O. Milewski, A. M. Beese, A. Wilson-Heid, A. De, W. Zhang, Additive manufacturing of metallic

- components – process, structure and properties, *Prog. Mater. Sci.* 92 (2018) 112–224, <https://doi.org/10.1016/j.jpmatsci.2017.10.001>.
- [12] D. Svetlizky, M. Das, B. Zheng, A.L. Vyatskikh, S. Bose, A. Bandyopadhyay, J. M. Schoenung, E.J. Lavernia, N. Eliaz, Directed energy deposition (DED) additive manufacturing: physical characteristics, defects, challenges and applications, *Mater. Today* 49 (2021) 271–295, <https://doi.org/10.1016/j.mattod.2021.03.020>.
- [13] Optomec, Quick Guide to Metal AM. <https://optomec.com/wp-content/uploads/2019/06/Metal-AM-Selection-Guide.pdf>. (Accessed 30 July 2021).
- [14] J.W. Pagues, M.A. Melia, R. Puckett, S.R. Whetten, N. Argibay, A.B. Kustas, Exploring additive manufacturing as a high-throughput screening tool for multiphase high entropy alloys, *Addit. Manuf.* 37 (2021), 101598, <https://doi.org/10.1016/j.addma.2020.101598>.
- [15] B. Heer, A. Bandyopadhyay, Compositationally graded magnetic-nonmagnetic bimetallic structure using laser engineered net shaping, *Mater. Lett.* 216 (2018) 16–19, <https://doi.org/10.1016/j.matlet.2017.12.129>.
- [16] F.F. Noecker, J.N. Dupont, Functionally Graded Copper – Steel Using Laser Engineered Net Shaping™ 2002, ICALEO, 2002, 185430 <https://doi.org/10.2351/1.5066217>.
- [17] J. Xie, Z. Huang, H. Lu, B. Zheng, X. Xu, J. Lei, Additive manufacturing of tantalum-zirconium alloy coating for corrosion and wear application by laser directed energy deposition on Ti6Al4V, *Surf. Coatings. Technol.* 411 (2021), 127006, <https://doi.org/10.1016/j.surcoat.2021.127006>.
- [18] A.K. Rai, B. Srinivasulu, C.P. Paul, R. Singh, S.K. Rai, G.K. Mishra, S. Bontha, K. S. Bindra, Development of thick SiC coating on thin wall tube of zircaloy-4 using laser based directed energy deposition technique, *Surf. Coatings. Technol.* 398 (2020), 126088, <https://doi.org/10.1016/j.surcoat.2020.126088>.
- [19] J.M. Wilson, C. Piya, Y.C. Shin, F. Zhao, K. Ramani, Remanufacturing of turbine blades by laser direct deposition with its energy and environmental impact analysis, *J. Clean. Prod.* 80 (2014) 170–178, <https://doi.org/10.1016/j.jclepro.2014.05.084>.
- [20] A. Saboori, A. Aversa, G. Marchese, S. Biamino, M. Lombardi, P. Fino, Application of directed energy deposition-based additive manufacturing in repair, *Appl. Sci.* 9 (2019) 3316, <https://doi.org/10.3390/app9163316>.
- [21] ASTM F3187-16: Standard Guide for Directed Energy Deposition of Metals, ASTM International, West Conshohocken, PA, 2016.
- [22] Ó. Barro, F. Arias-González, F. Lusquiños, R. Comesáñ, J. del Val, A. Riveiro, A. Badaoui, F. Gómez-Bano, J. Pou, Improved commercially pure titanium obtained by laser directed energy deposition for dental prosthetic applications, *Metals* 11 (2021) 70, <https://doi.org/10.3390/met11010070>.
- [23] B.-L. Chua, D.-G. Ahn, Estimation method of interpass time for the control of temperature during a directed energy deposition process of a Ti-6Al-4V planar layer, *Materials* 13 (2020) 4935, <https://doi.org/10.3390/ma13214935>.
- [24] E. Karayel, Y. Bozkurt, Additive manufacturing method and different welding applications, *J. Mater. Res. Technol.* 9 (2020) 11424–11438, <https://doi.org/10.1016/j.jmr.2020.08.039>.
- [25] J.H.K. Tan, S.L. Sing, W.Y. Yeong, Microstructure modelling for metallic additive manufacturing: a review, *Virtual Phys. Prototyp.* 15 (2020) 87–105, <https://doi.org/10.1080/17452759.2019.1677345>.
- [26] Z. Qi, B. Qi, B. Cong, H. Sun, G. Zhao, J. Ding, Microstructure and mechanical properties of wire + arc additively manufactured 2024 aluminum alloy components: as-deposited and post heat-treated, *J. Manuf. Process.* 40 (2019) 27–36, <https://doi.org/10.1016/j.jmapro.2019.03.003>.
- [27] A. Dass, A. Moridi, State of the art in directed energy deposition: from additive manufacturing to materials design, *Coatings* 9 (2019) 418, <https://doi.org/10.3390/coatings9070418>.
- [28] C. Baykasoglu, O. Akyildiz, M. Tunay, A.C. To, A process-microstructure finite element simulation framework for predicting phase transformations and microhardness for directed energy deposition of Ti6Al4V, *Addit. Manuf.* 35 (2020), 101252, <https://doi.org/10.1016/j.addma.2020.101252>.
- [29] Z. Wang, E. Denlinger, P. Michaleris, A.D. Stoica, D. Ma, A.M. Beese, Residual stress mapping in Inconel 625 fabricated through additive manufacturing: method for neutron diffraction measurements to validate thermomechanical model predictions, *Mater. Des.* 113 (2017) 169–177, <https://doi.org/10.1016/j.matedes.2016.10.003>.
- [30] L. Yan, Y. Chen, F. Liou, Additive manufacturing of functionally graded metallic materials using laser metal deposition, *Addit. Manuf.* 31 (2020), 100901, <https://doi.org/10.1016/j.addma.2019.100901>.
- [31] P. Bajaj, A. Hariharan, A. Kini, P. Kürnsteiner, D. Raabe, E.A. Jägle, Steels in additive manufacturing: a review of their microstructure and properties, *Mater. Sci. Eng.* 772 (2020), 138633, <https://doi.org/10.1016/j.msea.2019.138633>.
- [32] C. Zhang, F. Chen, Z. Huang, M. Jia, G. Chen, Y. Ye, Y. Lin, W. Liu, B. Chen, Q. Shen, Additive manufacturing of functionally graded materials: a review, *Mater. Sci. Eng.* 764 (2019), 138209, <https://doi.org/10.1016/j.msea.2019.138209>.
- [33] A. Bandyopadhyay, B. Heer, Additive manufacturing of multi-material structures, *Mater. Sci. Eng. R* 129 (2018) 1–16, <https://doi.org/10.1016/j.mser.2018.04.001>.
- [34] H. Attar, S. Ehtemam-Haghghi, D. Kent, M.S. Dargusch, Recent developments and opportunities in additive manufacturing of titanium-based matrix composites: a review, *Int. J. Mach. Tool Manufact.* 133 (2018) 85–102, <https://doi.org/10.1016/j.ijmachtools.2018.06.003>.
- [35] J. Zhang, B. Song, Q. Wei, D. Bourrell, Y. Shi, A review of selective laser melting of aluminum alloys: processing, microstructure, property and developing trends, *J. Mater. Sci. Technol.* 35 (2019) 270–284, <https://doi.org/10.1016/j.jmst.2018.09.004>.
- [36] T. Guan, S. Chen, X. Chen, J. Liang, C. Liu, M. Wang, Effect of laser incident energy on microstructures and mechanical properties of 12CrNi2Y alloy steel by direct laser deposition, *J. Mater. Sci. Technol.* 35 (2019) 395–402, <https://doi.org/10.1016/j.jmst.2018.10.024>.
- [37] Y. Yao, Y. Huang, B. Chen, C. Tan, Y. Su, J. Feng, Influence of processing parameters and heat treatment on the mechanical properties of 18Ni300 manufactured by laser based directed energy deposition, *Opt. Laser. Technol.* 105 (2018) 171–179, <https://doi.org/10.1016/j.optlastec.2018.03.011>.
- [38] R.S. Amano, P.K. Rohatgi, Laser engineered net shaping process for SAE 4140 low alloy steel, *Mater. Sci. Eng.* 528 (2011) 6680–6693, <https://doi.org/10.1016/j.msea.2011.05.036>.
- [39] H. Kim, Z. Liu, W. Cong, H.C. Zhang, Tensile fracture behavior and failure mechanism of additively-manufactured AISI 4140 low alloy steel by laser engineered net shaping, *Materials* 10 (2017) 1283, <https://doi.org/10.3390/mate10111283>.
- [40] J. Geng, I.C. Nlebedim, M.F. Besser, E. Simsek, R.T. Ott, Bulk Combinatorial synthesis and high throughput characterization for rapid assessment of magnetic materials: application of laser engineered net shaping (LENS™), *JOM* 68 (2016) 1972–1977, <https://doi.org/10.1007/s11837-016-1918-x>.
- [41] H. ping Duan, X. Liu, X. zhe Ran, J. Li, D. Liu, Mechanical properties and microstructure of 3D-printed high Co-Ni secondary hardening steel fabricated by laser melting deposition, *Int. J. Miner. Metall. Mater.* 24 (2017) 1027–1033, <https://doi.org/10.1007/s12613-017-1492-4>.
- [42] J. Liu, J. Li, X. Cheng, H. Wang, Microstructures and tensile properties of laser cladded AerMet100 steel coating on 300 M steel, *J. Mater. Sci. Technol.* 34 (2018) 643, <https://doi.org/10.1016/j.jmst.2017.11.037>.
- [43] R.A.R. Rashid, C.J. Barr, S. Palanisamy, K.A. Nazari, N. Orchowski, N. Matthews, M.S. Dargusch, Effect of clad orientation on the mechanical properties of laser-clad repaired ultra-high strength 300 M steel, *Surf. Coatings. Technol.* 380 (2019), 125090, <https://doi.org/10.1016/j.surcoat.2019.125090>.
- [44] S. Bhattacharya, G.P. Dinda, A.K. Dasgupta, J. Mazumder, Microstructural evolution of AISI 4340 steel during direct metal deposition process, *Mater. Sci. Eng.* 528 (2011) 2309–2318, <https://doi.org/10.1016/j.msea.2010.11.036>.
- [45] G. Sun, S. Bhattacharya, G.P. Dinda, A. Dasgupta, J. Mazumder, Microstructure evolution during laser-aided direct metal deposition of alloy tool steel, *Scripta Mater.* 64 (2011) 454–457, <https://doi.org/10.1016/j.scriptamat.2010.11.016>.
- [46] G. Sun, R. Zhou, J. Lu, J. Mazumder, Evaluation of defect density, microstructure, residual stress, elastic modulus, hardness and strength of laser-deposited AISI 4340 steel, *Acta Mater.* 84 (2015) 172–189, <https://doi.org/10.1016/j.actamat.2014.09.028>.
- [47] C. Huang, X. Lin, H. Yang, F. Liu, W. Huang, Microstructure and tribological properties of laser forming repaired 34CrNiMo6 steel, *Materials* 11 (2018) 1722, <https://doi.org/10.3390/ma11091722>.
- [48] L. Cao, S. Chen, M. Wei, Q. Guo, J. Liang, C. Liu, M. Wang, Effect of laser energy density on defects behavior of direct laser depositing 24CrNiMo alloy steel, *Opt. Laser. Technol.* 111 (2019) 541–553, <https://doi.org/10.1016/j.optlastec.2018.10.025>.
- [49] H. Chunping, L. Xin, L. Fencheng, C. Jun, L. Fenggang, H. Weidong, Effects of cooling condition on microstructure and mechanical properties in laser rapid forming of 34CrNiMo6 thin-wall component, *Int. J. Adv. Manuf. Technol.* 82 (2016) 1269–1279, <https://doi.org/10.1007/s00170-015-7453-z>.
- [50] H. El Kadiri, L. Wang, M.F. Horstemeyer, R.S. Yassar, J.T. Berry, S. Felicelli, P. T. Wang, Phase transformations in low-alloy steel laser deposits, *Mater. Sci. Eng.* 494 (2008) 10–20, <https://doi.org/10.1016/j.msea.2007.12.011>.
- [51] X. Zhao, Y. Lv, S. Dong, S. Yan, X. Liu, Y. Liu, P. He, T. Lin, B. Xu, H. Han, The martensitic strengthening of 12CrNi2 low-alloy steel using a novel scanning strategy during direct laser deposition, *Opt. Laser. Technol.* 132 (2020), 106487, <https://doi.org/10.1016/j.optlastec.2020.106487>.
- [52] Y.N. Aditya, T.D. Srichandra, M. Tak, G. Padmanabham, To study the laser cladding of ultra high strength AerMet-100 alloy powder on AISI-4340 steel for repair and refurbishment, *Mater. Today Proc.* 41 (2020) 1146–1155, <https://doi.org/10.1016/j.mtpr.2020.09.154>.
- [53] X. Cui, S. Zhang, C. Wang, C.H. Zhang, J. Chen, J.B. Zhang, Microstructure and fatigue behavior of a laser additive manufactured 12CrNi2 low alloy steel, *Mater. Sci. Eng.* 772 (2020), 138685, <https://doi.org/10.1016/j.msea.2019.138685>.
- [54] Y.H. Xu, C.H. Zhang, S. Zhang, R.Q. Qiao, J.B. Zhang, A.O. Abdullah, Scanning velocity influence on microstructure evolution and mechanical properties of laser melting deposited 12CrNi2 low alloy steel, *Vacuum* 177 (2020), 109387, <https://doi.org/10.1016/j.vacuum.2020.109387>.
- [55] Y. Zhou, S. Chen, X. Chen, J. Liang, C. Liu, M. Wang, The effect of laser scanning speed on microstructural evolution during direct laser deposition 12CrNi2 alloy steel, *Opt. Laser. Technol.* 125 (2020), 106041, <https://doi.org/10.1016/j.optlastec.2019.106041>.
- [56] X. Chen, S. Chen, T. Cui, J. Liang, C. Liu, M. Wang, A new 50Cr6Ni2Y alloy steel prepared by Direct laser Deposition: its design, microstructure and properties, *Opt. Laser. Technol.* 126 (2020), 106080, <https://doi.org/10.1016/j.optlastec.2020.106080>.
- [57] X. Kang, S. Dong, P. Men, X. Liu, S. Yan, H. Wang, B. Xu, Microstructure evolution and gradient performance of 24CrNiMo steel prepared via laser melting deposition, *Mater. Sci. Eng.* 777 (2020), 139004, <https://doi.org/10.1016/j.msea.2020.139004>.
- [58] M. Ebrahimpour, Y. Xie, C. Chi, Effect of cladding parameters on microstructure and defects in direct laser metal deposition of 24CrNiMo steel, *J. Laser Appl.* 33 (2020), 12007, <https://doi.org/10.2351/7.0000214>.
- [59] F. Liu, X. Lin, M. Song, H. Yang, K. Song, P. Guo, W. Huang, Effect of tempering temperature on microstructure and mechanical properties of laser solid formed

- 300M steel, *J. Alloys Compd.* 689 (2016) 225–232, <https://doi.org/10.1016/j.jallcom.2016.07.276>.
- [60] L. Cao, S. Chen, M. Wei, Q. Guo, J. Liang, C. Liu, M. Wang, Study of surface topography detection and analysis methods of direct laser deposition 24CrNiMo alloy steel, *Opt Laser. Technol.* 135 (2021), 106661, <https://doi.org/10.1016/j.optlastec.2020.106661>.
- [61] F. Liu, W. Zhang, X. Lin, C. Huang, Z. Wang, F. Liu, W. Huang, P. Wang, X. Li, Achieving superior ductility for laser directed energy deposition 300 M steel through isothermal bainitic transformation, *J. Manuf. Process.* 60 (2020) 426–434, <https://doi.org/10.1016/j.jmapro.2020.10.077>.
- [62] J.B. Ferguson, B.F. Schultz, A.D. Moghadam, P.K. Rohatgi, Semi-empirical model of deposit size and porosity in 420 stainless steel and 4140 steel using laser engineered net shaping, *J. Manuf. Process.* 19 (2015) 163–170, <https://doi.org/10.1016/j.jmapro.2015.06.026>.
- [63] M. Ansari, A. Mohammadiزاده, Y. Huang, V. Pasarin, E. Toyserkani, Laser directed energy deposition of water-atomized iron powder: process optimization and microstructure of single-tracks, *Opt Laser. Technol.* 112 (2019) 485–493, <https://doi.org/10.1016/j.optlastec.2018.11.054>.
- [64] C.M. Knapp, T.J. Lienert, C. Chen, D. Kovar, Additive manufacturing of 1018 steel : process observations and calculations, *Int. Solid Free. Fabr. Symp. – An Addit. Manuf. Conf.* 7 (2014) 334–342.
- [65] Y. Shi, Z. Lu, H. Xu, R. Xie, Y. Ren, G. Yang, Microstructure characterization and mechanical properties of laser additive manufactured oxide dispersion strengthened Fe-9Cr alloy, *J. Alloys Compd.* 791 (2019) 121–133, <https://doi.org/10.1016/j.jallcom.2019.03.284>.
- [66] M. Alimardani, V. Fallah, A. Khajepour, E. Toyserkani, The effect of localized dynamic surface preheating in laser cladding of Stellite 1, *Surf. Coatings. Technol.* 204 (2010) 3911–3919, <https://doi.org/10.1016/j.surcoat.2010.05.009>.
- [67] Y.N. Zavalov, A.V. Dubrov, F.K. Mirzade, V.D. Dubrov, Features of the estimation of temperature distribution on the bead formed by the laser aided metal powder deposition, *Opt. Meas. Syst. Ind. Insp. X.* 10329 (2017), 1032942, <https://doi.org/10.1117/12.2270239>.
- [68] J.X. Fang, S.Y. Dong, S.B. Li, Y.J. Wang, B.S. Xu, J. Li, B. Liu, Y.L. Jiang, Direct laser deposition as repair technology for a low transformation temperature alloy: microstructure, residual stress, and properties, *Mater. Sci. Eng.* 748 (2019) 119–127, <https://doi.org/10.1016/j.msea.2019.01.072>.
- [69] G.Y. Baek, G.Y. Shin, E.M. Lee, D.S. Shim, K.Y. Lee, H.S. Yoon, M.H. Kim, Mechanical characteristics of a tool steel layer deposited by using direct energy deposition, *Met. Mater. Int.* 23 (2017) 770–777, <https://doi.org/10.1007/s12540-017-6442-1>.
- [70] J.K. Mickovski, I.J. Lazarev, J. Lazarev, Microstructure case study of LENS™ processed cylinder from AISI H13 steel, *J. Technol. Plast.* 35 (2010) 61–74.
- [71] L. Xue, J. Chen, S.H. Wang, Freeform laser consolidated H13 and CPM 9V tool steels, *Metallogr. Microstruct. Anal.* 2 (2013) 67–78, <https://doi.org/10.1007/s13632-013-0061-0>.
- [72] D.S. Shim, G.Y. Baek, E.M. Lee, Effect of substrate preheating by induction heater on direct energy deposition of AISI M4 powder, *Mater. Sci. Eng.* 682 (2017) 550–562, <https://doi.org/10.1016/j.msea.2016.11.029>.
- [73] Y. Bai, A. Chaudhari, H. Wang, Investigation on the microstructure and machinability of ASTM A131 steel manufactured by directed energy deposition, *J. Mater. Process. Technol.* 276 (2020), 116410, <https://doi.org/10.1016/j.jmatprotec.2019.116410>.
- [74] G.Y. Baek, G.Y. Shin, K.Y. Lee, D.S. Shim, Effect of post-heat treatment on the AISI M4 layer deposited by directed energy deposition, *Metals* 10 (2020) 703, <https://doi.org/10.3390/met10060703>.
- [75] G.Y. Baek, G.Y. Shin, K.Y. Lee, D.S. Shim, Mechanical properties of tool steels with high wear resistance via directed energy deposition, *Metals* 9 (2019) 282, <https://doi.org/10.3390/met9030282>.
- [76] S. Choi, H. Kim, J. Sung, D. Lee, J. Seo, Properties of tool steels printed by directed energy deposition process on S45C base metal, *Materials* 13 (2020) 5068, <https://doi.org/10.3390/ma13225068>.
- [77] S.W. Choi, Y.S. Kim, Y.J. Yum, S.Y. Yang, A study on strengthening mechanical properties of a punch mold for cutting by using an HWS powder material and a DED semi-AM method of metal 3D printing, *J. Manuf. Mater. Process.* 4 (2020) 98, <https://doi.org/10.3390/jmmp4040098>.
- [78] R.T. Jardin, V. Tunineti, J.T. Tchuindjang, N. Hashemi, R. Carrus, A. Mertens, L. Duchêne, H.S. Tran, A.M. Habraken, Sensitivity analysis in the modeling of a high-speed, steel, thin wall produced by directed energy deposition, *Metals* 10 (2020) 1554, <https://doi.org/10.3390/met10111554>.
- [79] X. Zhao, Y. Lv, S. Dong, S. Yan, P. He, X. Liu, Y. Liu, T. Lin, B. Xu, The effect of thermal cycling on direct laser-deposited gradient H13 tool steel: microstructure evolution, nanoprecipitation behaviour, and mechanical properties, *Mater. Today Commun.* 25 (2020), 101390, <https://doi.org/10.1016/j.mtcomm.2020.101390>.
- [80] M.L. Griffith, M.E. Schiesser, L.D. Harwell, M.S. Oliver, M.D. Baldwin, M. T. Ensz, M. Essien, J. Brooks, C.V. Robino, J.E. Smugeresky, W.H. Hofmeister, M. J. Wert, D.V. Nelson, Understanding thermal behavior in the LENS process, *Mater. Des.* 20 (1999) 107–113, [https://doi.org/10.1016/S0261-3069\(99\)00016-3](https://doi.org/10.1016/S0261-3069(99)00016-3).
- [81] W. Hofmeister, M. Griffith, Solidification in direct metal deposition by LENS processing, *JOM* 53 (2001) 30–34, <https://doi.org/10.1007/s11837-001-0066-z>.
- [82] M.K. Imran, S.H. Masood, M. Brandt, S. Bhattacharya, J. Mazumder, Direct metal deposition (DMD) of H13 tool steel on copper alloy substrate: evaluation of mechanical properties, *Mater. Sci. Eng.* 528 (2011) 3342–3349, <https://doi.org/10.1016/j.msea.2010.12.099>.
- [83] G.Y. Baek, K.Y. Lee, S.H. Park, D.S. Shim, Effects of substrate preheating during direct energy deposition on microstructure, hardness, tensile strength, and notch toughness, *Met. Mater. Int.* 23 (2017) 1204–1215, <https://doi.org/10.1007/s12540-017-7049-2>.
- [84] D.S. Shim, G.Y. Baek, S.B. Lee, J.H. Yu, Y.S. Choi, S.H. Park, Influence of heat treatment on wear behavior and impact toughness of AISI M4 coated by laser melting deposition, *Surf. Coatings. Technol.* 328 (2017) 219–230, <https://doi.org/10.1016/j.surcoat.2017.08.059>.
- [85] D.S. Shim, G.Y. Baek, J.S. Seo, G.Y. Shin, K.P. Kim, K.Y. Lee, Effect of layer thickness setting on deposition characteristics in direct energy deposition (DED) process, *Opt. Laser. Technol.* 86 (2016) 69–78, <https://doi.org/10.1016/j.optlastec.2016.07.001>.
- [86] A.J. Pinkerton, L. Li, Direct additive laser manufacturing using gas- and water-atomised H13 tool steel powders, *Int. J. Adv. Manuf. Technol.* 25 (2005) 471–479, <https://doi.org/10.1007/s00170-003-1844-2>.
- [87] C.D. Naiju, P.M. Anil, Influence of operating parameters on the reciprocating sliding wear of direct metal deposition (DMD) components using Taguchi method, *Procedia Eng.* 174 (2017) 1016–1027, <https://doi.org/10.1016/j.proeng.2017.01.254>.
- [88] A. Yadollahi, N. Shamsaei, Y. Hammi, M.F. Horstemeyer, Quantification of tensile damage evolution in additive manufactured austenitic stainless steels, *Mater. Sci. Eng.* 657 (2016) 399–405, <https://doi.org/10.1016/j.msea.2016.01.067>.
- [89] P. Guo, B. Zou, C. Huang, H. Gao, Study on microstructure, mechanical properties and machinability of efficiently additive manufactured AISI 316L stainless steel by high-power direct laser deposition, *J. Mater. Process. Technol.* 240 (2017) 12–22, <https://doi.org/10.1016/j.jmatprotec.2016.09.005>.
- [90] P. Pratt, S.D. Felicelli, L. Wang, C.R. Hubbard, Residual stress measurement of laser-engineered net shaping AISI 410 thin plates using neutron diffraction, *Metall. Mater. Trans. S* 39 (2008) 3155–3163, <https://doi.org/10.1007/s11661-008-9660-9>.
- [91] L. Wang, S.D. Felicelli, P. Pratt, Residual stresses in LENS-deposited AISI 410 stainless steel plates, *Mater. Sci. Eng.* 496 (2008) 234–241, <https://doi.org/10.1016/j.msea.2008.05.044>.
- [92] Y. Liu, A. Li, X. Cheng, S.Q. Zhang, H.M. Wang, Effects of heat treatment on microstructure and tensile properties of laser melting deposited AISI 431 martensitic stainless steel, *Mater. Sci. Eng.* 666 (2016) 27–33, <https://doi.org/10.1016/j.msea.2016.04.014>.
- [93] X. Wang, D. Deng, M. Qi, H. Zhang, Influences of deposition strategies and oblique angle on properties of AISI 316L stainless steel oblique thin-walled part by direct laser fabrication, *Opt. Laser. Technol.* 80 (2016) 138–144, <https://doi.org/10.1016/j.optlastec.2016.01.002>.
- [94] J.A. Brooks, T.J. Headley, C.V. Robino, Microstructures of laser deposited 304L austenitic stainless steel, *MRS Online Proc. Libr.* 625 (2000) 21, <https://doi.org/10.1557/PROC-625-21>.
- [95] V.D. Manvatkar, A.A. Gokhale, G. Jagan Reddy, A. Venkataramana, A. De, Estimation of melt pool dimensions, thermal cycle, and hardness distribution in the laser-engineered net shaping process of austenitic stainless steel, *Metall. Mater. Trans. S* 42 (2011) 4080–4087, <https://doi.org/10.1007/s11661-011-0787-8>.
- [96] J.C. Haley, J.M. Schoenung, E.J. Lavernia, Observations of particle-melt pool impact events in directed energy deposition, *Addit. Manuf.* 22 (2018) 368–374, <https://doi.org/10.1016/j.addma.2018.04.028>.
- [97] K.L. Terrassa, J.C. Haley, B.E. MacDonald, J.M. Schoenung, Reuse of powder feedstock for directed energy deposition, *Powder Technol.* 338 (2018) 819–829, <https://doi.org/10.1016/j.powtec.2018.07.065>.
- [98] Z. peng Ye, Z. jing Zhang, X. Jin, M.Z. Xiao, J. zhou Su, Study of hybrid additive manufacturing based on pulse laser wire depositing and milling, *Int. J. Adv. Manuf. Technol.* 88 (2017) 2237–2248, <https://doi.org/10.1007/s00170-016-8894-8>.
- [99] T.R. Smith, J.D. Sugar, C. San Marchi, J.M. Schoenung, Strengthening mechanisms in directed energy deposited austenitic stainless steel, *Acta Mater.* 164 (2019) 728–740, <https://doi.org/10.1016/j.actamat.2018.11.021>.
- [100] C.A. Bronkhorst, J.R. Mayeur, V. Livescu, R. Pokharel, D.W. Brown, G.T. Gray, Structural representation of additively manufactured 316L austenitic stainless steel, *Int. J. Plast.* 118 (2019) 70–86, <https://doi.org/10.1016/j.ijplas.2019.01.012>.
- [101] M.H. Farshidianfar, A. Khajepour, A.P. Gerlich, Effect of real-time cooling rate on microstructure in Laser Additive Manufacturing, *J. Mater. Process. Technol.* 231 (2016) 468–478, <https://doi.org/10.1016/j.jmatprotec.2016.01.017>.
- [102] M. Ma, Z. Wang, X. Zeng, A comparison on metallurgical behaviors of 316L stainless steel by selective laser melting and laser cladding deposition, *Mater. Sci. Eng.* 685 (2017) 265–273, <https://doi.org/10.1016/j.msea.2016.12.112>.
- [103] N. Yang, J. Yee, B. Zheng, K. Gaiser, T. Reynolds, L. Clemon, W.Y. Lu, J. M. Schoenung, E.J. Lavernia, Process-structure-property relationships for 316L stainless steel fabricated by additive manufacturing and its implication for component engineering, *J. Therm. Spray Technol.* 26 (2017) 610–626, <https://doi.org/10.1007/s11666-016-0480-y>.
- [104] G.T. Gray, V. Livescu, P.A. Rigg, C.P. Trujillo, C.M. Cady, S.R. Chen, J. S. Carpenter, T.J. Lienert, S.J. Fensin, Structure/property (constitutive and spallation response) of additively manufactured 316L stainless steel, *Acta Mater.* 138 (2017) 140–149, <https://doi.org/10.1016/j.actamat.2017.07.045>.
- [105] A. Yadollahi, N. Shamsaei, S.M. Thompson, D.W. Seely, Effects of process time interval and heat treatment on the mechanical and microstructural properties of direct laser deposited 316L stainless steel, *Mater. Sci. Eng.* 644 (2015) 171–183, <https://doi.org/10.1016/j.msea.2015.07.056>.
- [106] F. Weng, S. Gao, J. Jiang, J.J. Wang, P. Guo, A novel strategy to fabricate thin 316L stainless steel rods by continuous directed energy deposition in Z direction,

- Addit. Manuf. 27 (2019) 474–481, <https://doi.org/10.1016/j.addma.2019.03.024>.
- [107] G.T. Gray III, V. Livescu, P.A. Rigg, C.P. Trujillo, C.M. Cady, S.R. Chen, J. S. Carpenter, T.J. Lienert, S. Fensin, Structure/property (constitutive and dynamic strength/damage) characterization of additively manufactured 316L SS, EPJ Web Conf. 94 (2015), 02006, <https://doi.org/10.1051/epjconf/20159402006>.
- [108] M. Ziatała, T. Durejko, M. Polański, I. Kunce, T. Płociński, W. Zieliński, M. Łazińska, W. Stępiński, T. Czujko, K.J. Kurzydowski, Z. Bojar, The microstructure, mechanical properties and corrosion resistance of 316 L stainless steel fabricated using laser engineered net shaping, Mater. Sci. Eng. 677 (2016) 1–10, <https://doi.org/10.1016/j.msea.2016.09.028>.
- [109] S. Karnati, N. Matta, T. Sparks, F. Liou, Vision-based process monitoring for Laser Metal deposition processes, in: 24th Int. Solid Freeform Fabrication Symp., 2013, pp. 88–94.
- [110] K. Zhang, S. Wang, W. Liu, X. Shang, Characterization of stainless steel parts by laser metal deposition shaping, Mater. Des. 55 (2014) 104–119, <https://doi.org/10.1016/j.matdes.2013.09.006>.
- [111] J.I. Arrizubieta, A. Lamikiz, F. Klocke, S. Martínez, K. Arntz, E. Ukar, Evaluation of the relevance of melt pool dynamics in Laser Material Deposition process modeling, Int. J. Heat Mass Tran. 115 (2017) 80–91, <https://doi.org/10.1016/j.ijheatmasstransfer.2017.07.011>.
- [112] J.I. Arrizubieta, A. Lamikiz, M. Cortina, E. Ukar, A. Alberdi, Hardness, grain size and porosity formation prediction on the Laser Metal Deposition of AISI 304 stainless steel, Int. J. Mach. Tool Manufact. 135 (2018) 53–64, <https://doi.org/10.1016/j.ijmachtools.2018.08.004>.
- [113] X. Xu, G. Mi, Y. Luo, P. Jiang, X. Shao, C. Wang, Morphologies, microstructures, and mechanical properties of samples produced using laser metal deposition with 316 L stainless steel wire, Opt. Laser. Eng. 94 (2017) 1–11, <https://doi.org/10.1016/j.optlaseng.2017.02.008>.
- [114] M. Rombouts, G. Maes, W. Hendrix, E. Delarbre, F. Motmans, Surface finish after laser metal deposition, Phys. Procedia 41 (2013) 810–814, <https://doi.org/10.1016/j.phpro.2013.03.152>.
- [115] L. Wang, P. Pratt, S.D. Felicelli, H. El Kadiri, J.T. Berry, P.T. Wang, M. F. Horstemeyer, Experimental analysis of porosity formation in laser-assisted powder deposition process, in: Suppl. Proc., vol. 1, TMS, 2009, pp. 389–396. *Fabrication, Materials, Processing and Properties*.
- [116] B. Vamsi Krishna, A. Bandyopadhyay, Surface modification of AISI 410 stainless steel using laser engineered net shaping (LENS™), Mater. Des. 30 (2009) 1490–1496, <https://doi.org/10.1016/j.matdes.2008.08.003>.
- [117] X. Wang, D. Deng, H. Yi, H. Xu, S. Yang, H. Zhang, Influences of pulse laser parameters on properties of AISI316L stainless steel thin-walled part by laser material deposition, Opt. Laser. Technol. 92 (2017) 5–14, <https://doi.org/10.1016/j.optlastec.2016.12.021>.
- [118] F. Ning, W. Cong, Microstructures and mechanical properties of Fe-Cr stainless steel parts fabricated by ultrasonic vibration-assisted laser engineered net shaping process, Mater. Lett. 179 (2016) 61–64, <https://doi.org/10.1016/j.matlet.2016.05.055>.
- [119] G.A. Ravi, X.J. Hao, N. Wain, X. Wu, M.M. Attallah, Direct laser fabrication of three dimensional components using SC420 stainless steel, Mater. Des. 47 (2013) 731–736, <https://doi.org/10.1016/j.matdes.2012.12.062>.
- [120] D.F. Susan, J.D. Puskar, J.A. Brooks, C.V. Robino, Quantitative characterization of porosity in stainless steel LENS powders and deposits, Mater. Char. 57 (2006) 36–43, <https://doi.org/10.1016/j.matchar.2005.12.005>.
- [121] Y.D. Wang, H.B. Tang, Y.L. Fang, H.M. Wang, Effect of heat treatment on microstructure and mechanical properties of laser melting deposited 1Cr12Ni2WMoVNb steel, Mater. Sci. Eng. 528 (2010) 474–479, <https://doi.org/10.1016/j.msea.2010.09.038>.
- [122] G.T. Gray, V. Livescu, P.A. Rigg, C.P. Trujillo, C.M. Cady, S.-R. Chen, J. S. Carpenter, T.J. Lienert, S.J. Fensin, C.M. Knapp, R.A. Beal, B. Morrow, O. F. Dippo, D.R. Jones, D.T. Martinez, J.A. Valdez, Technical report. LA-UR-16-27337: L2 milestone 5433: Characterization of Dynamic Behavior of AM and Conventionally Processed Stainless Steel (316L and 304L), National Nuclear Security Administration, USA, 2016, <https://doi.org/10.2172/1329535>.
- [123] L. Wang, S.D. Felicelli, J.E. Craig, Thermal modeling and experimental validation in the LENS™ process, in: Proc. 2007 Int. Solid Freeform Fabrication Symp., 2007, pp. 100–111, <https://doi.org/10.26153/tsw/7197>.
- [124] K.L. Terrassa, T.R. Smith, S. Jiang, J.D. Sugar, J.M. Schoenung, Improving build quality in directed energy deposition by cross-hatching, Mater. Sci. Eng. 765 (2019), 138269, <https://doi.org/10.1016/j.msea.2019.138269>.
- [125] B. Zheng, J.C. Haley, N. Yang, J. Yee, K.W. Terrassa, Y. Zhou, E.J. Lavernia, J. M. Schoenung, On the evolution of microstructure and defect control in 316L SS components fabricated via directed energy deposition, Mater. Sci. Eng. 764 (2019) 138243, <https://doi.org/10.1016/j.msea.2019.138243>.
- [126] Y. Xue, A. Pascu, M.F. Horstemeyer, L. Wang, P.T. Wang, Microporosity effects on cyclic plasticity and fatigue of LENS™-processed steel, Acta Mater. 58 (2010) 4029–4038, <https://doi.org/10.1016/j.actamat.2010.03.014>.
- [127] T.R. Smith, J.D. Sugar, C. San Marchi, J.M. Schoenung, Orientation effects on fatigue behavior of additively manufactured stainless steel, in: ASME 2017 Pressure Vessels and Piping Conf., Vol. 6A: Materials and Fabrication, American Society of Mechanical Engineers, 2017, <https://doi.org/10.1115/PVP2017-65948> paper PVP2017-65948.
- [128] M.A. Jackson, A. Kim, J.A. Manders, D.J. Thoma, F.E. Pfefferkorn, Production of mechanically-generated 316L stainless steel feedstock and its performance in directed energy deposition processing as compared to gas-atomized powder, CIRP J. Manuf. Sci. Technol. 31 (2020) 233–243, <https://doi.org/10.1016/j.cirpj.2020.05.014>.
- [129] D.R. Feenstra, V. Cruz, X. Gao, A. Molotnikov, N. Birbilis, Effect of build height on the properties of large format stainless steel 316L fabricated via directed energy deposition, Addit. Manuf. 34 (2020), 101205, <https://doi.org/10.1016/j.addma.2020.101205>.
- [130] Y. Hwa, C.S. Kumai, T.M. Devine, N. Yang, J.K. Yee, R. Hardwick, K. Burgmann, Microstructural banding of directed energy deposition-additively manufactured 316L stainless steel, J. Mater. Sci. Technol. 69 (2020) 96–105, <https://doi.org/10.1016/j.jmst.2020.08.022>.
- [131] J. Gordon, J. Hochhalter, C. Haden, D.G. Harlow, Enhancement in fatigue performance of metastable austenitic stainless steel through directed energy deposition additive manufacturing, Mater. Des. 168 (2019), 107630, <https://doi.org/10.1016/j.matdes.2019.107630>.
- [132] A. Aversa, A. Saboori, E. Librera, M. de Chirico, S. Biamino, M. Lombardi, P. Fino, The role of directed energy deposition atmosphere mode on the microstructure and mechanical properties of 316L samples, Addit. Manuf. 34 (2020), 101274, <https://doi.org/10.1016/j.addma.2020.101274>.
- [133] E. Azinpour, R. Darabi, J.C. de Sa, A. Santos, J. Hodek, J. Dzugan, Fracture analysis in directed energy deposition (DED) manufactured 316L stainless steel using a phase-field approach, Finite Elem. Anal. Des. 177 (2020), 103417, <https://doi.org/10.1016/j.finel.2020.103417>.
- [134] Y. Balit, L.-R. Joly, F. Szmytko, S. Durbecq, E. Charkaluk, A. Constantinescu, Self-heating behavior during cyclic loadings of 316L stainless steel specimens manufactured or repaired by Directed Energy Deposition, Mater. Sci. Eng. 768 (2020), 139476, <https://doi.org/10.1016/j.msea.2020.139476>.
- [135] R. Koike, T. Matsumoto, T. Aoyama, M. Kondo, Fabrication method for stainless steel foam block in directed energy deposition, CIRP Ann 69 (2020) 173–176, <https://doi.org/10.1016/j.cirp.2020.04.060>.
- [136] M.A. Jackson, J.D. Morrow, D.J. Thoma, F.E. Pfefferkorn, A comparison of 316 L stainless steel parts manufactured by directed energy deposition using gas-atomized and mechanically-generated feedstock, CIRP Ann 69 (2020) 165–168, <https://doi.org/10.1016/j.cirp.2020.04.042>.
- [137] L. Simoneau, A. Bois-Brochu, C. Blais, Tensile properties of built and rebuilt/repaired specimens of 316L stainless steel using directed energy deposition, J. Mater. Eng. Perform. 29 (2020) 6139–6146, <https://doi.org/10.1007/s11665-020-05087-z>.
- [138] Y. Balit, C. Guévenoux, A. Tanguy, M.V. Upadhyay, E. Charkaluk, A. Constantinescu, High resolution digital image correlation for microstructural strain analysis of a stainless steel repaired by Directed Energy Deposition, Mater. Lett. 270 (2020), 127632, <https://doi.org/10.1016/j.matlet.2020.127632>.
- [139] A. Saboori, G. Piscopo, M. Lai, A. Salmi, S. Biamino, An investigation on the effect of deposition pattern on the microstructure, mechanical properties and residual stress of 316L produced by Directed Energy Deposition, Mater. Sci. Eng. 780 (2020), 139179, <https://doi.org/10.1016/j.msea.2020.139179>.
- [140] K. Benarji, Y.R. Kumar, C.P. Paul, A.N. Jinoop, K.S. Bindra, Parametric investigation and characterization on SS316 built by laser-assisted directed energy deposition, Proc. Inst. Mech. Eng. L: J. Mater. Des. Appl. 234 (2020) 452–466, <https://doi.org/10.1177/1464420719894718>.
- [141] S. Kersten, M. Pranievicz, T. Kurfess, C. Saldana, Build orientation effects on mechanical properties of 316SS components produced by directed energy deposition, Procedia Manuf. 48 (2020) 730–736, <https://doi.org/10.1016/j.promfg.2020.05.106>.
- [142] P. Rangaswamy, M.L. Griffith, M.B. Prime, T.M. Holden, R.B. Rogge, J. M. Edwards, R.J. Sebring, Residual stresses in LENS® components using neutron diffraction and contour method, Mater. Sci. Eng. 399 (2005) 72–83, <https://doi.org/10.1016/j.msea.2005.02.019>.
- [143] X. Chen, B. Chen, X. Cheng, G. Li, Z. Huang, Microstructure and properties of hybrid additive manufacturing 316L component by directed energy deposition and laser remelting, J. Iron Steel Res. Int. 27 (2020) 842–848, <https://doi.org/10.1007/s42243-020-00396-y>.
- [144] P.Y. Lin, F.C. Shen, K.T. Wu, S.J. Hwang, H.H. Lee, Process optimization for directed energy deposition of SS316L components, Int. J. Adv. Manuf. Technol. 111 (2020) 1387–1400, <https://doi.org/10.1007/s00170-020-06113-z>.
- [145] N. Eliaz, N. Foucks, D. Geva, S. Oren, N. Shrikri, D. Vaknin, D. Fishman, O. Levi, Comparative quality control of titanium alloy Ti-6Al-4V, 17-4 PH stainless steel, and aluminum alloy 4047 either manufactured or repaired by laser engineered net shaping (LENS), Materials 13 (2020) 4171, <https://doi.org/10.3390/mater13184171>.
- [146] L. Wang, S. Felicelli, Y. Goorochurn, P.T. Wang, M.F. Horstemeyer, Optimization of the LENS® process for steady molten pool size, Mater. Sci. Eng. 474 (2008) 148–156, <https://doi.org/10.1016/j.msea.2007.04.119>.
- [147] W. Hofmeister, M. Griffith, M. Ensz, J. Smugeresky, Solidification in direct metal deposition by LENS processing, JOM 53 (2001) 30–34, <https://doi.org/10.1007/s11837-001-0066-z>.
- [148] J.C. Haley, B. Zheng, U.S. Bertoli, A.D. Dupuy, J.M. Schoenung, E.J. Lavernia, Working distance passive stability in laser directed energy deposition additive manufacturing, Mater. Des. 161 (2019) 86–94, <https://doi.org/10.1016/j.matdes.2018.11.021>.
- [149] B. Zheng, Y. Zhou, J.E. Smugeresky, J.M. Schoenung, E.J. Lavernia, Thermal behavior and microstructure evolution during laser deposition with laser-engineered net shaping: Part II. Experimental investigation and discussion, Metall. Mater. Trans. A Phys. Metall. Mater. Sci. 39 (2008) 2237–2245, <https://doi.org/10.1007/s11661-008-9566-6>.
- [150] A. Yadollahi, D. Seely, B. Patton, N. Shamsaei, S.M. Thompson, Mechanical and microstructural properties of lens-produced aisi 316L stainless steel, in: Proc. AIAA SciTech. 2015, American Institute of Aeronautics and Astronautics, 2015, <https://doi.org/10.2514/6.2015-1355>.

- [151] A. Revati, M. Das, V.K. Balla, D. Devika, D. Sen, G. Manivasagam, Surface engineering of LENSTi-6Al-4V to obtain nano- and micro-surface topography for orthopedic application, *Nanomed. Nanotechnol. Biol. Med.* 18 (2019) 157–168, <https://doi.org/10.1016/j.nano.2019.02.010>.
- [152] A. Revati, D. Mitun, V.K. Balla, S. Dwaipayan, D. Devika, G. Manivasagam, Surface properties and cytocompatibility of Ti-6Al-4V fabricated using laser engineered net shaping, *Mater. Sci. Eng. C* 100 (2019) 104–116, <https://doi.org/10.1016/j.msec.2019.02.099>.
- [153] M. Neikter, P. Åkerfeldt, R. Pederson, M.L. Antti, V. Sandell, Microstructural characterization and comparison of Ti-6Al-4V manufactured with different additive manufacturing processes, *Mater. Char.* 143 (2018) 68–75, <https://doi.org/10.1016/j.matchar.2018.02.003>.
- [154] G.J. Marshall, W.J. Young, S.M. Thompson, D. Seely, N. Shamsaei, Effect of substrate thickness on micro-hardness of direct laser deposited Ti-6Al-4V parts, in: 56th AIAA/ASCE/AHS/ASC Struct. Struct. Dyn. Mater. Conf., American Institute of Aeronautics and Astronautics, 2015, <https://doi.org/10.2514/6.2015-1356> paper AIAA 2015-1356.
- [155] Y.M. Ren, X. Lin, X. Fu, H. Tan, J. Chen, W.D. Huang, Microstructure and deformation behavior of Ti-6Al-4V alloy by high-power laser solid forming, *Acta Mater.* 132 (2017) 82–95, <https://doi.org/10.1016/j.actamat.2017.04.026>.
- [156] Q. Yang, P. Zhang, L. Cheng, Z. Min, M. Chyu, A.C. To, Finite element modeling and validation of thermomechanical behavior of Ti-6Al-4V in directed energy deposition additive manufacturing, *Addit. Manuf.* 12 (2016) 169–177, <https://doi.org/10.1016/j.addma.2016.06.012>.
- [157] O. Yelola, P. Crawforth, R. M'Saoubi, A.T. Clare, On the machinability of directed energy deposited Ti6Al4V, *Addit. Manuf.* 19 (2018) 39–50, <https://doi.org/10.1016/j.addma.2017.11.005>.
- [158] X. Lu, X. Lin, M. Chiumenti, M. Cervera, Y. Hu, X. Ji, L. Ma, H. Yang, W. Huang, Residual stress and distortion of rectangular and S-shaped Ti-6Al-4V parts by Directed Energy Deposition: modelling and experimental calibration, *Addit. Manuf.* 26 (2019) 166–179, <https://doi.org/10.1016/j.addma.2019.02.001>.
- [159] J. Li, Q. Wang, P. Michaleris, E.W. Reutzel, Model prediction for deposition height during a direct metal deposition process, in: American Control Conf, 2017, pp. 2188–2194, <https://doi.org/10.23919/ACC.2017.7963277>.
- [160] S.J. Wolff, S. Lin, E.J. Faierson, W.K. Liu, G.J. Wagner, J. Cao, A framework to link localized cooling and properties of directed energy deposition (DED)-processed Ti-6Al-4V, *Acta Mater.* 132 (2017) 106–117, <https://doi.org/10.1016/j.actamat.2017.04.027>.
- [161] H. Tan, M. Guo, A.T. Clare, X. Lin, J. Chen, W. Huang, Microstructure and properties of Ti-6Al-4V fabricated by low-power pulsed laser directed energy deposition, *J. Mater. Sci. Technol.* 35 (2019) 2027–2037, <https://doi.org/10.1016/j.jmst.2019.05.008>.
- [162] G.T. Loughnane, S.L. Kuntz, N. Klingbeil, J.M. Sosa, J. Irwin, A.R. Nassar, E. W. Reutzel, Application of a microstructural characterization uncertainty quantification framework to Widmanstätten-laths in additive manufactured Ti-6Al-4V, *Proc. 25th Int. Solid Free. Fabr. Symp.* (2015) 647–663.
- [163] H.R. Sandgren, Y. Zhai, D.A. Lados, P.A. Shade, J.C. Schuren, M.A. Groeber, P. Kenesei, A.G. Gavras, Characterization of fatigue crack growth behavior in LENSTi-6Al-4V using high-energy synchrotron x-ray micromotography, *Addit. Manuf.* 12 (2016) 132–141, <https://doi.org/10.1016/j.addma.2016.09.002>.
- [164] Y. Zhai, D.A. Lados, E.J. Brown, G.N. Vigilante, Fatigue crack growth behavior and microstructural mechanisms in Ti-6Al-4V manufactured by laser engineered net shaping, *Int. J. Fatig.* 93 (2016) 51–63, <https://doi.org/10.1016/j.ijfatigue.2016.08.009>.
- [165] A.R. Nassar, T.J. Spurgeon, E.E. Reutzel, Sensing defects during directed-energy additive manufacturing of metal parts using optical emissions spectroscopy, in: 25th Annu. Int. Solid Freeform Fabrication Symp., 2014, pp. 278–287, <https://doi.org/10.1017/CBO9781107415324.004>.
- [166] A.R. Nassar, E.W. Reutzel, Beyond layer-by-layer additive manufacturing – voxel-wise directed energy deposition, in: Annu. Int. Solid Freeform Fabrication Symp., 2013, pp. 19–43.
- [167] Y. Zhai, H. Galarraga, D.A. Lados, Microstructure evolution, tensile properties, and fatigue damage mechanisms in Ti-6Al-4V alloys fabricated by two additive manufacturing techniques, *Procedia Eng.* 114 (2015) 658–666, <https://doi.org/10.1016/j.proeng.2015.08.007>.
- [168] A.R. Nassar, E.W. Reutzel, Additive manufacturing of Ti-6Al-4V using a pulsed laser beam, *Metall. Mater. Trans.* 46 (2015) 2781–2789, <https://doi.org/10.1007/s11661-015-2838-z>.
- [169] G.J. Marshall, W.J. Young, S.M. Thompson, N. Shamsaei, S.R. Daniewicz, S. Shao, Understanding the microstructure formation of Ti-6Al-4V during direct laser deposition via in-situ thermal monitoring, *JOM* 68 (2016) 778–790, <https://doi.org/10.1007/s11837-015-1767-z>.
- [170] Y. Han, W. Lu, T. Jarvis, J. Shurvinton, X. Wu, Investigation on the microstructure of direct laser additive manufactured Ti6Al4V alloy, *Mater. Res.* 18 (2015) 24–28, <https://doi.org/10.1590/1516-1439.322214>.
- [171] K. Shah, A.J. Pinkerton, A. Salman, L. Li, Effects of melt pool variables and process parameters in laser direct metal deposition of aerospace alloys, *Mater. Manuf. Process.* 25 (2010) 1372–1380, <https://doi.org/10.1080/10426914.2010.480999>.
- [172] M. Buciumeanu, A. Bagheri, N. Shamsaei, S.M. Thompson, F.S. Silva, B. Henriques, Tribocorrosion behavior of additive manufactured Ti-6Al-4V biomedical alloy, *Tribol. Int.* 119 (2018) 381–388, <https://doi.org/10.1016/j.triboint.2017.11.032>.
- [173] S. Wolff, T. Lee, E. Faierson, K. Ehmann, J. Cao, Anisotropic properties of directed energy deposition (DED)-processed Ti-6Al-4V, *J. Manuf. Process.* 24 (2016) 397–405, <https://doi.org/10.1016/j.jmapro.2016.06.020>.
- [174] M. Gharbi, P. Peyre, C. Gorny, S. Morville, P. Le, D. Carron, R. Fabbro, Influence of various process conditions on surface finishes induced by the direct metal deposition laser technique on a Ti – 6Al – 4V alloy, *J. Mater. Process. Technol.* 213 (2013) 791–800, <https://doi.org/10.1016/j.jmaprotec.2012.11.015>.
- [175] B.A. Szost, S. Terzi, F. Martina, D. Boisselier, A. Prytuliak, T. Pirling, M. Hofmann, D.J. Jarvis, A comparative study of additive manufacturing techniques: residual stress and microstructural analysis of CLAD and WAAM printed Ti-6Al-4V components, *Mater. Des.* 89 (2016) 559–567, <https://doi.org/10.1016/j.matedes.2015.09.115>.
- [176] M.N. Ahsan, A.J. Pinkerton, R.J. Moat, J. Shackleton, A comparative study of laser direct metal deposition characteristics using gas and plasma-atomized Ti-6Al-4V powders, *Mater. Sci. Eng.* 528 (2011) 7648–7657, <https://doi.org/10.1016/j.mse.2011.06.074>.
- [177] A.W. Prabhu, T. Vincent, A. Chaudhary, W. Zhang, S.S. Babu, Effect of microstructure and defects on fatigue behaviour of directed energy deposited Ti-6Al-4V, *Sci. Technol. Weld. Join.* 20 (2015) 659–669, <https://doi.org/10.1179/1362171815Y.0000000050>.
- [178] D.A. Kriczky, J. Irwin, E.W. Reutzel, P. Michaleris, A.R. Nassar, J. Craig, 3D spatial reconstruction of thermal characteristics in directed energy deposition through optical thermal imaging, *J. Mater. Process. Technol.* 221 (2015) 172–186, <https://doi.org/10.1016/j.jmaprotec.2015.02.021>.
- [179] J. Li, Q. Wang, P. (Pan) Michaleris, E.W. Reutzel, A.R. Nassar, An extended lumped-parameter model of melt-pool geometry to predict part height for directed energy deposition, *J. Manuf. Sci. Eng.* 139 (2017), 091016, <https://doi.org/10.1115/1.4037235>.
- [180] A.R. Nassar, J.S. Keist, E.W. Reutzel, T.J. Spurgeon, Intra-layer closed-loop control of build plan during directed energy additive manufacturing of Ti-6Al-4V, *Addit. Manuf.* 6 (2015) 39–52, <https://doi.org/10.1016/j.addma.2015.03.005>.
- [181] Y. Byun, S. Lee, S.M. Seo, J. taek Yeom, S.E. Kim, N. Kang, J. Hong, Effects of Cr and Fe addition on microstructure and tensile properties of Ti-6Al-4V prepared by direct energy deposition, *Met. Mater. Int.* 24 (2018) 1213–1220, <https://doi.org/10.1007/s12540-018-0148-x>.
- [182] J.N. Rousseau, A. Bois-Brochu, C. Blais, Effect of oxygen content in new and reused powder on microstructural and mechanical properties of Ti6Al4V parts produced by directed energy deposition, *Addit. Manuf.* 23 (2018) 197–205, <https://doi.org/10.1016/j.addma.2018.08.011>.
- [183] M. Shukla, R.M. Mahamood, E.T. Akinlabi, S. Pityana, Effect of laser power and powder flow rate on properties of laser metal deposited Ti6Al4V, *Proc. World Acad. Sci. Eng. Technol.* 6 (2012) 1268, <https://doi.org/10.1016/j.matpr.2015.07.233>.
- [184] G.J. Marshall, S.M. Thompson, N. Shamsaei, Data indicating temperature response of Ti-6Al-4V thin-walled structure during its additive manufacture via Laser Engineered Net Shaping, *Data Brief* 7 (2016) 697–703, <https://doi.org/10.1016/j.dib.2016.02.084>.
- [185] Z. Li, X. Cheng, J. Li, H. Wang, Thermal expansion properties of laser melting deposited Ti-6.5Al-22r-1Mo-1V alloy during $\alpha + \beta$ zone annealing, *Mater. Char.* 128 (2017) 115–122, <https://doi.org/10.1016/j.matchar.2017.01.019>.
- [186] S. Lu, R. Bao, K. Wang, D. Liu, Y. Wu, B. Fei, Fatigue crack growth behaviour in laser melting deposited Ti-6.5Al-3.5Mo-1.5Zr-0.3Si alloy, *Mater. Sci. Eng.* 690 (2017) 378–386, <https://doi.org/10.1016/j.mse.2017.03.001>.
- [187] F. Zhang, M. Mei, K. Al-Hamdan, H. Tan, A.T. Clare, Novel nucleation mechanisms through satelliting in direct metal deposition of Ti-15Mo, *Mater. Lett.* 213 (2018) 197–200, <https://doi.org/10.1016/j.matlet.2017.11.036>.
- [188] X.J. Tian, S.Q. Zhang, A. Li, H.M. Wang, Effect of annealing temperature on the notch impact toughness of a laser melting deposited titanium alloy Ti-4Al-1.5Mn, *Mater. Sci. Eng.* 527 (2010) 1821–1827, <https://doi.org/10.1016/j.msea.2009.11.014>.
- [189] X.J. Tian, S.Q. Zhang, H.M. Wang, The influences of anneal temperature and cooling rate on microstructure and tensile properties of laser deposited Ti-4Al-1.5Mn titanium alloy, *J. Alloys Compd.* 608 (2014) 95–101, <https://doi.org/10.1016/j.jallcom.2014.04.058>.
- [190] Y. Zhu, X. Tian, J. Li, H. Wang, Microstructure evolution and layer bands of laser melting deposition Ti-6.5Al-3.5Mo-1.5Zr-0.3Si titanium alloy, *J. Alloys Compd.* 616 (2014) 468–474, <https://doi.org/10.1016/j.jallcom.2014.07.161>.
- [191] K.I. Schwendner, R. Banerjee, P.C. Collins, C.A. Brice, H.L. Fraser, Direct laser deposition of alloys from elemental powder blends, *Scripta Mater.* 45 (2001) 1123–1129, [https://doi.org/10.1016/S1359-6462\(01\)01107-1](https://doi.org/10.1016/S1359-6462(01)01107-1).
- [192] R. Banerjee, P.C. Collins, H.L. Fraser, Phase evolution in laser-deposited titanium-chromium alloys, *Metall. Mater. Trans.* 33 (2002) 2129–2138, <https://doi.org/10.1007/s11661-002-0044-2>.
- [193] S.A. Mantri, R. Banerjee, Microstructure and micro-texture evolution of additively manufactured β -Ti alloys, *Addit. Manuf.* 23 (2018) 86–98, <https://doi.org/10.1016/j.addma.2018.07.013>.
- [194] R.M. Mahamood, E.T. Akinlabi, Effect of laser power on surface finish during laser metal deposition process, *Proc. World Congr. Eng. Computer Sci. II* (2014) 22–24.
- [195] Y. Zhai, D.A. Lados, E.J. Brown, G.N. Vigilante, Understanding the microstructure and mechanical properties of Ti-6Al-4V and inconel 718 alloys manufactured by laser engineered net shaping, *Addit. Manuf.* 27 (2019) 334–344, <https://doi.org/10.1016/j.addma.2019.02.017>.
- [196] H. Mohseni, P. Nandwana, A. Tsoi, R. Banerjee, T.W. Scharf, In situ nitrided titanium alloys: microstructural evolution during solidification and wear, *Acta Mater.* 83 (2015) 61–74, <https://doi.org/10.1016/j.actamat.2014.09.026>.

- [197] Y. Zhai, H. Galarraga, D.A. Lados, Microstructure, static properties, and fatigue crack growth mechanisms in Ti-6Al-4V fabricated by additive manufacturing: LENS and EBM, Eng. Fail. Anal. 69 (2016) 3–14, <https://doi.org/10.1016/j.engfailanal.2016.05.036>.
- [198] M.S. Dargusch, G. Wang, D. Kent, M. Bermingham, J. Venezuela, J.E. Frith, Z. Yu, S. Yu, Z. Shi, Comparison of the microstructure and biocorrosion properties of additively manufactured and conventionally fabricated near β Ti-25Nb-3Zr-3Mo-2Sn alloy, ACS Biomater. Sci. Eng. 5 (2019) 5844–5856, <https://doi.org/10.1021/acsbiomaterials.9b00596>.
- [199] S. Liu, Y.C. Shin, Prediction of 3D microstructure and phase distributions of Ti6Al4V built by the directed energy deposition process via combined multi-physics models, Addit. Manuf. 34 (2020), 101234, <https://doi.org/10.1016/j.addma.2020.101234>.
- [200] J. Wang, Q. Luo, H. Wang, Y. Wu, X. Cheng, H. Tang, Microstructure characteristics and failure mechanisms of Ti-48Al-2Nb-2Cr titanium aluminide intermetallic alloy fabricated by directed energy deposition technique, Addit. Manuf. 32 (2020), 101007, <https://doi.org/10.1016/j.addma.2019.101007>.
- [201] R. Chen, C. Tan, Z. You, Z. Li, S. Zhang, Z. Nie, X. Yu, X. Zhao, Effect of α phase on high-strain rate deformation behavior of laser melting deposited Ti-6.5 Al-1Mo-1V-2Zr titanium alloy, Mater. Sci. Eng. 750 (2019) 81–90, <https://doi.org/10.1016/j.msea.2019.01.060>.
- [202] T. Wang, X. He, X. Wang, Y. Li, P-S-N curve description of laser metal deposition Ti-6.5 Al-2Zr-1Mo-1V titanium alloy after duplex annealing, Materials 12 (2019) 418, <https://doi.org/10.3390/ma12030418>.
- [203] X. Wang, X. He, T. Wang, Y. Li, The influence of the microtexture and orientation of columnar grains on the fatigue crack growth of directed energy deposited Ti-6.5 Al-2Cr-Mo-V alloys, Addit. Manuf. 35 (2020), 101174, <https://doi.org/10.1016/j.addma.2020.101174>.
- [204] Y. Wang, R. Chen, X. Cheng, Y. Zhu, J. Zhang, H. Wang, Effects of microstructure on fatigue crack propagation behavior in a bi-modal TC11 titanium alloy fabricated via laser additive manufacturing, J. Mater. Sci. Technol. 35 (2019) 403–408, <https://doi.org/10.1016/j.jmst.2018.10.031>.
- [205] D.R. Waryoba, J.S. Keist, C. Ranger, T.A. Palmer, Microtexture in additively manufactured Ti-6Al-4V fabricated using directed energy deposition, Mater. Sci. Eng. 734 (2018) 149–163, <https://doi.org/10.1016/j.msea.2018.07.098>.
- [206] K. Wang, R. Bao, S. Ren, D. Liu, C. Yan, Effect of microstructure on fatigue crack tip field of laser melting deposited Ti-5Al-5Mo-5V-1Cr-1Fe titanium alloy, MATEC Web Conf., EDP Sciences 165 (2018), 02009, <https://doi.org/10.1051/matecconf/201816502009>.
- [207] T. Bhardwaj, M. Shukla, N.K. Prasad, C.P. Paul, K.S. Bindra, Direct laser deposition-additive manufacturing of Ti-15Mo alloy: effect of build orientation induced surface topography on corrosion and bioactivity, Met. Mater. Int. 26 (2020) 1015–1029, <https://doi.org/10.1007/s12540-019-00464-3>.
- [208] J.D. Avila, M. Isik, A. Bandyopadhyay, Titanium-silicon on CoCr alloy for load-bearing implants using directed energy deposition-based additive manufacturing, ACS Appl. Mater. Interfaces 12 (2020) 51263–51272, <https://doi.org/10.1021/acsami.0c15279>.
- [209] A. Bandyopadhyay, M. Upadhyayula, K.D. Traxel, B. Onuiken, Influence of deposition orientation on fatigue response of LENSTM processed Ti6Al4V, Mater. Lett. 255 (2019), 126541, <https://doi.org/10.1016/j.matlet.2019.126541>.
- [210] A. Antolak-Dudka, P. Piatek, T. Durejko, P. Baranowski, J. Małachowski, M. Sarzyński, T. Czujko, Static and dynamic loading behavior of Ti6Al4V honeycomb structures manufactured by laser engineered net shaping (LENSTM) technology, Materials 12 (2019) 1225, <https://doi.org/10.3390/ma12081225>.
- [211] A. Szafrańska, A. Antolak-Dudka, P. Baranowski, P. Bogusz, D. Zasada, J. Małachowski, T. Czujko, Identification of mechanical properties for titanium alloy Ti-6Al-4V produced using LENSTM technology, Materials 12 (2019) 886, <https://doi.org/10.3390/ma12060886>.
- [212] S.M. Razavi, G.G. Bordonaro, P. Ferro, J. Torgersen, F. Berto, Fatigue behavior of porous Ti-6Al-4V made by laser-engineered net shaping, Materials 11 (2018) 284, <https://doi.org/10.3390/ma11020284>.
- [213] A. Sterling, N. Shamsaei, B. Torries, S.M. Thompson, Fatigue behaviour of additively manufactured Ti-6Al-4V, Procedia Eng. 133 (2015) 576–589, <https://doi.org/10.1016/j.proeng.2015.12.632>.
- [214] S.M.J. Razavi, F. Berto, Directed energy deposition versus wrought Ti-6Al-4V: a comparison of microstructure, fatigue behavior, and notch sensitivity, Adv. Eng. Mater. 21 (2019), 1900220, <https://doi.org/10.1002/adem.201900220>.
- [215] A.J. Sterling, B. Torries, N. Shamsaei, S.M. Thompson, D.W. Seely, Fatigue behavior and failure mechanisms of direct laser deposited Ti-6Al-4V, Mater. Sci. Eng. 655 (2016) 100–112, <https://doi.org/10.1016/j.mse.2015.12.026>.
- [216] M.N. Ahsan, R. Bradley, A.J. Pinkerton, Microcomputed tomography analysis of intralayer porosity generation in laser direct metal deposition and its causes, J. Laser Appl. 23 (2011), 022009, <https://doi.org/10.2351/1.3582311>.
- [217] K. Mutombo, Metallurgical evaluation of laser additive manufactured Ti6Al4V components, in: Rapid Product Development Association of South Africa (RAPDASA) Conf., 2013, pp. 4–6, <http://hdl.handle.net/10204/7243>.
- [218] B. Torries, N. Shamsaei, Fatigue behavior and modeling of additively manufactured Ti-6Al-4V including interlayer time interval effects, JOM (J. Occup. Med.) 69 (2017) 2698–2705, <https://doi.org/10.1007/s11837-017-2625-y>.
- [219] J. Li, X. Cheng, D. Liu, S.Q. Zhang, Z. Li, B. He, H.M. Wang, Phase evolution of a heat-treatable aluminum alloy during laser additive manufacturing, Mater. Lett. 214 (2018) 56–59, <https://doi.org/10.1016/j.matlet.2017.11.111>.
- [220] A. Singh, A. Ramakrishnan, G. Dinda, Direct Laser Metal Deposition of Al 7050 Alloy, 2017, <https://doi.org/10.4271/2017-01-0286>. SAE Technical Paper 2017-01-0286.
- [221] S. Ja-Ye, S. Do-Sik, Compressive behavior of porous materials fabricated by laser melting deposition using AlSi12 powder and foaming agent, Mater. Res. Express 6 (2019), 066581, <https://doi.org/10.1088/2053-1591/aafc5a>.
- [222] Y. Gao, J. Zhao, Y. Zhao, Z. Wang, H. Song, M. Gao, Effect of processing parameters on solidification defects behavior of laser deposited AlSi10Mg alloy, Vacuum 167 (2019) 471–478, <https://doi.org/10.1016/j.vacuum.2019.06.042>.
- [223] Y. Liu, C. Liu, W. Liu, Y. Ma, S. Tang, C. Liang, Q. Cai, C. Zhang, Optimization of parameters in laser powder deposition AlSi10Mg alloy using Taguchi method, Opt. Laser. Technol. 111 (2019) 470–480, <https://doi.org/10.1016/j.optlastec.2018.10.030>.
- [224] X. Wang, L. Li, J. Qu, W. Tao, Microstructure and mechanical properties of laser metal deposited AlSi10Mg alloys, Mater. Sci. Technol. 35 (2019) 2284–2293, <https://doi.org/10.1080/02670836.2019.1674022>.
- [225] F. Lv, L. Shen, H. Liang, D. Xie, C. Wang, Z. Tian, Mechanical properties of AlSi10Mg alloy fabricated by laser melting deposition and improvements via heat treatment, Optik 179 (2019) 8–18, <https://doi.org/10.1016/j.jleco.2018.10.112>.
- [226] A. Singh, Additive Manufacturing of Al 4047 and Al 7050 Alloys Using Direct Laser Metal Deposition Process, PhD Dissertation, Wayne State University, 2017, <https://digitalcommons.wayne.edu/etd/1878>.
- [227] A. Bhagavatam, A. Ramakrishnan, V.S.K. Adapa, G.P. Dinda, Laser metal deposition of aluminum 7075 alloy, Int. J. Mater. Sci. Res. 1 (2018) 50–55, <https://doi.org/10.18689/ijmsr-1000108>.
- [228] D. Svetlizky, B. Zheng, T. Buta, Y. Zhou, O. Golan, U. Breiman, R. Haj-Ali, J. M. Schoenung, E.J. Lavernia, N. Eliaz, Directed energy deposition of Al 5xxx alloy using laser engineered net shaping (LENS®), Mater. Des. 192 (2020), 108763, <https://doi.org/10.1016/j.matdes.2020.108763>.
- [229] F. Caiazzo, V. Alfieri, Simulation of laser-assisted directed energy deposition of aluminum powder: prediction of geometry and temperature evolution, Materials 12 (2019) 2100, <https://doi.org/10.3390/ma12132100>.
- [230] S.P. Isanaka, S. Karnati, F. Liou, Blown powder deposition of 4047 aluminum on 2024 aluminum substrates, Manuf. Lett. 7 (2016) 11–14, <https://doi.org/10.1016/j.mfglet.2015.11.007>.
- [231] A. Langebeck, A. Bohlen, R. Rentsch, F. Vollertsen, Mechanical properties of high strength aluminum alloy EN AW-7075 additively manufactured by directed energy deposition, Metals 10 (2020) 579, <https://doi.org/10.3390/met10050579>.
- [232] P. Kiani, A.D. Dupuy, K. Ma, J.M. Schoenung, Directed energy deposition of AlSi10Mg: single track nonscalability and bulk properties, Mater. Des. 194 (2020), 108847, <https://doi.org/10.1016/j.matdes.2020.108847>.
- [233] Z. Wang, X. Lin, N. Kang, J. Chen, Y. Tang, H. Tan, X. Yu, H. Yang, W. Huang, Directed energy deposition additive manufacturing of a Sc/Zr-modified Al-Mg alloy: effect of thermal history on microstructural evolution and mechanical properties, Mater. Sci. Eng. 802 (2020), 140606, <https://doi.org/10.1016/j.msea.2020.140606>.
- [234] P. Kürnsteiner, P. Bajaj, A. Gupta, M.B. Wilms, A. Weisheit, X. Li, C. Leinenbach, B. Gault, E.A. Jägle, D. Raabe, Control of thermally stable core-shell nanoparticles in additively manufactured Al-Sc-Zr alloys, Addit. Manuf. 32 (2020), 100910, <https://doi.org/10.1016/j.addma.2019.100910>.
- [235] A.I. García-Moreno, J.M. Alvarado-Orozco, J. Ibarra-Medina, E. Martínez-Franco, Image-based porosity classification in Al-alloys by laser metal deposition using random forests, Int. J. Adv. Manuf. Technol. 110 (2020) 2827–2845, <https://doi.org/10.1007/s00170-020-05887-6>.
- [236] Z. Wang, X. Lin, N. Kang, Y. Hu, J. Chen, W. Huang, Strength-ductility synergy of selective laser melted Al-Mg-Sc-Zr alloy with a heterogeneous grain structure, Addit. Manuf. 34 (2020), 101260, <https://doi.org/10.1016/j.addma.2020.101260>.
- [237] Z. Wang, X. Lin, Y. Tang, N. Kang, X. Gao, S. Shi, W. Huang, Laser-based directed energy deposition of novel Sc/Zr-modified Al-Mg alloys: columnar-to-equiaxed transition and aging hardening behavior, J. Mater. Sci. Technol. 69 (2021) 168–179, <https://doi.org/10.1016/j.jmst.2020.08.003>.
- [238] N. Eliaz, D. Svetlizky, J. Schoenung, E. Lavernia, Y. Zhou, B. Zheng, Deposition of Al 5xxx alloy using laser engineered net shaping, patent application PCT/US2020/065373, filed December 16, 2020.
- [239] F.A. España, V.K. Balla, A. Bandyopadhyay, Laser processing of bulk Al-12Si alloy: influence of microstructure on thermal properties, Philos. Mag. 91 (2011) 574–588, <https://doi.org/10.1080/14786435.2010.526650>.
- [240] A. Plotkowski, O. Rios, N. Sridharan, Z. Sims, K. Unocic, R.T. Ott, R.R. Dehoff, S. S. Babu, Evaluation of an Al-Ce alloy for laser additive manufacturing, Acta Mater. 126 (2017) 507–519, <https://doi.org/10.1016/j.actamat.2016.12.065>.
- [241] P.A. Rometsch, H. Zhong, K.M. Nairn, T. Jarvis, X. Wu, Characterization of a laser-fabricated hypereutectic Al-Sc alloy bar, Scripta Mater. 87 (2014) 13–16, <https://doi.org/10.1016/j.scriptamat.2014.05.021>.
- [242] M. Javidani, J. Arreguin-Zavala, J. Danovitch, Y. Tian, M. Brochu, Additive manufacturing of AlSi10Mg alloy using direct energy deposition: microstructure and hardness characterization, J. Therm. Spray Technol. 26 (2017) 587–597, <https://doi.org/10.1007/s11666-016-0495-4>.
- [243] B. Chen, Y. Yao, X. Song, C. Tan, L. Cao, J. Feng, Microstructure and mechanical properties of additive manufacturing AlSi10Mg alloy using direct metal deposition, Ferroelectrics 523 (2018) 153–166, <https://doi.org/10.1080/00150193.2018.1392147>.
- [244] A. Singh, A. Ramakrishnan, G. Dinda, Fabrication of Al-11.2 Si components by direct laser metal deposition for automotive applications, J. Weld. Join. 35 (2017) 67–73, <https://doi.org/10.5781/JWJ.2017.35.4.10>.
- [245] A. Singh, A. Ramakrishnan, D. Baker, A. Biswas, G.P. Dinda, Laser metal deposition of nickel coated Al 7050 alloy, J. Alloys Compd. 719 (2017) 151–158, <https://doi.org/10.1016/j.jallcom.2017.05.171>.

- [246] Y. Liu, C. Liu, W. Liu, Y. Ma, S. Tang, C. Liang, Q. Cai, C. Zhang, Optimization of parameters in laser powder deposition AlSi10Mg alloy using Taguchi method, *Opt Laser. Technol.* 111 (2019) 470–480, <https://doi.org/10.1016/j.optlastec.2018.10.030>.
- [247] M. Renderos, F. Girot, A. Lamikiz, A. Torregaray, N. Saintier, Ni based powder reconditioning and reuse for LMD process, *Phys. Procedia* 83 (2016) 769–777, <https://doi.org/10.1016/j.phpro.2016.08.079>.
- [248] K. Zhang, S. Wang, W. Liu, R. Long, Effects of substrate preheating on the thin-wall part built by laser metal deposition shaping, *Appl. Surf. Sci.* 317 (2014) 839–855, <https://doi.org/10.1016/j.apsusc.2014.08.113>.
- [249] A.N. Jinoop, C.P. Paul, K.S. Bindra, Laser assisted direct energy deposition of Hastelloy-X, *Opt Laser. Technol.* 109 (2019) 14–19, <https://doi.org/10.1016/j.optlastec.2018.07.037>.
- [250] D.Y. Zhang, Z. Feng, C.J. Wang, Z. Liu, D.D. Dong, Y. Zhou, R. Wu, Modeling of temperature field evolution during multilayered direct laser metal deposition, *J. Therm. Spray Technol.* 26 (2017) 831–845, <https://doi.org/10.1007/s11666-017-0554-5>.
- [251] M.G. Glavacic, K.A. Sargent, P.A. Kobryn, S.L. Semiatin, The Repair of Single Crystal Nickel Superalloy Turbine Blades Using Laser Engineered Net Shape (LENS) Technology, *Report No. 2003-01-01*, UES, Inc., Dayton, OH, 2003.
- [252] P.A. Carroll, P. Brown, F. Ng, R. Scudamore, A.J. Pinkerton, W.U.H. Syed, H. K. Sezer, L. Li, J. Allen, The effect of powder recycling in direct metal laser deposition of powder and manufactured part characteristics, in: Proc. Cost Effective Manufacture via Net-Shape Processing, vol. 139, 2006 paper 18, <http://eprints.lancs.ac.uk/id/eprint/59645>. (Accessed 30 July 2021).
- [253] R.J. Moat, A.J. Pinkerton, L. Li, P.J. Withers, M. Preuss, Residual stresses in laser direct metal deposited Waspaloy, *Mater. Sci. Eng.* 528 (2011) 2288–2298, <https://doi.org/10.1016/j.msea.2010.12.010>.
- [254] L.L. Parimi, G. Ravi, D. Clark, M.M. Attallah, Microstructural and texture development in direct laser fabricated IN718, *Mater. Char.* 89 (2014) 102–111, <https://doi.org/10.1016/j.matchar.2013.12.012>.
- [255] Y. Kakinuma, M. Mori, Y. Oda, T. Mori, M. Kashihara, A. Hansel, M. Fujishima, Influence of metal powder characteristics on product quality with directed energy deposition of Inconel 625, *CIRP Ann. - Manuf. Technol.* 65 (2016) 209–212, <https://doi.org/10.1016/j.cirp.2016.04.058>.
- [256] J. Jones, M. Whittaker, R. Buckingham, R. Johnston, M. Bache, D. Clark, Microstructural characterisation of a nickel alloy processed via blown powder direct laser deposition (DLD), *Mater. Des.* 117 (2017) 47–57, <https://doi.org/10.1016/j.matdes.2016.12.062>.
- [257] Y.L. Hu, X. Lin, Y.L. Li, J. Wang, S.Y. Zhang, X.F. Lu, W.D. Huang, Effect of heat treatment on the microstructural evolution and mechanical properties of GH4099 additive-manufactured by directed energy deposition, *J. Alloys Compd.* 800 (2019) 163–173, <https://doi.org/10.1016/j.jallcom.2019.05.348>.
- [258] Z. Liu, H. Kim, W. Liu, W. Cong, Q. Jiang, H. Zhang, Influence of energy density on macro/micro structures and mechanical properties of as-deposited Inconel 718 parts fabricated by laser engineered net shaping, *J. Manuf. Process.* 42 (2019) 96–105, <https://doi.org/10.1016/j.jmapro.2019.04.020>.
- [259] S. Sui, H. Tan, J. Chen, C. Zhong, Z. Li, W. Fan, A. Gasser, W. Huang, The influence of Laves phases on the room temperature tensile properties of Inconel 718 fabricated by powder feeding laser additive manufacturing, *Acta Mater.* 164 (2019) 413–427, <https://doi.org/10.1016/j.actamat.2018.10.032>.
- [260] N. Pirch, S. Linnenbrink, A. Gasser, K. Wissenbach, R. Poprawe, Analysis of track formation during laser metal deposition, *J. Laser Appl.* 29 (2017), 022506, <https://doi.org/10.2351/1.4983231>.
- [261] C. Zhong, N. Pirch, A. Gasser, R. Poprawe, J. Schleifenzbaum, The influence of the powder stream on high-deposition-rate laser metal deposition with Inconel 718, *Metals* 7 (2017) 443, <https://doi.org/10.3390/met7100443>.
- [262] N.A. Kistler, A.R. Nassar, E.W. Reutzel, D.J. Corbin, A.M. Beese, Effect of directed energy deposition processing parameters on laser deposited Inconel ® 718: microstructure, fusion zone morphology, and hardness, *J. Laser Appl.* 29 (2017), 022005, <https://doi.org/10.2351/1.4979702>.
- [263] M. Gao, Z. Wang, X. Li, X. Zeng, The effect of deposition patterns on the deformation of substrates during direct laser fabrication, *J. Eng. Mater. Technol.* 135 (2013), 034502, <https://doi.org/10.1115/1.4024195>.
- [264] A.S. Johnson, S. Shuai, N. Shamsaei, S.M. Thompson, L. Bian, Fatigue behavior and failure mechanisms of direct laser deposited Inconel 718, in: Proc. 27th Annu. Int. Solid Freeform Fabrication Symp. – an Additive Manufacturing Conf., 2016, pp. 499–511.
- [265] A.R. Nassar, B. Starr, E.W. Reutzel, Process monitoring of directed-energy deposition of Inconel-718 via plume imaging, in: proc. 26th Ann. Int. Solid Freeform Fabr. (SFF) Symp. Addit. Manuf. Conf. (2015) 284–294.
- [266] E.L. Stevens, J. Toman, A.C. To, M. Chmielus, Variation of hardness, microstructure, and Laves phase distribution in direct laser deposited alloy 718 cuboids, *Mater. Des.* 119 (2017) 188–198, <https://doi.org/10.1016/j.matdes.2017.01.031>.
- [267] C. Zhong, T. Biermann, A. Gasser, R. Poprawe, Experimental study of effects of main process parameters on porosity, track geometry, deposition rate, and powder efficiency for high deposition rate laser metal deposition, *J. Laser Appl.* 27 (2015), 042003, <https://doi.org/10.2351/1.4923335>.
- [268] A.N. Jinoop, J. Denny, C.P. Paul, J. Ganesh Kumar, K.S. Bindra, Effect of post heat-treatment on the microstructure and mechanical properties of Hastelloy-X structures manufactured by laser based Directed Energy Deposition, *J. Alloys Compd.* 797 (2019) 399–412, <https://doi.org/10.1016/j.jallcom.2019.05.050>.
- [269] A. Ramakrishnan, G.P. Dinda, Direct laser metal deposition of Inconel 738, *Mater. Sci. Eng.* 740-741 (2019) 1–13, <https://doi.org/10.1016/j.msea.2018.10.020>, 1–13.
- [270] D. Kotoban, S. Grigoriev, I. Shishkovsky, Study of 3D laser cladding for Ni85Al15 superalloy, *Phys. Procedia* 56 (2014) 262–268, <https://doi.org/10.1016/j.phipro.2014.08.170>.
- [271] M. Fujishima, Y. Oda, R. Ashida, K. Takezawa, M. Kondo, Study on factors for pores and cladding shape in the deposition processes of Inconel 625 by the directed energy deposition (DED) method, *CIRP J. Manuf. Sci. Technol.* 19 (2017) 200–204, <https://doi.org/10.1016/j.cirpj.2017.04.003>.
- [272] Z. Liu, H. Qi, L. Jiang, Control of crystal orientation and continuous growth through inclination of coaxial nozzle in laser powder deposition of single-crystal superalloy, *J. Mater. Process. Technol.* 230 (2016) 177–186, <https://doi.org/10.1016/j.jmatprotec.2015.11.017>.
- [273] Y.L. Hu, X. Lin, S.Y. Zhang, Y.M. Jiang, X.F. Lu, H.O. Yang, W.D. Huang, Effect of solution heat treatment on the microstructure and mechanical properties of Inconel 625 superalloy fabricated by laser solid forming, *J. Alloys Compd.* 767 (2018) 330–344, <https://doi.org/10.1016/j.jallcom.2018.07.087>.
- [274] X. Zhang, Z. Chai, H. Chen, J. Xu, L. Xu, H. Lu, X. Chen, A novel method to prevent cracking in directed energy deposition of Inconel 738 by in-situ doping Inconel 718, *Mater. Des.* 197 (2021), 109214, <https://doi.org/10.1016/j.matdes.2020.109214>.
- [275] X. Yu, X. Lin, H. Tan, Y. Hu, S. Zhang, F. Liu, H. Yang, W. Huang, Microstructure and fatigue crack growth behavior of Inconel 718 superalloy manufactured by laser directed energy deposition, *Int. J. Fatig.* 143 (2021), 106005, <https://doi.org/10.1016/j.ijfatigue.2020.106005>.
- [276] M.J. Kim, C. Saldaña, Thin wall deposition of IN625 using directed energy deposition, *J. Manuf. Process.* 56B (2020) 1366–1373, <https://doi.org/10.1016/j.jmapro.2020.04.032>.
- [277] P.D. Nezhadfar, A.S. Johnson, N. Shamsaei, Fatigue behavior and microstructural evolution of additively manufactured Inconel 718 under cyclic loading at elevated temperature, *Int. J. Fatig.* 136 (2020), 105598, <https://doi.org/10.1016/j.ijfatigue.2020.105598>.
- [278] X. Yu, X. Lin, F. Liu, L. Wang, Y. Tang, J. Li, S. Zhang, W. Huang, Influence of post-heat-treatment on the microstructure and fracture toughness properties of Inconel 718 fabricated with laser directed energy deposition additive manufacturing, *Mater. Sci. Eng.* 798 (2020), 140092, <https://doi.org/10.1016/j.msea.2020.140092>.
- [279] G. Bi, C.N. Sun, H. chi Chen, F.L. Ng, C.C.K. Ma, Microstructure and tensile properties of superalloy IN100 fabricated by micro-laser aided additive manufacturing, *Mater. Des.* 60 (2014) 401–408, <https://doi.org/10.1016/j.matdes.2014.04.020>.
- [280] Z. Li, J. Chen, S. Sui, C. Zhong, X. Lu, X. Lin, The microstructure evolution and tensile properties of Inconel 718 fabricated by high-deposition-rate laser directed energy deposition, *Addit. Manuf.* 31 (2020), 100941, <https://doi.org/10.1016/j.addma.2019.100941>.
- [281] S. Sui, J. Chen, Z. Li, H. Li, X. Zhao, H. Tan, Investigation of dissolution behavior of laves phase in inconel 718 fabricated by laser directed energy deposition, *Addit. Manuf.* 32 (2020), 101055, <https://doi.org/10.1016/j.addma.2020.101055>.
- [282] Y.L. Hu, X. Lin, Y.L. Li, S.Y. Zhang, X.H. Gao, F.G. Liu, X. Li, W.D. Huang, Plastic deformation behavior and dynamic recrystallization of Inconel 625 superalloy fabricated by directed energy deposition, *Mater. Des.* 186 (2020), 108359, <https://doi.org/10.1016/j.matdes.2019.108359>.
- [283] J. Denny, A.N. Jinoop, C.P. Paul, R. Singh, K.S. Bindra, Fatigue crack propagation behaviour of inconel 718 structures built using directed energy deposition based laser additive manufacturing, *Mater. Lett.* 276 (2020), 128241, <https://doi.org/10.1016/j.matlet.2020.128241>.
- [284] Y.L. Hu, Y.L. Li, S.Y. Zhang, X. Lin, Z.H. Wang, W.D. Huang, Effect of solution temperature on static recrystallization and ductility of Inconel 625 superalloy fabricated by directed energy deposition, *Mater. Sci. Eng.* 772 (2020), 138711, <https://doi.org/10.1016/j.msea.2019.138711>.
- [285] F. Liu, F. Lyu, F. Liu, X. Lin, C. Huang, Laves phase control of inconel 718 superalloy fabricated by laser direct energy deposition via δ aging and solution treatment, *J. Mater. Res. Technol.* 9 (2020) 9753–9765, <https://doi.org/10.1016/j.jmrt.2020.06.011>.
- [286] G.E. Huanez-Alvan, B. Aydogan, H. Sahasrabudhe, S.K. Chakrapani, Ultrasonic properties of Inconel 718 fabricated via laser-directed energy deposition, *J. Acoust. Soc. Am.* 148 (2020) 2648, <https://doi.org/10.1121/1.5147361>.
- [287] T. Pan, X. Zhang, T. Yamazaki, A. Sutton, W. Cui, L. Li, F. Liou, Characteristics of Inconel 625–copper bimetallic structure fabricated by directed energy deposition, *Int. J. Adv. Manuf. Technol.* 109 (2020) 1261–1274, <https://doi.org/10.1007/s00170-020-05713-z>.
- [288] Y.-J. Liang, X. Cheng, J. Li, H.-M. Wang, Microstructural control during laser additive manufacturing of single-crystal nickel-base superalloys: new processing–microstructure maps involving powder feeding, *Mater. Des.* 130 (2017) 197–207, <https://doi.org/10.1016/j.matdes.2017.05.066>.
- [289] E.C. Santos, K. Kida, P. Carroll, R. Vilar, Optimization of laser deposited Ni-based single crystal superalloys microstructure, *Adv. Mater. Res.* 154–155 (2011) 1405–1414, <https://doi.org/10.4028/www.scientific.net/AMR.154-155.1405>.
- [290] A.S. Johnson, S. Shao, N. Shamsaei, S.M. Thompson, L. Bian, Microstructure, fatigue behavior, and failure mechanisms of direct laser-deposited inconel 718, *JOM* 69 (2017) 597–603, <https://doi.org/10.1007/s11837-016-2225-2>.
- [291] W. Liu, J.N. DuPont, Direct laser deposition of a single-crystal Ni3Al-based IC221W alloy, *Metall. Mater. Trans.* 36 (2005) 3397–3406, <https://doi.org/10.1007/s11661-005-0013-7>.
- [292] S.S. Babu, N. Raghavan, J. Raplee, S.J. Foster, C. Frederick, M. Haines, R. Dinwiddie, M.K. Kirk, A. Plotkowski, Y. Lee, R.R. Dehoff, Additive manufacturing of nickel superalloys: opportunities for innovation and challenges

- related to qualification, *Metall. Mater. Trans.* 49 (2018) 3764–3780, <https://doi.org/10.1007/s11661-018-4702-4>.
- [293] V. Dhinakaran, J. Ajith, A. Fathima Yasin Fahmidha, T. Jagadeesha, T. Sathish, B. Stalin, Wire arc additive manufacturing (WAAM) process of nickel based superalloys – a review, *Mater. Today Proc.* 21 (2020) 920–925, <https://doi.org/10.1016/j.matpr.2019.08.159>.
- [294] Q. Yu, C. Wang, Z. Zhao, C. Dong, Y. Zhang, New Ni-based superalloys designed for laser additive manufacturing, *J. Alloys Compd.* 861 (2021), 157979, <https://doi.org/10.1016/j.jallcom.2020.157979>.
- [295] T.D. Anderson, J.N. DuPont, T. DebRoy, Stray grain formation in welds of single-crystal Ni-base superalloy CMSX-4, *Metall. Mater. Trans.* 41 (2009) 181, <https://doi.org/10.1007/s11661-009-0078-9>.
- [296] C. Zhong, J. Kittel, A. Gasser, J.H. Schleifenbaum, Study of nickel-based superalloys Inconel 718 and Inconel 625 in high-deposition-rate laser metal deposition, *Opt. Laser Technol.* 109 (2019) 352–360, <https://doi.org/10.1016/j.optlastec.2018.08.003>.
- [297] H. Kim, W. Cong, H.C. Zhang, Z. Liu, Laser engineered net shaping of nickel-based superalloy inconel 718 powders onto aisi 4140 alloy steel substrates: interface bond and fracture failure mechanism, *Materials* 10 (2017) 341, <https://doi.org/10.3390/ma10040431>.
- [298] C. Kumara, A. Segerstark, F. Hanning, N. Dixit, S. Joshi, J. Moverare, P. Nylén, Microstructure modelling of laser metal powder directed energy deposition of alloy 718, *Addit. Manuf.* 25 (2019) 357–364, <https://doi.org/10.1016/j.addma.2018.11.024>.
- [299] Z. Liu, T. Li, F. Ning, W. Cong, H. Kim, Q. Jiang, H. Zhang, Effects of deposition variables on molten pool temperature during laser engineered net shaping of Inconel 718 superalloy, *Int. J. Adv. Manuf. Technol.* 102 (2019) 969–976, <https://doi.org/10.1007/s00170-018-03245-1>.
- [300] M.K. Mallik, C.S. Rao, V.V.S. Kesava Rao, Effect of heat treatment on hardness of Co-Cr-Mo alloy deposited with laser engineered net shaping, *Procedia Eng.* 97 (2014) 1718–1723, <https://doi.org/10.1016/j.proeng.2014.12.323>.
- [301] K.M. Mantrala, M. Das, V.K. Balla, C.S. Rao, V.V.S. Kesava Rao, Additive manufacturing of Co-Cr-Mo alloy: influence of heat treatment on microstructure, tribological, and electrochemical properties, *Front. Mech. Eng.* 1 (2015) 1–7, <https://doi.org/10.3389/fmech.2015.00002>.
- [302] B. Ren, C. Chen, M. Zhang, Effect of heat treatment on the microstructure of Co-Cr-W alloy fabricated by laser additive manufacturing, *Opt. Eng.* 57 (2018), 41409, <https://doi.org/10.1117/1.OE.57.4.041409>.
- [303] G. Suresh, K.L. Narayana, M.K. Mallik, V. Srinivas, G.J. Reddy, Processing & characterization of LENS™ deposited Co-Cr-W alloy for bio-medical applications, *Int. J. Pharmacol.* Res. 10 (2018) 276–285.
- [304] A. Bandyopadhyay, A. Shivaram, M. Isik, J.D. Avila, W.S. Dernell, S. Bose, Additively manufactured calcium phosphate reinforced CoCrMo alloy: biotribological and biocompatibility evaluation for load-bearing implants, *Addit. Manuf.* 28 (2019) 312–324, <https://doi.org/10.1016/j.addma.2019.04.020>.
- [305] B. Stucker, C. Esplin, D. Justin, An investigation of LENS®-deposited medical-grade CoCrMo alloys, in: *Proc. 2004 Int. Solid Freeform Fabrication Symp.*, 2004, pp. 68–79, <https://doi.org/10.26153/tsw/5709>.
- [306] F.A. España, V.K. Balla, S. Bose, A. Bandyopadhyay, Design and fabrication of CoCrMo alloy based novel structures for load bearing implants using laser engineered net shaping, *Mater. Sci. Eng. C* 30 (2010) 50–57, <https://doi.org/10.1016/j.msec.2009.08.006>.
- [307] O. Nenadl, V. Ocelík, J.T.M. De Hosson, Texture development in direct powder deposition, *J. Laser Appl.* 29 (2017), 042007, <https://doi.org/10.2351/1.5007944>.
- [308] G.D.J. Ram, C.K. Esplin, B.E. Stucker, Microstructure and wear properties of LENS® deposited medical grade CoCrMo, *J. Mater. Sci. Mater. Med.* 19 (2008) 2105–2111, <https://doi.org/10.1007/s10856-007-3078-6>.
- [309] G. Suresh, K.L. Narayana, M.K. Mallik, Bio-compatible processing of LENS™ deposited Co-Cr-W alloy for medical applications, *Int. J. Eng. Technol.* 7 (2018) 362–366, <https://doi.org/10.14419/ijet.v7i2.20.16734>.
- [310] M.K. Mallik, K.L. Narayana, Impact strength and fracture analysis of Co-Cr-Mo alloy deposited with Laser Engineered Net Shaping – an additive manufacturing technology, *Proc. World Congr. Eng.* (2019). London, UK.
- [311] G. Suresh, K.L. Narayana, M.K. Mallik, Characterization and wear properties of Co-Cr-W alloy deposited with laser engineered net shaping, *Int. J. Recent Technol. Eng.* 4 (2018) 151–155.
- [312] K.D. Traxel, A. Bandyopadhyay, First demonstration of additive manufacturing of cutting tools using directed energy deposition system: Stellite™-based cutting tools, *Addit. Manuf.* 25 (2019) 460–468, <https://doi.org/10.1016/j.addma.2018.11.019>.
- [313] K. Karczewski, M. Dąbrowska, M. Zielińska, M. Polański, Fe-Al thin walls manufactured by laser engineered net shaping, *J. Alloys Compd.* 696 (2017) 1105–1112, <https://doi.org/10.1016/j.jallcom.2016.12.034>.
- [314] M. Łazińska, T. Durejko, T. Czujko, Z. Bojar, The effect of the traverse feed rate on the microstructure and mechanical properties of laser deposited Fe₃Al (Zr, B) intermetallic alloy, *Materials* 11 (2018) 792, <https://doi.org/10.3390/ma11050792>.
- [315] G. Rolink, S. Vogt, L. Senčekova, A. Weisheit, R. Poprawe, M. Palm, Laser metal deposition and selective laser melting of Fe–28 at.% Al, *J. Mater. Res.* 29 (2014) 2036–2043, <https://doi.org/10.1557/jmr.2014.131>.
- [316] W. Liu, J.N. Dupont, In-situ reactive processing of nickel aluminides by laser-engineered net shaping, *Metall. Mater. Trans.* 34 (2003) 2633–2641, <https://doi.org/10.1007/s11661-003-0022-3>.
- [317] M. Tłotleng, Microstructural properties of heat-treated LENS in situ additively manufactured titanium aluminide, *J. Mater. Eng. Perform.* 28 (2019) 701–708, <https://doi.org/10.1007/s11665-018-3789-5>.
- [318] T. Durejko, M. Zielińska, M. Łazińska, S. Lipiński, W. Polkowski, T. Czujko, R. A. Varin, Structure and properties of the Fe₃Al-type intermetallic alloy fabricated by laser engineered net shaping (LENS), *Mater. Sci. Eng.* 650 (2016) 374–381, <https://doi.org/10.1016/j.msea.2015.10.076>.
- [319] M. Łazińska, T. Durejko, D. Zasadka, Z. Bojar, Microstructure and mechanical properties of a Fe-28%Al-5%Cr-1%Nb-2%B alloy fabricated by laser engineered net shaping, *Mater. Lett.* 196 (2017) 87–90, <https://doi.org/10.1016/j.matlet.2017.03.022>.
- [320] D. Kotoban, A. Nazarov, I. Shishkovsky, Comparative study of selective laser melting and direct laser metal deposition of Ni₃Al intermetallic alloy, *Procedia IUTAM* 23 (2017) 138–146, <https://doi.org/10.1016/j.piutam.2017.06.014>.
- [321] R. Łyszkowski, High-temperature oxidation of Fe₃Al intermetallic alloy prepared by additive manufacturing LENS, *Materials* 8 (2015) 1499–1512, <https://doi.org/10.3390/ma8041499>.
- [322] V.K. Balla, M. Das, A. Mohammad, A.M. Al-Ahmari, Additive manufacturing of γ-TiAl: processing, microstructure, and properties, *Adv. Eng. Mater.* 18 (2016) 1208–1215, <https://doi.org/10.1002/adem.201500588>.
- [323] M. Kwiatkowska, D. Zasadka, J. Bystrzycki, M. Polański, Synthesis of Fe-Al-Ti based intermetallics with the use of laser engineered net shaping (LENS), *Materials* 8 (2015) 2311–2331, <https://doi.org/10.3390/ma8052311>.
- [324] B.V. Krishna, S. Bose, A. Bandyopadhyay, Laser processing of net-shape NiTi shape memory alloy, *Metall. Mater. Trans.* 38 (2007) 1096–1103, <https://doi.org/10.1007/s11661-007-9127-4>.
- [325] R.F. Hamilton, T.A. Palmer, B.A. Bimber, Spatial characterization of the thermal-induced phase transformation throughout as-deposited additive manufactured NiTi bulk builds, *Scripta Mater.* 101 (2015) 56–59, <https://doi.org/10.1016/j.scriptamat.2015.01.018>.
- [326] A. Bagheri, M.J. Mahtabi, N. Shamsaei, Fatigue behavior and cyclic deformation of additive manufactured NiTi, *J. Mater. Process. Technol.* 252 (2018) 440–453, <https://doi.org/10.1016/j.jmatprotec.2017.10.006>.
- [327] R.F. Hamilton, B.A. Bimber, M. Taheri Andani, M. Elahinia, Multi-scale shape memory effect recovery in NiTi alloys additive manufactured by selective laser melting and laser directed energy deposition, *J. Mater. Process. Technol.* 250 (2017) 55–64, <https://doi.org/10.1016/j.jmatprotec.2017.06.027>.
- [328] S. Bernard, V.K. Balla, S. Bose, A. Bandyopadhyay, Rotating bending fatigue response of laser processed porous NiTi alloy, *Mater. Sci. Eng. C* 31 (2011) 815–820, <https://doi.org/10.1016/j.msec.2010.12.007>.
- [329] X. Xu, X. Lin, M. Yang, J. Chen, W. Huang, Microstructure evolution in laser solid forming of Ti-50 wt% Ni alloy, *J. Alloys Compd.* 480 (2009) 782–787, <https://doi.org/10.1016/j.jallcom.2009.02.056>.
- [330] A. Baran, M. Polanski, Microstructure and properties of LENS (laser engineered net shaping) manufactured Ni-Ti shape memory alloy, *J. Alloys Compd.* 750 (2018) 863–870, <https://doi.org/10.1016/j.jallcom.2018.03.400>.
- [331] S. Shiva, I.A. Palani, S.K. Mishra, C.P. Paul, L.M. Kukreja, Investigations on the influence of composition in the development of Ni-Ti shape memory alloy using laser based additive manufacturing, *Opt. Laser. Technol.* 69 (2015) 44–51, <https://doi.org/10.1016/j.joptlastec.2014.12.014>.
- [332] B.A. Bimber, R.F. Hamilton, T.A. Palmer, Ni-concentration dependence of directed energy deposited NiTi alloy microstructures, *Shape Mem. Superelasticity*. 5 (2019) 182–187, <https://doi.org/10.1007/s40830-019-00215-8>.
- [333] S. Bernard, V. Krishna Balla, S. Bose, A. Bandyopadhyay, Compression fatigue behavior of laser processed porous NiTi alloy, *J. Mech. Behav. Biomed. Mater.* 13 (2012) 62–68, <https://doi.org/10.1016/j.jmbbm.2012.04.010>.
- [334] J. Lee, Y.C. Shin, Effects of composition and post heat treatment on shape memory characteristics and mechanical properties for laser direct deposited Nitinol, *Lasers Manuf. Mater. Process.* 6 (2019) 41–58, <https://doi.org/10.1007/s40516-019-0079-5>.
- [335] C. Wang, X.P. Tan, Z. Du, S. Chandra, Z. Sun, C.W.J. Lim, S.B. Tor, C.S. Lim, C. H. Wong, Additive manufacturing of NiTi shape memory alloys using pre-mixed powders, *J. Mater. Process. Technol.* 271 (2019) 152–161, <https://doi.org/10.1016/j.jmatprotec.2019.03.025>.
- [336] P.R. Halani, I. Kaya, Y.C. Shin, H.E. Karaca, Phase transformation characteristics and mechanical characterization of nitinol synthesized by laser direct deposition, *Mater. Sci. Eng.* 559 (2013) 836–843, <https://doi.org/10.1016/j.msea.2012.09.031>.
- [337] S. Kumar, L. Marandi, V.K. Balla, S. Bysakh, D. Piorunek, G. Eggeler, M. Das, I. Sen, Microstructure–property correlations for additively manufactured NiTi based shape memory alloys, *Materialia* 8 (2019), 100456, <https://doi.org/10.1016/j.mtla.2019.100456>.
- [338] S. Khademzadeh, N. Parvin, P.F. Bariani, Production of NiTi alloy by direct metal deposition of mechanically alloyed powder mixtures, *Int. J. Precis. Eng. Manuf.* 16 (2015) 2333–2338, <https://doi.org/10.1007/s12541-015-0300-1>.
- [339] J. Toman, P. Müllner, M. Chmielus, Properties of as-deposited and heat-treated Ni-Mn-Ga magnetic shape memory alloy processed by directed energy deposition, *J. Alloys Compd.* 752 (2018) 455–463, <https://doi.org/10.1016/j.jallcom.2018.04.059>.
- [340] C. Lauhoff, N. Sommer, M. Vollmer, G. Mienert, P. Kroos, S. Böhm, T. Niendorf, Excellent superelasticity in a Co-Ni-Ga high-temperature shape memory alloy processed by directed energy deposition, *Mater. Res. Lett.* 8 (2020) 314–320, <https://doi.org/10.1080/21663831.2020.1756495>.

- [341] J. Toman, Directed Energy Deposition of Ni-Mn-Ga Magnetic Shape Memory Alloy, MSc thesis, University of Pittsburgh, USA, 2017. <http://d-scholarship.pitt.edu/id/eprint/30306>.
- [342] T. Paplham, J. Toman, M. Chmielus, Characterization of hierarchical structures in remelted Ni-Mn-Ga substrates for directed energy deposition manufacturing of single crystals, *Ingenium* 6 (2020) 77–80, <https://doi.org/10.18117/af64-w271>.
- [343] D. Zhang, Y. Li, H. Wang, W. Cong, Ultrasonic vibration-assisted laser directed energy deposition in-situ synthesis of NiTi alloys: effects on microstructure and mechanical properties, *J. Manuf. Process.* 60 (2020) 328–339, <https://doi.org/10.1016/j.jmapro.2020.10.058>.
- [344] B. Lu, X. Cui, W. Ma, M. Dong, Y. Fang, X. Wen, G. Jin, D. Zeng, Promoting the heterogeneous nucleation and the functional properties of directed energy deposited NiTi alloy by of La₂O₃ addition, *Addit. Manuf.* 33 (2020), 101150, <https://doi.org/10.1016/j.addma.2020.10.1150>.
- [345] J. Wang, Z. Pan, Y. Wang, L. Wang, L. Su, D. Cuiuri, Y. Zhao, H. Li, Evolution of crystallographic orientation, precipitation, phase transformation and mechanical properties realized by enhancing deposition current for dual-wire arc additive manufactured Ni-rich NiTi alloy, *Addit. Manuf.* 34 (2020), 101240, <https://doi.org/10.1016/j.addma.2020.10.1240>.
- [346] Z. Zeng, B.Q. Cong, J.P. Oliveira, W.C. Ke, N. Schell, B. Peng, Z.W. Qi, F.G. Ge, W. Zhang, S.S. Ao, Wire and arc additive manufacturing of a Ni-rich NiTi shape memory alloy: microstructure and mechanical properties, *Addit. Manuf.* 32 (2020), 101051, <https://doi.org/10.1016/j.addma.2020.10.1051>.
- [347] R.F. Hamilton, B.A. Bimber, T.A. Palmer, Correlating microstructure and superelasticity of directed energy deposition additive manufactured Ni-rich NiTi alloys, *J. Alloys Compd.* 739 (2018) 712–722, <https://doi.org/10.1016/j.jallcom.2017.12.270>.
- [348] K. Malukhin, K. Ehmann, Material characterization of NiTi based memory alloys fabricated by the laser direct metal deposition process, *J. Manuf. Sci. Eng.* 128 (2006) 691, <https://doi.org/10.1115/1.2193553>.
- [349] J.J. Marattukalam, V.K. Balla, M. Das, S. Bontha, S.K. Kalpathy, Effect of heat treatment on microstructure, corrosion, and shape memory characteristics of laser deposited NiTi alloy, *J. Alloys Compd.* 744 (2018) 337–346, <https://doi.org/10.1016/j.jallcom.2018.01.174>.
- [350] J.J. Marattukalam, A.K. Singh, S. Datta, M. Das, V.K. Balla, S. Bontha, S. K. Kalpathy, Microstructure and corrosion behavior of laser processed NiTi alloy, *Mater. Sci. Eng. C* 57 (2015) 309–313, <https://doi.org/10.1016/j.msec.2015.07.067>.
- [351] B.V. Krishna, S. Bose, A. Bandyopadhyay, Fabrication of porous NiTi shape memory alloy structures using laser engineered net shaping, *J. Biomed. Mater. Res. B Appl. Biomater.* 89 (2009) 481–490, <https://doi.org/10.1002/jbm.b.31238>.
- [352] P.R. Halani, Y.C. Shin, In situ synthesis and characterization of shape memory alloy nitinol by laser direct deposition, *Metall. Mater. Trans. A Phys. Metall. Mater. Sci.* 43 (2012) 650–657, <https://doi.org/10.1007/s11661-011-0890-x>.
- [353] B.A. Bimber, R.F. Hamilton, J. Keist, T.A. Palmer, Anisotropic microstructure and superelasticity of additive manufactured NiTi alloy bulk builds using laser directed energy deposition, *Mater. Sci. Eng.* 674 (2016) 125–134, <https://doi.org/10.1016/j.msea.2016.07.059>.
- [354] S. Guan, D. Wan, K. Solberg, F. Berto, T. Welo, T.M. Yue, K.C. Chan, Additive manufacturing of fine-grained and dislocation-populated CrMnFeCoNi high entropy alloy by laser engineered net shaping, *Mater. Sci. Eng.* 761 (2019), 138056, <https://doi.org/10.1016/j.msea.2019.138056>.
- [355] I. Kunce, M. Polanski, J. Bystrzycki, Structure and hydrogen storage properties of a high entropy ZrTiCrFeNi alloy synthesized using Laser Engineered Net Shaping (LENS), *Int. J. Hydrogen Energy* 38 (2013) 12180–12189, <https://doi.org/10.1016/j.ijhydene.2013.05.071>.
- [356] S. Xiang, J. Li, H. Luan, A. Amar, S. Lu, K. Li, L. Zhang, X. Liu, G. Le, X. Wang, F. Qu, W. Zhang, D. Wang, Q. Li, Effects of process parameters on microstructures and tensile properties of laser melting deposited CrMnFeCoNi high entropy alloys, *Mater. Sci. Eng.* 743 (2019) 412–417, <https://doi.org/10.1016/j.msea.2018.11.110>.
- [357] R. Wang, K. Zhang, C. Davies, X. Wu, Evolution of microstructure, mechanical and corrosion properties of AlCoCrFeNi high-entropy alloy prepared by direct laser fabrication, *J. Alloys Compd.* 694 (2017) 971–981, <https://doi.org/10.1016/j.jallcom.2016.10.138>.
- [358] Z. Tong, X. Ren, J. Jiao, W. Zhou, Y. Ren, Y. Ye, E.A. Larson, J. Gu, Laser additive manufacturing of FeCrCoMnNi high-entropy alloy: effect of heat treatment on microstructure, residual stress and mechanical property, *J. Alloys Compd.* 785 (2019) 1144–1159, <https://doi.org/10.1016/j.jallcom.2019.01.213>.
- [359] M.A. Melia, J.D. Carroll, S.R. Whetten, S.N. Esmaeily, J. Locke, E. White, I. Anderson, M. Chandross, J.R. Michael, N. Argibay, Mechanical and corrosion properties of additively manufactured CoCrFeMnNi high entropy alloy, *Addit. Manuf.* 29 (2019), 100833, <https://doi.org/10.1016/j.addma.2019.100833>.
- [360] M. Zheng, C. Li, X. Zhang, Z. Ye, X. Yang, J. Gu, The influence of columnar to equiaxed transition on deformation behavior of FeCoCrNiMn high entropy alloy fabricated by laser-based directed energy deposition, *Addit. Manuf.* 37 (2020), 101660, <https://doi.org/10.1016/j.addma.2020.101660>.
- [361] Z. Tong, H. Liu, J. Jiao, W. Zhou, Y. Yang, X. Ren, Improving the strength and ductility of laser directed energy deposited CrMnFeCoNi high-entropy alloy by laser shock peening, *Addit. Manuf.* 35 (2020), 101417, <https://doi.org/10.1016/j.addma.2020.101417>.
- [362] F. Wang, Y. Chew, Z. Zhu, X. Yao, L. Wang, F.L. Ng, S. Liu, G. Bi, Excellent combination of strength and ductility of CoCrNi medium entropy alloy fabricated by laser aided directed energy deposition, *Addit. Manuf.* 34 (2020), 101202, <https://doi.org/10.1016/j.addma.2020.101202>.
- [363] M. Zhang, J. Li, Y. Li, J. Wang, Z. Li, X. Cheng, Effect of Al addition on the microstructure and hardness of the (Al_xCoCrFe) 50Ni high-entropy alloy prepared by directed energy deposition technique, *Mater. Lett.* 285 (2021), 128778, <https://doi.org/10.1016/j.matlet.2020.128778>.
- [364] J.T. Moon, E.J. Schindelholz, M.A. Melia, A.B. Kustas, D. Chidambaram, Corrosion of additively manufactured CoCrFeMnNi high entropy alloy in molten NaNO₃-KNO₃, *J. Electrochem. Soc.* 167 (2020), 81509, <https://doi.org/10.1149/1945-7111/ab8ddf>.
- [365] J.W. Pegues, M.A. Melia, R. Puckett, S.R. Whetten, N. Argibay, A.B. Kustas, Exploring additive manufacturing as a high-throughput screening tool for multiphase high entropy alloys, *Addit. Manuf.* 37 (2020), 101598, <https://doi.org/10.1016/j.addma.2020.101598>.
- [366] I. Kunce, M. Polanski, K. Karczewski, T. Plocinski, K.J. Kurzydlowski, Microstructural characterisation of high-entropy alloy AlCoCrFeNi fabricated by laser engineered net shaping, *J. Alloys Compd.* 648 (2015) 751–758, <https://doi.org/10.1016/j.jallcom.2015.05.144>.
- [367] M.S.K.K.Y. Nartu, T. Alam, S. Dasari, S.A. Mantri, S. Gorsse, H. Siller, N. Dahotre, R. Banerjee, Enhanced tensile yield strength in laser additively manufactured Al_{0.3}CoCrFeNi high entropy alloy, *Materialia* 9 (2020), 100522, <https://doi.org/10.1016/j.mtla.2019.100522>.
- [368] J. Joseph, N. Stanford, P. Hodgson, D.M. Fabijanic, Tension/compression asymmetry in additive manufactured face centered cubic high entropy alloy, *Scripta Mater.* 129 (2017) 30–34, <https://doi.org/10.1016/j.scriptamat.2016.10.023>.
- [369] Y. Chew, G.J. Bi, Z.G. Zhu, F.L. Ng, F. Wang, S.B. Liu, S.M.L. Nai, B.Y. Lee, Microstructure and enhanced strength of laser aided additive manufactured CoCrFeNiMn high entropy alloy, *Mater. Sci. Eng.* 744 (2019) 137–144, <https://doi.org/10.1016/j.msea.2018.12.005>.
- [370] H. Zhang, W. Wu, Y. He, M. Li, S. Guo, Formation of core-shell structure in high entropy alloy coating by laser cladding, *Appl. Surf. Sci.* 363 (2016) 543–547, <https://doi.org/10.1016/j.apsusc.2015.12.059>.
- [371] J. Joseph, N. Stanford, P. Hodgson, D.M. Fabijanic, Understanding the mechanical behaviour and the large strength/ductility differences between FCC and BCC Al_xCoCrFeNi high entropy alloys, *J. Alloys Compd.* 726 (2017) 885–895, <https://doi.org/10.1016/j.jallcom.2017.08.067>.
- [372] J. Joseph, T. Jarvis, X. Wu, N. Stanford, P. Hodgson, D.M. Fabijanic, Comparative study of the microstructures and mechanical properties of direct laser fabricated and arc-melted Al_xCoCrFeNi high entropy alloys, *Mater. Sci. Eng.* 633 (2015) 184–193, <https://doi.org/10.1016/j.msea.2015.02.072>.
- [373] I. Kunce, M. Polanski, T. Czujko, Microstructures and hydrogen storage properties of La-Ni-Fe-V-Mn alloys, *Int. J. Hydrogen Energy* 42 (2017) 27154–27164, <https://doi.org/10.1016/j.ijhydene.2017.09.039>.
- [374] I. Kunce, M. Polanski, J. Bystrzycki, Microstructure and hydrogen storage properties of a TiZrNbMoV high entropy alloy synthesized using Laser Engineered Net Shaping (LENS), *Int. J. Hydrogen Energy* 39 (2014) 9904–9910, <https://doi.org/10.1016/j.ijhydene.2014.02.067>.
- [375] G. Ma, S. Yan, F. Niu, Y. Zhang, D. Wu, Microstructure and mechanical properties of solid Al₂O₃-ZrO₂ (Y₂O₃) eutectics prepared by laser engineered net shaping, *J. Laser Appl.* 29 (2017), 22305, <https://doi.org/10.2351/1.4983258>.
- [376] Z. Fan, Y. Zhao, Q. Tan, N. Mo, M.X. Zhang, M. Lu, H. Huang, Nanostructured Al₂O₃-YAG-ZrO₂ ternary eutectic components prepared by laser engineered net shaping, *Acta Mater.* 170 (2019) 24–37, <https://doi.org/10.1016/j.actamat.2019.03.020>.
- [377] S. Yan, D. Wu, F. Niu, G. Ma, R. Kang, Al₂O₃-ZrO₂ eutectic ceramic via ultrasonic-assisted laser engineered net shaping, *Ceram. Int.* 43 (2017) 15905–15910, <https://doi.org/10.1016/j.ceramint.2017.08.165>.
- [378] F. Niu, D. Wu, G. Ma, J. Wang, M. Guo, B. Zhang, Nanosized microstructure of Al₂O₃-ZrO₂(Y₂O₃) eutectics fabricated by laser engineered net shaping, *Scripta Mater.* 95 (2015) 39–41, <https://doi.org/10.1016/j.scriptamat.2014.09.026>.
- [379] Y. Li, Y. Hu, W. Cong, L. Zhi, Z. Guo, Additive manufacturing of alumina using laser engineered net shaping: effects of deposition variables, *Ceram. Int.* 43 (2017) 7768–7775, <https://doi.org/10.1016/j.ceramint.2017.03.085>.
- [380] S.A. Bernard, V.K. Balla, S. Bose, A. Bandyopadhyay, Direct laser processing of bulk lead zirconate titanate ceramics, *Mater. Sci. Eng. B* 172 (2010) 85–88, <https://doi.org/10.1016/j.mseb.2010.04.022>.
- [381] Y. Hu, F. Ning, W. Cong, Y. Li, X. Wang, H. Wang, Ultrasonic vibration-assisted laser engineering net shaping of ZrO₂-Al₂O₃ bulk parts: effects on crack suppression, microstructure, and mechanical properties, *Ceram. Int.* 44 (2018) 2752–2760, <https://doi.org/10.1016/j.ceramint.2017.11.013>.
- [382] V.K. Balla, M. Das, S. Bose, G.D. Janaki Ram, I. Manna, Laser surface modification of 316 L stainless steel with bioactive hydroxyapatite, *Mater. Sci. Eng. C* 33 (2013) 4594–4598, <https://doi.org/10.1016/j.msec.2013.07.015>.
- [383] S. Nag, S.R. Paital, P. Nandawana, K. Mahdak, Y.H. Ho, H.D. Vora, R. Banerjee, N. B. Dahotre, Laser deposited biocompatible Ca-P coatings on Ti-6Al-4V: microstructural evolution and thermal modeling, *Mater. Sci. Eng. C* 33 (2013) 165–173, <https://doi.org/10.1016/j.msec.2012.08.024>.
- [384] Y. Zhang, H. Sahasrabudhe, A. Bandyopadhyay, Additive manufacturing of Ti-Si-N ceramic coatings on titanium, *Appl. Surf. Sci.* 346 (2015) 428–437, <https://doi.org/10.1016/j.apsusc.2015.03.184>.
- [385] T.M. Yue, K.J. Huang, H.C. Man, Laser cladding of Al₂O₃ coating on aluminium alloy by thermite reactions, *Surf. Coatings Technol.* 194 (2005) 232–237, <https://doi.org/10.1016/j.surcoat.2004.09.026>.
- [386] G.J. Cheng, D. Pirzada, M. Cai, P. Mohanty, A. Bandyopadhyay, Bioceramic coating of hydroxyapatite on titanium substrate with Nd-YAG laser, *Mater. Sci. Eng. C* 25 (2005) 541–547, <https://doi.org/10.1016/j.msec.2005.05.002>.

- [387] S. Yan, D. Wu, G. Ma, F. Niu, R. Kang, D. Guo, Formation mechanism and process optimization of nano Al₂O₃-ZrO₂ eutectic ceramic via laser engineered net shaping (LENS), Ceram. Int. 43 (2017) 14742–14747, <https://doi.org/10.1016/j.ceramint.2017.07.214>.
- [388] F. Niu, D. Wu, S. Zhou, G. Ma, Power prediction for laser engineered net shaping of Al₂O₃ ceramic parts, J. Eur. Ceram. Soc. 34 (2014) 3811–3817, <https://doi.org/10.1016/j.jeurceramsoc.2014.06.023>.
- [389] G. Ma, S. Yan, D. Wu, Q. Miao, M. Liu, F. Niu, Microstructure evolution and mechanical properties of ultrasonic assisted laser clad yttria stabilized zirconia coating, Ceram. Int. 43 (2017) 9622–9629, <https://doi.org/10.1016/j.ceramint.2017.04.103>.
- [390] G.K. Mishra, C.P. Paul, A.K. Rai, A.K. Agrawal, S.K. Rai, K.S. Bindra, Experimental investigation on Laser Directed Energy Deposition based additive manufacturing of Al₂O₃ bulk structures, Ceram. Int. 47 (2020) 5708–5720, <https://doi.org/10.1016/j.ceramint.2020.10.157>.
- [391] S. Nam, I.H. Jung, Y.M. Kim, DED type laser additive manufacturing technology of oxide ceramics, J. Weld. Join. 38 (2020) 469–478, <https://doi.org/10.5781/JWJ.2020.38.5.6>.
- [392] D. Wu, J. San, F. Niu, D. Zhao, X. Liang, S. Yan, G. Ma, Effect and mechanism of ZrO₂ doping on the cracking behavior of melt-grown Al₂O₃ ceramics prepared by directed laser deposition, Int. J. Appl. Ceram. Technol. 17 (2020) 227–238, <https://doi.org/10.1111/ijac.13374>.
- [393] S. Yan, Y. Huang, D. Zhao, F. Niu, G. Ma, D. Wu, 3D printing of nano-scale Al₂O₃-ZrO₂ eutectic ceramic: principle analysis and process optimization of pores, Addit. Manuf. 28 (2019) 120–126, <https://doi.org/10.1016/j.addma.2019.04.024>.
- [394] J.M. Pappas, A.R. Thakur, X. Dong, Effects of zirconia doping on additively manufactured alumina ceramics by laser direct deposition, Mater. Des. 192 (2020), 108711, <https://doi.org/10.1016/j.matdes.2020.108711>.
- [395] Y. Hu, H. Wang, W. Cong, B. Zhao, Directed energy deposition of zirconia-toughened alumina ceramic: novel microstructure formation and mechanical performance, J. Manuf. Sci. Eng. 142 (2020) 021005, <https://doi.org/10.1115/1.4045626>.
- [396] D. Wu, J. San, F. Niu, D. Zhao, Y. Huang, G. Ma, Directed laser deposition of Al₂O₃-ZrO₂ melt-grown composite ceramics with multiple composition ratios, J. Mater. Sci. 55 (2020) 6794–6809, <https://doi.org/10.1007/s10853-020-04524-7>.
- [397] J.M. Pappas, X. Dong, Direct 3D printing of silica doped transparent magnesium aluminate spinel ceramics, Materials 13 (2020) 4810, <https://doi.org/10.3390/ma13214810>.
- [398] V.K. Balla, S. Bose, A. Bandyopadhyay, Processing of bulk alumina ceramics using laser engineered net shaping, Int. J. Appl. Ceram. Technol. 5 (2008) 234–242, <https://doi.org/10.1111/j.1744-7402.2008.02202.x>.
- [399] J.M. Pappas, A.R. Thakur, E.C. Kinzel, X. Dong, Direct 3D printing of transparent magnesium aluminate spinel ceramics, J. Laser Appl. 33 (2021), 12018, <https://doi.org/10.2351/7.000327>.
- [400] J.M. Pappas, X. Dong, Porosity characterization of additively manufactured transparent MgAl₂O₄ spinel by laser direct deposition, Ceram. Int. 46 (2020) 6745–6755, <https://doi.org/10.1016/j.ceramint.2019.11.164>.
- [401] J.M. Pappas, E.C. Kinzel, X. Dong, Laser direct deposited transparent magnesium aluminate spinel ceramics, Manuf. Lett. 24 (2020) 92–95, <https://doi.org/10.1016/j.mfglet.2020.04.003>.
- [402] K. Vartanian, T. McDonald, Accelerating industrial adoption of metal additive manufacturing technology, JOM 68 (2016) 806–810, <https://doi.org/10.1007/s11837-015-1794-9>.
- [403] Y. Xiong, J.E. Smugeresky, J.M. Schoenung, The influence of working distance on laser deposited WC-Co, J. Mater. Process. Technol. 209 (2009) 4935–4941, <https://doi.org/10.1016/j.jmatprot.2009.01.016>.
- [404] Y. Xiong, M. Kim, O. Seo, J.M. Schoenung, S. Kang, (Ti,W)C-Ni cermets by laser engineered net shaping, Powder Metall. 53 (2010) 41–46, <https://doi.org/10.1179/174329009X380581>.
- [405] Y. Xiong, W.H. Hofmeister, Z. Cheng, J.E. Smugeresky, E.J. Lavernia, J. M. Schoenung, In situ thermal imaging and three-dimensional finite element modeling of tungsten carbide-cobalt during laser deposition, Acta Mater. 57 (2009) 5419–5429, <https://doi.org/10.1016/j.actamat.2009.07.038>.
- [406] F. Niu, D. Wu, G. Ma, S. Zhou, B. Zhang, Effect of second-phase doping on laser deposited Al₂O₃ ceramics, Rapid Prototyp. J. 21 (2015) 201–206, <https://doi.org/10.1108/RPJ-12-2014-0167>.
- [407] F. Niu, D. Wu, G. Ma, J. Wang, J. Zhuang, Z. Jin, Rapid fabrication of eutectic ceramic structures by laser engineered net shaping, Procedia CIRP 42 (2016) 91–95, <https://doi.org/10.1016/j.procir.2016.02.196>.
- [408] Z. Liu, K. Song, B. Gao, T. Tian, H. Yang, X. Lin, W. Huang, Microstructure and mechanical properties of Al₂O₃/ZrO₂ directionally solidified eutectic ceramic prepared by laser 3D printing, J. Mater. Sci. Technol. 32 (2016) 320–325, <https://doi.org/10.1016/j.jmst.2015.11.017>.
- [409] S. Yan, D. Wu, F. Niu, Y. Huang, N. Liu, G. Ma, Effect of ultrasonic power on forming quality of nano-sized Al₂O₃-ZrO₂ eutectic ceramic via laser engineered net shaping (LENS), Ceram. Int. 44 (2018) 1120–1126, <https://doi.org/10.1016/j.ceramint.2017.10.067>.
- [410] S. Yan, D. Wu, G. Ma, F. Niu, R. Kang, D. Guo, Nano-sized Al₂O₃-ZrO₂ eutectic ceramic structures prepared by ultrasonic-assisted laser engineered net shaping, Mater. Lett. 212 (2018) 8–11, <https://doi.org/10.1016/j.matlet.2017.10.053>.
- [411] F.Y. Niu, D.J. Wu, S. Yan, G.Y. Ma, B. Zhang, Process optimization for suppressing cracks in laser engineered net shaping of Al₂O₃ ceramics, JOM 69 (2017) 557–562, <https://doi.org/10.1007/s11837-016-2191-8>.
- [412] B. Zheng, T. Topping, J.E. Smugeresky, Y. Zhou, A. Biswas, D. Baker, E. J. Lavernia, The influence of Ni-coated TiC on laser-deposited IN625 metal matrix composites, Metall. Mater. Trans. A Phys. Metall. Mater. Sci. 41 (2010) 568–573, <https://doi.org/10.1007/s11661-009-0126-5>.
- [413] M.Y. Shen, X.J. Tian, D. Liu, H.B. Tang, X. Cheng, Microstructure and fracture behavior of TiC particles reinforced Inconel 625 composites prepared by laser additive manufacturing, J. Alloys Compd. 734 (2018) 188–195, <https://doi.org/10.1016/j.jallcom.2017.10.280>.
- [414] R. Banerjee, A. Genç, D. Hill, P.C. Collins, H.L. Fraser, Nanoscale TiB precipitates in laser deposited Ti-matrix composites, Scripta Mater. 53 (2005) 1433–1437, <https://doi.org/10.1016/j.scriptamat.2005.08.014>.
- [415] S. Roy, M. Das, A.K. Mallik, V.K. Balla, Laser melting of titanium-diamond composites: microstructure and mechanical behavior study, Mater. Lett. 178 (2016) 284–287, <https://doi.org/10.1016/j.matlet.2016.05.023>.
- [416] B. Zheng, J.E. Smugeresky, Y. Zhou, D. Baker, E.J. Lavernia, Microstructure and properties of laser-deposited Ti6Al4V metal matrix composites using Ni-Coated powder, Metall. Mater. Trans. A Phys. Metall. Mater. Sci. 39 (2008) 1196–1205, <https://doi.org/10.1007/s11661-008-9498-1>.
- [417] F. Wang, J. Mei, H. Jiang, X. Wu, Laser fabrication of Ti6Al4V/TiC composites using simultaneous powder and wire feed, Mater. Sci. Eng. 445–446 (2007) 461–466, <https://doi.org/10.1016/j.msea.2006.09.093>.
- [418] S. Liu, Y.C. Shin, The influences of melting degree of TiC reinforcements on microstructure and mechanical properties of laser direct deposited Ti6Al4V-TiC composites, Mater. Des. 136 (2017) 185–195, <https://doi.org/10.1016/j.matesdes.2017.09.063>.
- [419] J. Wang, L. Li, C. Tan, H. Liu, P. Lin, Microstructure and tensile properties of TiCp/Ti6Al4V titanium matrix composites manufactured by laser melting deposition, J. Mater. Process. Technol. 252 (2018) 524–536, <https://doi.org/10.1016/j.jmatprotec.2017.10.005>.
- [420] C.A. Brice, K.I. Schwendner, S. Amacherla, H.L. Fraser, X.D. Zhang, Characterization of laser deposited niobium and molybdenum silicides, MRS Online Proc. Libr. 625 (2000) 31, <https://doi.org/10.1557/PROC-625-31>.
- [421] T. Wang, J. Liu, L. Qin, J. Tang, J. Wu, Laser direct deposition of CoCrAlSiY/YSZ composites: densification, microstructure and mechanical properties, J. Therm. Spray Technol. 28 (2019) 862–879, <https://doi.org/10.1007/s11666-019-00859-z>.
- [422] R.S. Amano, S. Marek, B.F. Schultz, P.K. Rohatgi, Laser engineered net shaping process for 316L/15% nickel coated titanium carbide metal matrix composite, J. Manuf. Sci. Eng. 136 (2014), 051007, <https://doi.org/10.1115/1.4027758>.
- [423] N. Preprint, T.W. Scharf, A. Neira, J.Y. Hwang, J. Tiley, R. Banerjee, Solid Lubrication of Laser Deposited Carbon Nanotube Reinforced Nickel Matrix, 2009.
- [424] T.W. Scharf, A. Neira, J.Y. Hwang, J. Tiley, R. Banerjee, Self-lubricating carbon nanotube reinforced nickel matrix composites, J. Appl. Phys. 106 (2009) 013508, <https://doi.org/10.1063/1.3158360>.
- [425] S. Gopagni, J.Y. Hwang, A.R.P. Singh, B.A. Mensah, N. Bunce, J. Tiley, T. W. Scharf, R. Banerjee, Microstructural evolution in laser deposited nickel-titanium-carbon in situ metal matrix composites, J. Alloys Compd. 509 (2011) 1255–1260, <https://doi.org/10.1016/j.jallcom.2010.09.208>.
- [426] Y. Hu, B. Zhao, F. Ning, H. Wang, W. Cong, In-situ ultrafine three-dimensional quasi-continuous network microstructural TiB reinforced titanium matrix composites fabrication using laser engineered net shaping, Mater. Lett. 195 (2017) 116–119, <https://doi.org/10.1016/j.matlet.2017.02.112>.
- [427] Y. Hu, W. Cong, X. Wang, Y. Li, F. Ning, H. Wang, Laser deposition-additive manufacturing of TiB-Ti composites with novel three-dimensional quasi-continuous network microstructure: effects on strengthening and toughening, Compos. B Eng. 133 (2018) 91–100, <https://doi.org/10.1016/j.compositesb.2017.09.019>.
- [428] B.M. Arkhurst, J.J. Park, C.H. Lee, J.H. Kim, Direct laser deposition of 14Cr oxide dispersion strengthened steel powders using Y₂O₃ and HfO₂ dispersoids, J. Korean Inst. Met. Mater. 55 (2017) 550–558, <https://doi.org/10.3365/KJMM.2017.55.8.550>.
- [429] Y. Hu, F. Ning, H. Wang, W. Cong, B. Zhao, Laser engineered net shaping of quasi-continuous network microstructural TiB reinforced titanium matrix bulk composites: microstructure and wear performance, Opt. Laser. Technol. 99 (2018) 174–183, <https://doi.org/10.1016/j.optlastec.2017.08.032>.
- [430] T. Gualtieri, A. Bandyopadhyay, Niobium carbide composite coatings on SS304 using laser engineered net shaping (LENS™), Mater. Lett. 189 (2017) 89–92, <https://doi.org/10.1016/j.matlet.2016.11.071>.
- [431] H. Tan, D. Hao, K. Al-Hamdan, F. Zhang, Z. Xu, A.T. Clare, Direct metal deposition of TiB₂/AlSi10Mg composites using satellited powders, Mater. Lett. 214 (2018) 123–126, <https://doi.org/10.1016/j.matlet.2017.11.121>.
- [432] S. Cao, D. Gu, Q. Shi, Relation of microstructure, microhardness and underlying thermodynamics in molten pools of laser melting deposition processed TiC/Inconel 625 composites, J. Alloys Compd. 692 (2017) 758–769, <https://doi.org/10.1016/j.jallcom.2016.09.098>.
- [433] J.A. Vreeling, V. Ocelík, G.A. Hamstra, Y.T. Pei, J.T.M. De Hosson, In-situ microscopy investigation of failure mechanisms in Al/SiCp metal matrix composite produced by laser embedding, Scripta Mater. 42 (2000) 589–595, [https://doi.org/10.1016/S1359-6462\(99\)00404-2](https://doi.org/10.1016/S1359-6462(99)00404-2).
- [434] S. Pouzet, P. Peyre, C. Gorny, O. Castelnau, T. Baudin, F. Brisset, C. Colin, P. Gadaud, Additive layer manufacturing of titanium matrix composites using the direct metal deposition laser process, Mater. Sci. Eng. 677 (2016) 171–181, <https://doi.org/10.1016/j.msea.2016.09.002>.
- [435] J.M. Wilson, Y.C. Shin, Microstructure and wear properties of laser-deposited functionally graded Inconel 690 reinforced with TiC, Surf. Coatings. Technol. 207 (2012) 517–522, <https://doi.org/10.1016/j.surcoat.2012.07.058>.
- [436] L. Li, J. Wang, P. Lin, H. Liu, Microstructure and mechanical properties of functionally graded TiCp/Ti6Al4V composite fabricated by laser melting

- deposition, Ceram. Int. 43 (2017) 16638–16651, <https://doi.org/10.1016/j.ceramint.2017.09.054>.
- [437] W. Liu, J.N. DuPont, Fabrication of functionally graded TiC/Ti composites by laser engineered net shaping, Scripta Mater. 48 (2003) 1337–1342, [https://doi.org/10.1016/S1359-6462\(03\)00020-4](https://doi.org/10.1016/S1359-6462(03)00020-4).
- [438] T. Zhao, M. Dahmen, W. Cai, M. Alkhayat, J. Schaible, P. Albus, C. Zhong, C. Hong, T. Biermann, H. Zhang, Laser metal deposition for additive manufacturing of AA5024 and nanoparticulate TiC modified AA5024 alloy composites prepared with balling milling process, Opt. Laser. Technol. 131 (2020), 106438, <https://doi.org/10.1016/j.optlastec.2020.106438>.
- [439] J. Wang, L. Li, P. Lin, J. Wang, Effect of TiC particle size on the microstructure and tensile properties of TiCp/Ti6Al4V composites fabricated by laser melting deposition, Opt. Laser Technol. 105 (2018) 195–206, <https://doi.org/10.1016/j.optlastec.2018.03.009>.
- [440] L.C. Naidoo, O.S. Fatoba, S.A. Akinlabi, R.M. Mahamood, M.Y. Shatalov, E. V. Murashkin, S. Hassan, E.T. Akinlabi, Study of additive manufactured Ti-Al-Si-Cu/Ti-6Al-4V composite coating by direct laser metal deposition (DLMD) technique, in: S.S. Emamian, M. Awang, F. Yusof (Eds.), Advances in Manufacturing Engineering, Lecture Notes in Mechanical Engineering, Springer, Singapore, 2020, pp. 503–513, https://doi.org/10.1007/978-981-15-5753-8_46.
- [441] S. Su, Y. Lu, Laser directed energy deposition of Zr-based bulk metallic glass composite with tensile strength, Mater. Lett. 247 (2019) 79–81, <https://doi.org/10.1016/j.matlet.2019.03.111>.
- [442] P.K. Farayibi, T.E. Abioye, A. Kennedy, A.T. Clare, Development of metal matrix composites by direct energy deposition of ‘satellited’ powders, J. Manuf. Process. 45 (2019) 429–437, <https://doi.org/10.1016/j.jmapro.2019.07.029>.
- [443] X. Li, C.H. Zhang, S. Zhang, C.L. Wu, J.B. Zhang, H.T. Chen, A.O. Abdullah, Design, preparation, microstructure and properties of novel wear-resistant stainless steel-base composites using laser melting deposition, Vacuum 165 (2019) 139–147, <https://doi.org/10.1016/j.vacuum.2019.04.016>.
- [444] H. Sahasrabudhe, S. Bose, A. Bandyopadhyay, Laser processed calcium phosphate reinforced CoCrMo for load-bearing applications: processing and wear induced damage evaluation, Acta Biomater. 66 (2018) 118–128, <https://doi.org/10.1016/j.actbio.2017.11.022>.
- [445] G. Ma, C. Yu, B. Tang, Y. Li, F. Niu, D. Wu, G. Bi, S. Liu, High-mass-proportion TiCp/Ti6Al4V titanium matrix composites prepared by directed energy deposition, Addit. Manuf. 35 (2020), 101323, <https://doi.org/10.1016/j.addma.2020.101323>.
- [446] A.S.P. Pereira, TiC-Reinforced Inconel X750 Metal Matrix Composite Produced through Laser Directed Energy Deposition, MSc thesis, Universidade Federal de Santa Catarina, Florianópolis, Brazil, 2020.
- [447] L. Constantini, L. Fan, M. Pontoreau, F. Wang, B. Cui, J.-L. Battaglia, J.-F. Silvain, Y.F. Lu, Additive manufacturing of copper/diamond composites for thermal management applications, Manuf. Lett. 24 (2020) 61–66, <https://doi.org/10.1016/j.mfglet.2020.03.014>.
- [448] J.D. Avila, Z. Alrawahi, S. Bose, A. Bandyopadhyay, Additively manufactured Ti6Al4V-Si-Hydroxyapatite composites for articulating surfaces of load-bearing implants, Addit. Manuf. 34 (2020), 101241, <https://doi.org/10.1016/j.addma.2020.101241>.
- [449] Y. Huang, D. Wu, D. Zhao, F. Niu, H. Zhang, S. Yan, G. Ma, Process optimization of melt growth alumina/aluminum titanate composites directed energy deposition: effects of scanning speed, Addit. Manuf. 35 (2020), 101210, <https://doi.org/10.1016/j.addma.2020.101210>.
- [450] H. Sahasrabudhe, A. Bandyopadhyay, Additive manufacturing of reactive in situ Zr based ultra-high temperature ceramic composites, JOM 68 (2016) 822–830, <https://doi.org/10.1007/s11837-015-1777-x>.
- [451] S. Yan, D. Wu, Y. Huang, N. Liu, Y. Zhang, F. Niu, G. Ma, C fiber toughening $\text{Al}_2\text{O}_3\text{-ZrO}_2$ eutectic via ultrasonic-assisted directed laser deposition, Mater. Lett. 235 (2019) 228–231, <https://doi.org/10.1016/j.matlet.2018.10.047>.
- [452] J. Yao, J. Zhang, G. Wu, L. Wang, Q. Zhang, R. Liu, Microstructure and wear resistance of laser cladded composite coatings prepared from pre-alloyed WC-NiCrMo powder with different laser spots, Opt. Laser. Technol. 101 (2018) 520–530, <https://doi.org/10.1016/j.optlastec.2017.12.007>.
- [453] C.L. Wu, S. Zhang, C.H. Zhang, J.B. Zhang, Y. Liu, Formation mechanism and phase evolution of in situ synthesizing TiC-reinforced 316L stainless steel matrix composites by laser melting deposition, Mater. Lett. 217 (2018) 304–307, <https://doi.org/10.1016/j.matlet.2018.01.097>.
- [454] D. Wu, Y. Huang, F. Niu, G. Ma, S. Yan, C. Li, J. Ding, Effects of TiO_2 doping on microstructure and properties of directed laser deposition alumina/aluminum titanate composites, Virtual Phys. Prototyp. 14 (2019) 371–381, <https://doi.org/10.1080/17452759.2019.1622987>.
- [455] J.Y. Hwang, A. Neira, T.W. Scharf, J. Tiley, R. Banerjee, Laser-deposited carbon nanotube reinforced nickel matrix composites, Scripta Mater. 59 (2008) 487–490, <https://doi.org/10.1016/j.scriptamat.2008.04.032>.
- [456] S. Su, Y. Lu, Densified WCu composite fabricated via laser additive manufacturing, Int. J. Refract. Metals Hard Mater. 87 (2020), 105122, <https://doi.org/10.1016/j.ijrmhm.2019.105122>.
- [457] K. Stenberg, S. Dittrick, S. Bose, A. Bandyopadhyay, Influence of simultaneous addition of carbon nanotubes and calcium phosphate on wear resistance of 3D-printed Ti6Al4V, J. Mater. Res. 33 (2018) 2077–2086, <https://doi.org/10.1557/jmr.2018.234>.
- [458] H. Sahasrabudhe, J. Soderlind, A. Bandyopadhyay, Laser processing of in situ TiN/Ti composite coating on titanium, J. Mech. Behav. Biomed. Mater. 53 (2016) 239–249, <https://doi.org/10.1016/j.jmbbm.2015.08.013>.
- [459] K.D. Traxel, A. Bandyopadhyay, Reactive-deposition-based additive manufacturing of Ti-Zr-BN composites, Addit. Manuf. 24 (2018) 353–363, <https://doi.org/10.1016/j.addma.2018.10.005>.
- [460] M. Isik, J.D. Avila, A. Bandyopadhyay, Alumina and tricalcium phosphate added CoCr alloy for load-bearing implants, Addit. Manuf. 36 (2020), 101553, <https://doi.org/10.1016/j.addma.2020.101553>.
- [461] S. Nag, S. Samuel, A. Puthucode, R. Banerjee, Characterization of novel borides in Ti-Nb-Zr-Ta+2B metal-matrix composites, Mater. Char. 60 (2009) 106–113, <https://doi.org/10.1016/j.matchar.2008.07.011>.
- [462] J.D. Avila, A. Bandyopadhyay, Influence of boron nitride reinforcement to improve high temperature oxidation resistance of titanium, J. Mater. Res. 34 (2019) 1279–1289, <https://doi.org/10.1557/jmr.2019.11>.
- [463] M. Das, K. Bhattacharya, S.A. Dittrick, C. Mandal, V.K. Balla, T.S. Sampath Kumar, A. Bandyopadhyay, I. Manna, In situ synthesized TiB-TiN reinforced Ti6Al4V alloy composite coatings: microstructure, tribological and in-vitro biocompatibility, J. Mech. Behav. Biomed. Mater. 29 (2014) 259–271, <https://doi.org/10.1016/j.jmbbm.2013.09.006>.
- [464] R. Banerjee, P.C. Collins, H.L. Fraser, Laser deposition of in situ Ti-TiB composites, Adv. Eng. Mater. 4 (2002) 847–851, [https://doi.org/10.1002/1527-2648\(20021105\)4:11<847::AID-ADEM847>3.0.CO;2-C](https://doi.org/10.1002/1527-2648(20021105)4:11<847::AID-ADEM847>3.0.CO;2-C).
- [465] B. Zheng, Y. Li, J.E. Smugeresky, Y. Zhou, D. Baker, E.J. Lavernia, Hybrid Al+ Al_3Ni metallic foams synthesized in situ via laser engineered net shaping, Philos. Mag. 91 (2011) 3473–3497, <https://doi.org/10.1080/14786435.2011.586375>.
- [466] S. Wang, S. Zhang, C.H. Zhang, C.L. Wu, J. Chen, M.B. Shahzad, Effect of Cr₃C₂ content on 316L stainless steel fabricated by laser melting deposition, Vacuum 147 (2018) 92–98, <https://doi.org/10.1016/j.vacuum.2017.10.027>.
- [467] M. Policelli, Development of a New Method to Fabricate Titanium Metal Matrix Composites via LENS with Improved Material Properties, BSc Thesis, The Pennsylvania State University, August 2011.
- [468] S. Samuel, Surface Engineering and Characterization of Laser Deposited Metallic Biomaterials, MSc thesis, University of North Texas, May 2007.
- [469] S. Samuel, S. Nag, T.W. Scharf, R. Banerjee, Wear resistance of laser-deposited boride reinforced Ti-Nb-Zr-Ta alloy composites for orthopedic implants, Mater. Sci. Eng. C 28 (2008) 414–420, <https://doi.org/10.1016/j.msec.2007.04.029>.
- [470] M. Das, V.K. Balla, D. Basu, I. Manna, T.S. Sampath Kumar, A. Bandyopadhyay, Laser processing of in situ synthesized TiB-TiN-reinforced Ti6Al4V alloy coatings, Scripta Mater. 66 (2012) 578–581, <https://doi.org/10.1016/j.scriptamat.2012.01.010>.
- [471] M. Iazińska, T. Durejko, W. Polkowski, The effect of nanometric $\alpha\text{-Al}_2\text{O}_3$ addition on structure and mechanical properties of feal alloys fabricated by lens technique, Arch. Metall. Mater. 62 (2017) 1703–1712, <https://doi.org/10.1515/amm-2017-0260>.
- [472] A. Emamian, M.H. Farshidianfar, A. Khajepour, Thermal monitoring of microstructure and carbide morphology in direct metal deposition of Fe-Ti-C metal matrix composites, J. Alloys Compd. 710 (2017) 20–28, <https://doi.org/10.1016/j.jallcom.2017.03.207>.
- [473] A. Amar, J. Li, S. Xiang, X. Liu, Y. Zhou, G. Le, X. Wang, F. Qu, S. Ma, W. Dong, Q. Li, Additive manufacturing of high-strength CrMnFeCoNi-based high entropy alloys with TiC addition, Intermetallics 109 (2019) 162–166, <https://doi.org/10.1016/j.intermet.2019.04.005>.
- [474] A. Reichardt, R.P. Dillon, J.P. Borgonia, A.A. Shapiro, B.W. McEnerney, T. Momose, P. Hosemann, Development and characterization of Ti-6Al-4V to 304L stainless steel gradient components fabricated with laser deposition additive manufacturing, Mater. Des. 104 (2016) 404–413, <https://doi.org/10.1016/j.matedes.2016.05.016>.
- [475] W. Li, S. Karnati, C. Kriewall, F. Liou, J. Newkirk, K.M. Brown Taminger, W. J. Seufzer, Fabrication and characterization of a functionally graded material from Ti-6Al-4V to SS316 by laser metal deposition, Addit. Manuf. 14 (2017) 95–104, <https://doi.org/10.1016/j.addma.2016.12.006>.
- [476] P.C. Collins, R. Banerjee, H.L. Fraser, Laser deposition of compositionally graded titanium-vanadium and titanium-molybdenum alloys, Mater. Sci. Eng. 352 (2003) 118–128, [https://doi.org/10.1016/S0921-5093\(02\)00909-7](https://doi.org/10.1016/S0921-5093(02)00909-7).
- [477] M.Y. Mendoza, P. Samimi, D.A. Brice, B.W. Martin, M.R. Rolchigo, R. LeSar, P. C. Collins, Microstructures and grain refinement of additive-manufactured Ti-xW alloys, Metall. Mater. Trans. 48 (2017) 3594–3605, <https://doi.org/10.1007/s11661-017-4117-7>.
- [478] B.A. Welk, M.A. Gibson, H.L. Fraser, A combinatorial approach to the investigation of metal systems that form both bulk metallic glasses and high entropy alloys, JOM 68 (2016) 1021–1026, <https://doi.org/10.1007/s11837-015-1779-8>.
- [479] Q. Wang, S. Zhang, C.H. Zhang, C. Wu, J. Wang, J. Chen, Z. Sun, Microstructure evolution and EBSD analysis of a graded steel fabricated by laser additive manufacturing, Vacuum 141 (2017) 68–81, <https://doi.org/10.1016/j.vacuum.2017.03.021>.
- [480] D.C. Hofmann, S. Roberts, R. Otis, J. Kolodziejska, R.P. Dillon, J.O. Suh, A. A. Shapiro, Z.K. Liu, J.P. Borgonia, Developing gradient metal alloys through radial deposition additive manufacturing, Sci. Rep. 4 (2014) 5357, <https://doi.org/10.1038/srep05357>.
- [481] C.H. Zhang, H. Zhang, C.L. Wu, S. Zhang, Z.L. Sun, S.Y. Dong, Multi-layer functional graded stainless steel fabricated by laser melting deposition, Vacuum 141 (2017) 181–187, <https://doi.org/10.1016/j.vacuum.2017.04.020>.
- [482] T. Hwang, Y.Y. Woo, S.W. Han, Y.H. Moon, Functionally graded properties in directed-energy-deposition titanium parts, Opt. Laser. Technol. 105 (2018) 80–88, <https://doi.org/10.1016/j.optlastec.2018.02.057>.

- [483] T. Borkar, R. Conteri, X. Chen, R.V. Ramanujan, R. Banerjee, Laser additive processing of functionally-graded Fe–Si–B–Cu–Nb soft magnetic materials, *Mater. Manuf. Process.* 32 (2017) 1581–1587, <https://doi.org/10.1080/10426914.2016.1244849>.
- [484] R.R. Unocic, J.N. DuPont, Composition control in the direct laser-deposition process, *Metall. Mater. Trans. B* 34 (2003) 439–445, <https://doi.org/10.1007/s11663-003-0070-5>.
- [485] R.M. Mahamood, E.T. Akinlabi, Laser metal deposition of functionally graded Ti6Al4V/TiC, *Mater. Des.* 84 (2015) 402–410, <https://doi.org/10.1016/j.matdes.2015.06.135>.
- [486] D.D. Lima, S.A. Mantri, C.V. Mikler, R. Contieri, C.J. Yannetta, K.N. Campo, E.S. Lopes, M.J. Styles, T. Borkar, R. Caram, R. Banerjee, Laser additive processing of a functionally graded internal fracture fixation plate, *Mater. Des.* 130 (2017) 8–15, <https://doi.org/10.1016/j.matdes.2017.05.034>.
- [487] M. Tlotengl, S. Pityana, Effects of Al and heat treatment on the microstructure and hardness of Ti-Al synthesized via in situ melting using LENS, *Metals* 9 (2019) 623, <https://doi.org/10.3390/met9060623>.
- [488] S.S. Kumar, I.I.T. Bombay, Development of a Co-Cr-Mo to tantalum transition using LENS for orthopedic applications, in: *Int. Solid Freeform Fabrication Symp.*, 2005, pp. 273–282.
- [489] B.E. Carroll, R.A. Otis, J.P. Borgonia, J.O. Suh, R.P. Dillon, A.A. Shapiro, D.C. Hofmann, Z.K. Liu, A.M. Beese, Functionally graded material of 304L stainless steel and inconel 625 fabricated by directed energy deposition: characterization and thermodynamic modeling, *Acta Mater.* 108 (2016) 46–54, <https://doi.org/10.1016/j.actamat.2016.02.019>.
- [490] O. Oyelola, P. Crawforth, R. M'Saoubi, A.T. Clare, Machining of functionally graded Ti6Al4V/WC produced by directed energy deposition, *Addit. Manuf.* 24 (2018) 20–29, <https://doi.org/10.1016/j.addma.2018.09.007>.
- [491] C. Schneider-Maunoury, L. Weiss, P. Acquier, D. Boisselier, P. Laheurte, Functionally graded Ti6Al4V-Mo alloy manufactured with DED-CLAD® process, *Addit. Manuf.* 17 (2017) 55–66, <https://doi.org/10.1016/j.addma.2017.07.008>.
- [492] H. Knoll, S. Ocylok, A. Weisheit, H. Springer, E. Jägle, D. Raabe, Combinatorial alloy design by laser additive manufacturing, *Steel Res. Int.* 88 (2017) 1–11, <https://doi.org/10.1002/srin.201600416>.
- [493] P. Tsai, K.M. Flores, High-throughput discovery and characterization of multicomponent bulk metallic glass alloys, *Acta Mater.* 120 (2016) 426–434, <https://doi.org/10.1016/j.actamat.2016.08.068>.
- [494] B. Onuike, A. Bandyopadhyay, Additive manufacturing of Inconel 718 – Ti6Al4V bimetallic structures, *Addit. Manuf.* 22 (2018) 844–851, <https://doi.org/10.1016/j.addma.2018.06.025>.
- [495] K. Zhang, W. Li, Y. Xu, B. Liu, Y. Li, D. Liu, X. Ding, X. Jin, Rapid construction of multicomponent TRIP stainless steel by powder feeding laser deposition for comprehensive properties, *Mater. Des.* 184 (2019), 108171, <https://doi.org/10.1016/j.matdes.2019.108171>.
- [496] L.D. Bobbio, B. Bocklund, R. Otis, J.P. Borgonia, R.P. Dillon, A.A. Shapiro, B. McEnery, Z.K. Liu, A.M. Beese, Characterization of a functionally graded material of Ti-6Al-4V to 304L stainless steel with an intermediate V section, *J. Alloys Compd.* 742 (2018) 1031–1036, <https://doi.org/10.1016/j.jallcom.2018.01.156>.
- [497] A. Almeida, D. Gupta, C. Loable, R. Vilar, Laser-assisted synthesis of Ti–Mo alloys for biomedical applications, *Mater. Sci. Eng. C* 32 (2012) 1190–1195, <https://doi.org/10.1016/j.msec.2012.03.007>.
- [498] H. Sahasrabudhe, R. Harrison, C. Carpenter, A. Bandyopadhyay, Stainless steel to titanium bimetallic structure using LENS, *Addit. Manuf.* 5 (2015) 1–8, <https://doi.org/10.1016/j.addma.2014.10.002>.
- [499] F. Wang, J. Mei, X. Wu, Compositationally graded Ti6Al4V+TiC made by direct laser fabrication using powder and wire, *Mater. Des.* 28 (2007) 2040–2046, <https://doi.org/10.1016/j.matdes.2006.06.010>.
- [500] Y. Zhang, Z. Wei, L. Shi, M. Xi, Characterization of laser powder deposited Ti–TiC composites and functional gradient materials, *J. Mater. Process. Technol.* 206 (2008) 438–444, <https://doi.org/10.1016/j.jmatprotc.2007.12.055>.
- [501] J. Obielodan, B. Stucker, Characterization of LENS-fabricated Ti6Al4V and Ti6Al4V/TiC dual-material transition joints, *Int. J. Adv. Manuf. Technol.* 66 (2013) 2053–2061, <https://doi.org/10.1007/s00170-012-4481-9>.
- [502] Y. Zhang, A. Bandyopadhyay, Direct fabrication of compositionally graded Ti-Al₂O₃ multi-material structures using Laser Engineered Net Shaping, *Addit. Manuf.* 21 (2018) 104–111, <https://doi.org/10.1016/j.addma.2018.03.001>.
- [503] X. Zhang, Y. Chen, F. Liou, Fabrication of SS316L-IN625 functionally graded materials by powder-fed directed energy deposition, *Sci. Technol. Weld. Join.* 24 (2019) 504–516, <https://doi.org/10.1080/13621718.2019.1589086>.
- [504] W. Meng, Y. Xiaohui, W. Zhang, F. Junfei, G. Lijie, M. Qunshuang, C. Bing, Additive manufacturing of a functionally graded material from Inconel625 to Ti6Al4V by laser synchronous preheating, *J. Mater. Process. Technol.* 275 (2020), 116368, <https://doi.org/10.1016/j.jmatprotc.2019.116368>.
- [505] T. Durejko, M. Zietala, W. Polkowski, T. Czujko, Thin wall tubes with Fe₃Al/SS316L graded structure obtained by using laser engineered net shaping technology, *Mater. Des.* 63 (2014) 766–774, <https://doi.org/10.1016/j.matdes.2014.07.011>.
- [506] W. Meng, W. Zhang, W. Zhang, X. Yin, L. Guo, B. Cui, Additive fabrication of 316L/Inconel625/Ti6Al4V functionally graded materials by laser synchronous preheating, *Int. J. Adv. Manuf. Technol.* 104 (2019) 2525–2538, <https://doi.org/10.1007/s00170-019-04061-x>.
- [507] A. Thiriet, C. Schneider-Maunoury, P. Laheurte, D. Boisselier, L. Weiss, Multiscale study of different types of interface of a buffer material in powder-based directed energy deposition: example of Ti6Al4V/Ti6Al4V-Mo/Mo-Inconel 718, *Addit. Manuf.* 27 (2019) 118–130, <https://doi.org/10.1016/j.addma.2019.02.007>.
- [508] F. Khodabakhshi, M.H. Farshidianfar, S. Bakhshivash, A.P. Gerlich, A. Khajepour, Dissimilar metals deposition by directed energy based on powder-fed laser additive manufacturing, *J. Manuf. Process.* 43 (2019) 83–97, <https://doi.org/10.1016/j.jmapro.2019.05.018>.
- [509] Y. Su, B. Chen, C. Tan, X. Song, J. Feng, Influence of composition gradient variation on the microstructure and mechanical properties of 316 L/Inconel 718 functionally graded material fabricated by laser additive manufacturing, *J. Mater. Process. Technol.* 283 (2020), 116702, <https://doi.org/10.1016/j.jmatprotec.2020.116702>.
- [510] T. Kunimine, R. Miyazaki, Y. Yamashita, Y. Funada, Effects of laser-beam defocus on microstructural features of compositionally graded WC/Co-alloy composites additively manufactured by multi-beam laser directed energy deposition, *Sci. Rep.* 10 (2020) 1–11, <https://doi.org/10.1038/s41598-020-65429-8>.
- [511] J.S. Zuback, T.A. Palmer, T. DebRoy, Additive manufacturing of functionally graded transition joints between ferritic and austenitic alloys, *J. Alloys Compd.* 770 (2019) 995–1003, <https://doi.org/10.1016/j.jallcom.2018.08.197>.
- [512] J.S. Zuback, *Additive Manufacturing of Functionally Graded Materials between Ferritic and Austenitic Alloys*, PhD Dissertation, The Pennsylvania State University, August 2019.
- [513] C. Schneider-Maunoury, L. Weiss, O. Perroud, D. Jouyet, D. Boisselier, P. Laheurte, An application of differential injection to fabricate functionally graded Ti-Nb alloys using DED-CLAD® process, *J. Mater. Process. Technol.* 268 (2019) 171–180, <https://doi.org/10.1016/j.jmatprotec.2019.01.018>.
- [514] B. Chen, Y. Su, Z. Xie, C. Tan, J. Feng, Development and characterization of 316L/Inconel625 functionally graded material fabricated by laser direct metal deposition, *Opt. Laser. Technol.* 123 (2020), 105916, <https://doi.org/10.1016/j.optlastec.2019.105916>.
- [515] C. Shen, X. Hua, M. Reid, K.-D. Liss, G. Mou, Z. Pan, Y. Huang, H. Li, Thermal induced phase evolution of Fe–Fe₃Ni functionally graded material fabricated using the wire-arc additive manufacturing process: an in-situ neutron diffraction study, *J. Alloys Compd.* 826 (2020), 154097, <https://doi.org/10.1016/j.jallcom.2020.154097>.
- [516] T. Borkar, B. Gwalani, D. Choudhuri, C.V. Mikler, C.J. Yannetta, X. Chen, R. V. Ramanujan, M.J. Styles, M.A. Gibson, R. Banerjee, A combinatorial assessment of Al_xCuFeNi₂ (0 < x < 1.5) complex concentrated alloys: microstructure, microhardness, and magnetic properties, *Acta Mater.* 116 (2016) 63–76, <https://doi.org/10.1016/j.actamat.2016.06.025>.
- [517] G. Lu, X. Shi, X. Liu, H. Zhou, Y. Chen, Z. Yang, Y. Huang, Tribological performance of functionally graded structure of graphene nanoplatelets reinforced Ni3Al metal matrix composites prepared by laser melting deposition, *Wear* 428–429 (2019) 417–429, <https://doi.org/10.1016/j.wear.2019.04.009>.
- [518] A. Ramakrishnan, G.P. Dinda, Functionally graded metal matrix composite of Haynes 282 and SiC fabricated by laser metal deposition, *Mater. Des.* 179 (2019), 107877, <https://doi.org/10.1016/j.matdes.2019.107877>.
- [519] S.M. Banait, C.P. Paul, A.N. Jinoop, H. Kumar, R.S. Pawade, K.S. Bindra, Experimental investigation on laser directed energy deposition of functionally graded layers of Ni-Cr-B-Si and SS316L, *Opt. Laser. Technol.* 121 (2020), 105787, <https://doi.org/10.1016/j.optlastec.2019.105787>.
- [520] N. Kang, X. Lin, M. El Mansori, Q.Z. Wang, J.L. Lu, C. Coddet, W.D. Huang, On the effect of the thermal cycle during the directed energy deposition application to the in-situ production of a Ti-Mo alloy functionally graded structure, *Addit. Manuf.* 31 (2020), 100911, <https://doi.org/10.1016/j.addma.2019.100911>.
- [521] T. Zhang, H. Xu, Z. Li, H. She, D. Du, A. Dong, H. Xing, D. Wang, G. Zhu, B. Sun, Microstructure and properties of TC4/TNTZO multi-layered composite by direct laser deposition, *J. Mech. Behav. Biomed. Mater.* 109 (2020), 103842, <https://doi.org/10.1016/j.jmbbm.2020.103842>.
- [522] W. Meng, W. Zhang, W. Zhang, X. Yin, B. Cui, Fabrication of steel-Inconel functionally graded materials by laser melting deposition integrating with laser synchronous preheating, *Opt. Laser. Technol.* 131 (2020), 106451, <https://doi.org/10.1016/j.optlastec.2020.106451>.
- [523] L.D. Bobbio, B. Bocklund, A. Reichardt, R. Otis, J.P. Borgonia, R.P. Dillon, A. A. Shapiro, B.W. McEnery, P. Hosemann, Z.-K. Liu, Analysis of formation and growth of the σ phase in additively manufactured functionally graded materials, *J. Alloys Compd.* 814 (2020) 151729, <https://doi.org/10.1016/j.jallcom.2019.151729>.
- [524] D.R. Feenstra, A. Molotnikov, N. Birbilis, Effect of energy density on the interface evolution of stainless steel 316L deposited upon INC 625 via directed energy deposition, *J. Mater. Sci.* 55 (2020) 13314–13328, <https://doi.org/10.1007/s10853-020-04913-y>.
- [525] K.D. Traxel, A. Bandyopadhyay, Naturally architected microstructures in structural materials via additive manufacturing, *Addit. Manuf.* 34 (2020), 101243, <https://doi.org/10.1016/j.addma.2020.101243>.
- [526] B. Onuike, A. Heer, A. Bandyopadhyay, Additive manufacturing of Inconel 718–copper alloy bimetallic structure using laser engineered net shaping (LENSTM), *Addit. Manuf.* 21 (2018) 133–140, <https://doi.org/10.1016/j.addma.2018.02.007>.
- [527] M. Polanski, M. Kwiatkowska, I. Kunce, J. Bystrzycki, Combinatorial synthesis of alloy libraries with a progressive composition gradient using laser engineered net shaping (LENS): hydrogen storage alloys, *Int. J. Hydrogen Energy* 38 (2013) 12159–12171, <https://doi.org/10.1016/j.ijhydene.2013.05.024>.
- [528] B. Onuike, A. Bandyopadhyay, Functional bimetallic joints of Ti6Al4V to SS410, *Addit. Manuf.* 31 (2020), 100931, <https://doi.org/10.1016/j.addma.2019.100931>.
- [529] B. Heer, A. Bandyopadhyay, Compositionally graded magnetic-nonmagnetic bimetallic structure using laser engineered net shaping, *Mater. Lett.* 216 (2018) 16–19, <https://doi.org/10.1016/j.matlet.2017.12.129>.

- [530] T. Gualtieri, A. Bandyopadhyay, Additive manufacturing of compositionally gradient metal-ceramic structures: stainless steel to vanadium carbide, *Mater. Des.* 139 (2018) 419–428, <https://doi.org/10.1016/j.matdes.2017.11.007>.
- [531] U. Articek, M. Milfener, I. Anzel, Synthesis of functionally graded material H13/Cu by LENS technology, *Adv. Prod. Eng. Manag.* 8 (2013) 169–176, <https://doi.org/10.14743/apem2013.3.164>.
- [532] V.K. Balla, P.P. Bandyopadhyay, S. Bose, A. Bandyopadhyay, Compositively graded yttria-stabilized zirconia coating on stainless steel using laser engineered net shaping (LENSTM), *Scripta Mater.* 57 (2007) 861–864, <https://doi.org/10.1016/j.scriptamat.2007.06.055>.
- [533] I.V. Shishkovsky, A.P. Nazarov, D.V. Kotoban, N.G. Kakovkina, Comparison of additive technologies for gradient aerospace part fabrication from nickel-based superalloys, in: M. Aliofkazraei (Ed.), *Superalloys*, Intech, 2015, pp. 221–245, <https://doi.org/10.5772/61121>. Ch. 10.
- [534] P.K. Farayibi, J.A. Folkes, A.T. Clare, Laser deposition of Ti-6Al-4V wire with WC powder for functionally graded components, *Mater. Manuf. Process.* 28 (2013) 514–518, <https://doi.org/10.1080/10426914.2012.718477>.
- [535] Y. Chen, X. Zhang, M.M. Parvez, F. Liou, A review on metallic alloys fabrication using elemental powder blends by laser powder directed energy deposition process, *Materials* 13 (2020) 3562, <https://doi.org/10.3390/ma13163562>.
- [536] R. Ghanaati, H. Naffakh-Moosavy, Additive manufacturing of functionally graded metallic materials: a review of experimental and numerical studies, *J. Mater. Res. Technol.* 13 (2021) 1628–1664, <https://doi.org/10.1016/j.jmrt.2021.05.022>.
- [537] R. Ma, Z. Liu, W. Wang, G. Xu, W. Wang, Microstructures and mechanical properties of Ti6Al4V-Ti48Al2Cr2Nb alloys fabricated by laser melting deposition of powder mixtures, *Mater. Char.* 164 (2020), 110321, <https://doi.org/10.1016/j.matchar.2020.110321>.
- [538] R. Banerjee, D. Bhattacharyya, P.C. Collins, G.B. Viswanathan, H.L. Fraser, Precipitation of grain boundary α in a laser deposited compositionally graded Ti-8Al-xV alloy - an orientation microscopy study, *Acta Mater.* 52 (2004) 377–385, <https://doi.org/10.1016/j.actamat.2003.09.038>.
- [539] P.W. Hochanadel, R.D. Field, G.K. Lewis, Microstructure and properties of laser deposited and wrought alloy K-500 (UNS N05500), *Weld. World* 56 (2012) 51–58, <https://doi.org/10.1007/BF03321395>.
- [540] W. Li, L. Yan, X. Chen, J. Zhang, X. Zhang, F. Liou, Directed energy depositing a new Fe-Cr-Ni alloy with gradually changing composition with elemental powder mixes and particle size' effect in fabrication process, *J. Mater. Process. Technol.* 255 (2018) 96–104, <https://doi.org/10.1016/j.jmatprote.2017.12.010>.
- [541] L.D. Bobbio, R.A. Otis, J.P. Borgonia, R.P. Dillon, A.A. Shapiro, Z.K. Liu, A. M. Beese, Additive manufacturing of a functionally graded material from Ti-6Al-4V to Invar: experimental characterization and thermodynamic calculations, *Acta Mater.* 127 (2017) 133–142, <https://doi.org/10.1016/j.actamat.2016.12.070>.
- [542] J.T. Black, R.A. Kohser, *DeGarmo's Materials and Processes in Manufacturing*, thirteenth ed., John Wiley & Sons, 2019.
- [543] M.P. Groover, *Fundamentals of Modern Manufacturing: Materials, Processes, and Systems*, seventh ed., John Wiley & Sons, NY, USA, 2020.
- [544] D. Herzog, V. Seyda, E. Wycisk, C. Emmelmann, Additive manufacturing of metals, *Acta Mater.* 117 (2016) 371–392, <https://doi.org/10.1016/j.actamat.2016.07.019>.
- [545] J.S. Park, J.H. Park, M.G. Lee, J.H. Sung, K.J. Cha, D.H. Kim, Effect of energy input 7on the characteristic of AISI H13 and D2 tool steels deposited by a directed energy deposition process, *Metall. Mater. Trans.* 47 (2016) 2529–2535, <https://doi.org/10.1007/s11661-016-3427-5>.
- [546] N.U. Rahman, L. Capuano, S. Cabeza, M. Feinaeugle, A. Garcia-Junceda, M.B. de Rooij, D.T.A. Matthews, G. Walmag, I. Gibson, G. Römer, Directed energy deposition and characterization of high-carbon high speed steels, *Addit. Manuf.* 30 (2019), 100838, <https://doi.org/10.1016/j.addma.2019.100838>.
- [547] N. Eliaz, Corrosion of metallic biomaterials: a review, *Materials* 12 (2019) 407, <https://doi.org/10.3390/ma12030407>.
- [548] N. Eliaz, E. Gileadi, *Physical Electrochemistry: Fundamentals, Techniques, and Applications*, second ed., Wiley-VCH, Weinheim, Germany, 2019.
- [549] A. Basak, S. Das, Epitaxy and microstructure evolution in metal additive manufacturing, *Annu. Rev. Mater. Res.* 46 (2016) 125–149, <https://doi.org/10.1146/annurev-matsci-070115-031728>.
- [550] J.V. Gordon, C.V. Haden, H.F. Nied, R.P. Vinci, D.G. Harlow, Fatigue crack growth anisotropy, texture and residual stress in austenitic steel made by wire and arc additive manufacturing, *Mater. Sci. Eng.* 724 (2018) 431–438, <https://doi.org/10.1016/j.mse.2018.03.075>.
- [551] W. Cong, F. Ning, A fundamental investigation on ultrasonic vibration-assisted laser engineered net shaping of stainless steel, *Int. J. Mach. Tool Manufact.* 121 (2017) 61–69, <https://doi.org/10.1016/j.ijmachtools.2017.04.008>.
- [552] L. Bian, S.M. Thompson, N. Shamsaei, Mechanical properties and microstructural features of direct laser-deposited Ti-6Al-4V, *JOM* 67 (2015) 629–638, <https://doi.org/10.1007/s11837-015-1308-9>.
- [553] A.M. Beese, B.E. Carroll, Review of mechanical properties of Ti-6Al-4V made by laser-based additive manufacturing using powder feedstock, *JOM* 68 (2016) 724–734, <https://doi.org/10.1007/s11837-015-1759-z>.
- [554] S.-B. Hong, N. Eliaz, G.G. Leisk, E.M. Sachs, R.M. Latanision, S.M. Allen, A new Ti-5Ag alloy for customized prostheses by three-dimensional printing (3DP™), *J. Dent. Res.* 80 (2001) 860–863, <https://doi.org/10.1177/00220234501080003031>.
- [555] S.B. Hong, N. Eliaz, E.M. Sachs, S.M. Allen, R.M. Latanision, Corrosion behavior of advanced titanium-based alloys made by three-dimensional printing (3DP™) for biomedical applications, *Corrosion Sci.* 43 (2001) 1781–1791, [https://doi.org/10.1016/S0010-938X\(00\)00181-5](https://doi.org/10.1016/S0010-938X(00)00181-5).
- [556] H. Attar, S. Ehtemam-Haghghi, D. Kent, M.S. Dargusch, Recent developments and opportunities in additive manufacturing of titanium-based matrix composites: a review, *Int. J. Mach. Tool Manufact.* 133 (2018) 85–102, <https://doi.org/10.1016/j.ijmachtools.2018.06.003>.
- [557] N.U. Navi, J. Tenenbaum, E. Sabatani, G. Kimmel, R. Ben David, B.A. Rosen, Z. Barkay, V. Ezersky, E. Tiferet, Y.I. Ganor, N. Eliaz, Hydrogen effects on electrochemically charged additive manufactured by electron beam melting (EBM) and wrought Ti-6Al-4V alloys, *Int. J. Hydrogen Energy* 45 (2020) 25523–25540, <https://doi.org/10.1016/j.ijhydene.2020.06.277>.
- [558] A. Saboori, D. Gallo, S. Biamino, P. Fino, M. Lombardi, An overview of additive manufacturing of titanium components by directed energy deposition: microstructure and mechanical properties, *Appl. Sci.* 7 (2017) 883, <https://doi.org/10.3390/app7090883>.
- [559] A. Azarniya, X.G. Colera, M.J. Mirzaali, S. Sovizi, F. Bartolomeu, M.K. St Węglowski, W.W. Wits, C.Y. Yap, J. Ahn, G. Miranda, F.S. Silva, H.R. Madaah Hosseini, S. Ramakrishna, A.A. Zadpoor, Additive manufacturing of Ti-6Al-4V parts through laser metal deposition (LMD): process, microstructure, and mechanical properties, *J. Alloys Compd.* 804 (2019) 163–191, <https://doi.org/10.1016/j.jallcom.2019.04.255>.
- [560] R. Molaei, A. Fatemi, N. Sanaei, J. Pegues, N. Shamsaei, S. Shao, P. Li, D. H. Warner, N. Phan, Fatigue of additive manufactured Ti-6Al-4V, Part II: the relationship between microstructure, material cyclic properties, and component performance, *Int. J. Fatig.* 132 (2020), 105363, <https://doi.org/10.1016/j.ijfatigue.2019.105363>.
- [561] H.K. Rafi, N.V. Karthik, H. Gong, T.L. Starr, B.E. Stucker, Microstructures and mechanical properties of Ti6Al4V parts fabricated by selective laser melting and electron beam melting, *J. Mater. Eng. Perform.* 22 (2013) 3872–3883, <https://doi.org/10.1007/s11665-013-0658-0>.
- [562] P.A. Kobryń, S.L. Semiatin, Mechanical properties of laser-deposited Ti-6Al-4V, in: Proc. Int. Solid Freeform Fabrication Symp., 2001, pp. 179–186, <https://doi.org/10.26153/itsw/3261>.
- [563] I. Polmear, D. StJohn, J.-F. Nie, M. Qian, *Light Alloys: Metallurgy of the Light Metals*, fifth ed., Butterworth-Heinemann, London, UK, 2017.
- [564] Y. Ding, J.A. Muñiz-Lerma, M. Trask, S. Chou, A. Walker, M. Brochu, Microstructure and mechanical property considerations in additive manufacturing of aluminum alloys, *MRS Bull.* 41 (2016) 745–751, <https://doi.org/10.1557/mrs.2016.214>.
- [565] G.K. Lewis, in: C. Guo, S.C. Singh (Eds.), Rapid manufacturing, in *Handbook of Laser Technology and Application*, 2nd, CRC Press, Boca Raton, 2021, pp. 71–79, <https://doi.org/10.1201/9781315310855>. Ch. 6.
- [566] E.O. Olakanmi, Selective laser sintering/melting (SLS/SLM) of pure Al, Al-Mg, and Al-Si powders: effect of processing conditions and powder properties, *J. Mater. Process. Technol.* 213 (2013) 1387–1405, <https://doi.org/10.1016/j.jmatprote.2013.03.009>.
- [567] H. Ye, An overview of the development of Al-Si-alloy based material for engine applications, *J. Mater. Eng. Perform.* 12 (2003) 288–297, <https://doi.org/10.1361/105994903770343132>.
- [568] G.R. Thellaputta, P.S. Chandra, C.S.P. Rao, Machinability of nickel based superalloys: a review, *Mater. Today Proc.* 4 (2017) 3712–3721, <https://doi.org/10.1016/j.mtpr.2017.02.266>.
- [569] D. Ulutan, T. Ozel, Machining induced surface integrity in titanium and nickel alloys: a review, *Int. J. Mach. Tool Manufact.* 51 (2011) 250–280, <https://doi.org/10.1016/j.ijmachtools.2010.11.003>.
- [570] A. Kracke, A. Alvac, Superalloys, the most successful alloy system of modern times-past, present and future, in: E.A. Ott, J.R. Groh, A. Banik, I. Dempster, T. P. Gabb, R. Helmink, X. Liu, A. Mitchell, G.P. Sjöberg, A. Wusatowska-Sarnek (Eds.), Proc. 7th Int. Symp. Superalloy 718 and Derivatives, TMS, 2010, pp. 13–50, https://doi.org/10.7449/2010Superalloys_2010_13_50.
- [571] A. Thakur, S. Gangopadhyay, State-of-the-art in surface integrity in machining of nickel-based super alloys, *Int. J. Mach. Tool Manufact.* 100 (2016) 25–54, <https://doi.org/10.1016/j.ijmachtools.2015.10.001>.
- [572] N. Eliaz, G. Shemesh, R.M. Latanision, Hot corrosion in gas turbine components, *Eng. Fail. Anal.* 9 (2002) 31–43, [https://doi.org/10.1016/S1350-6307\(00\)00035-2](https://doi.org/10.1016/S1350-6307(00)00035-2).
- [573] C.K. Stimpson, J.C. Snyder, K.A. Thole, D. Mongillo, Scaling roughness effects on pressure loss and heat transfer of additively manufactured channels, *J. Turbomach.* 139 (2017), 021003, <https://doi.org/10.1115/1.4034555>.
- [574] R.S. Bunker, Innovative gas turbine cooling techniques, in: WIT Trans. State Art Sci. Eng., vol. 42, WIT Press, 2008, pp. 199–229, <https://doi.org/10.2495/978-1-84564-062-0/07>. Ch. 7.
- [575] K.M. Manralta, M. Das, V.K. Balla, C. Srinivasa Rao, V.V.S. Kesava Rao, Laser-deposited CoCrMo alloy: microstructure, wear, and electrochemical properties, *J. Mater. Res.* 29 (2014) 2021–2027, <https://doi.org/10.1557/jmr.2014.163>.
- [576] J.V. Giacchi, C.N. Morando, O. Fornaro, H.A. Palacio, Microstructural characterization of as-cast biocompatible Co-Cr-Mo alloys, *Mater. Char.* 62 (2011) 53–61, <https://doi.org/10.1016/j.matchar.2010.10.011>.
- [577] Y. Jiang, Y. He, C.T. Liu, Review of porous intermetallic compounds by reactive synthesis of elemental powders, *Intermetallics* 93 (2018) 217–226, <https://doi.org/10.1016/j.intermet.2017.06.003>.
- [578] A.Y. Lee, J. An, C.K. Chua, Two-way 4D printing: a review on the reversibility of 3D-printed shape memory materials, *Engineering* 3 (2017) 663–674, <https://doi.org/10.1016/J.ENG.2017.05.014>.
- [579] M. Elahinia, N. Shayesteh Moghaddam, M. Taheri Andani, A. Amerinatanzi, B. A. Bimber, R.F. Hamilton, Fabrication of NiTi through additive manufacturing: a review, *Prog. Mater. Sci.* 83 (2016) 630–663, <https://doi.org/10.1016/j.pmatsci.2016.08.001>.

- [580] N.B. Morgan, Medical shape memory alloy applications—the market and its products, *Mater. Sci. Eng.* 378 (2004) 16–23, <https://doi.org/10.1016/j.msea.2003.10.326>.
- [581] B. Carpenter, J. Lyons, EO-1 technology validation report: lightweight flexible solar array experiment, in: Tech. Report, NASA Godard Space Flight Center, Greenbelt, MD, August 2001.
- [582] J. Van Humebeck, Shape memory alloys: a material and a technology, *Adv. Eng. Mater.* 3 (2001) 837–850, [https://doi.org/10.1002/1527-2648\(200111\)3:11<837::AID-ADEM837>3.0.CO;2-0](https://doi.org/10.1002/1527-2648(200111)3:11<837::AID-ADEM837>3.0.CO;2-0).
- [583] S.K. Wu, H.C. Lin, C.C. Chen, A study on the machinability of a Ti49.6Ni50.4 shape memory alloy, *Mater. Lett.* 40 (1999) 27–32, [https://doi.org/10.1016/S0167-577X\(99\)00044-0](https://doi.org/10.1016/S0167-577X(99)00044-0).
- [584] M.H. Elahinia, Shape Memory Alloy Actuators: Design, Fabrication, and Experimental Evaluation, John Wiley & Sons, West Sussex, UK, 2016, <https://doi.org/10.1002/9781118426913>.
- [585] C. Scheitler, O. Hentschel, T. Krebs, K.Y. Nagulin, M. Schmidt, Laser metal deposition of NiTi shape memory alloy on Ti sheet metal: influence of preheating on dissimilar build-up, *J. Laser Appl.* 29 (2017), 22309, <https://doi.org/10.2351/1.4983246>.
- [586] H. Meier, C. Haberland, J. Frenzel, R. Zarnetta, Selective laser melting of NiTi shape memory components, in: Innovative Developments in Design and Manufacturing: Advanced Research in Virtual and Rapid Prototyping, CRC Press, London, 2010, pp. 233–238.
- [587] K. Otsuka, C.M. Wayman (Eds.), Shape Memory Materials, Cambridge University Press, UK, 1999.
- [588] H. Kalaantari, Development of Co-ni-Ga Ferromagnetic Shape Memory Alloys (FSMAs) by Investigating the Effects of Solidification Processing Parameters, Dissertation, PhD Dissertation, University of California Riverside, USA, March 2013.
- [589] M.P. Caputo, A.E. Berkowitz, A. Armstrong, P. Müllner, C.V. Solomon, 4D printing of net shape parts made from Ni-Mn-Ga magnetic shape-memory alloys, *Addit. Manuf.* 21 (2018) 579–588, <https://doi.org/10.1016/j.addma.2018.03.028>.
- [590] A. Saren, D. Musienko, A.R. Smith, J. Tellinen, K. Ullakko, Modeling and design of a vibration energy harvester using the magnetic shape memory effect, *Smart Mater. Struct.* 24 (2015), 95002, <https://doi.org/10.1088/0964-1726/24/9/095002>.
- [591] R. Yin, F. Wendler, B. Krevet, M. Kohl, A magnetic shape memory microactuator with intrinsic position sensing, *Sensors Actuators A Phys.* 246 (2016) 48–57, <https://doi.org/10.1016/j.sna.2016.05.013>.
- [592] S.M. Ueland, C.A. Schuh, Grain boundary and triple junction constraints during martensitic transformation in shape memory alloys, *J. Appl. Phys.* 114 (2013), 53503, <https://doi.org/10.1063/1.4817170>.
- [593] Y.F. Ye, Q. Wang, J. Lu, C.T. Liu, Y. Yang, High-entropy alloy: challenges and prospects, *Mater. Today* 19 (2016) 349–362, <https://doi.org/10.1016/j.mattod.2015.11.026>.
- [594] M.H. Tsai, J.W. Yeh, High-entropy alloys: a critical review, *Mater. Res. Lett.* 2 (2014) 107–123, <https://doi.org/10.1016/j.mattod.2015.11.026>.
- [595] E.P. George, D. Raabe, R.O. Ritchie, High-entropy alloys, *Nat. Rev. Mater.* 4 (2019) 515–534, <https://doi.org/10.1038/s41578-019-0121-4>.
- [596] Y. Zhang, T.T. Zuo, Z. Tang, M.C. Gao, K.A. Dahmen, P.K. Liaw, Z.P. Lu, Microstructures and properties of high-entropy alloys, *Prog. Mater. Sci.* 61 (2014) 1–93, <https://doi.org/10.1016/j.jpmatsci.2013.10.001>.
- [597] M. Zhang, X. Zhou, X. Yu, J. Li, Synthesis and characterization of refractory TiZrNbWMo high-entropy alloy coating by laser cladding, *Surf. Coatings. Technol.* 311 (2017) 321–329, <https://doi.org/10.1016/j.surco.2017.01.012>.
- [598] Q. Ye, K. Feng, Z. Li, F. Lu, R. Li, J. Huang, Y. Wu, Microstructure and corrosion properties of CrMnFeCoNi high entropy alloy coating, *Appl. Surf. Sci.* 396 (2017) 1420–1426, <https://doi.org/10.1016/j.apsusc.2016.11.176>.
- [599] F.Y. Shu, S. Liu, H.Y. Zhao, W.X. He, S.H. Sui, J. Zhang, P. He, B.S. Xu, Structure and high-temperature property of amorphous composite coating synthesized by laser cladding FeCrCoNiSiB high-entropy alloy powder, *J. Alloys Compd.* 731 (2018) 662–666, <https://doi.org/10.1016/j.jallcom.2017.08.248>.
- [600] F.Y. Shu, L. Wu, H.Y. Zhao, S.H. Sui, L. Zhou, J. Zhang, W.X. He, P. He, B.S. Xu, Microstructure and high-temperature wear mechanism of laser cladded CoCrBFeNiSi high-entropy alloy amorphous coating, *Mater. Lett.* 211 (2018) 235–238, <https://doi.org/10.1016/j.matlet.2017.09.056>.
- [601] Z. Cai, X. Cui, Z. Liu, Y. Li, M. Dong, G. Jin, Microstructure and wear resistance of laser cladded Ni-Cr-Co-Ti-V high-entropy alloy coating after laser remelting processing, *Opt. Laser. Technol.* 99 (2018) 276–281, <https://doi.org/10.1016/j.optlastec.2017.09.012>.
- [602] S. Minghong, Z. Li, Z. Junwei, L. Na, L. Taizeng, W. Ning, Effects of annealing on the microstructure and wear resistance of AlCoCrFeNiTi 0.5 high-entropy alloy coating prepared by laser cladding, *Rare Met. Mater. Eng.* 46 (2017) 1237–1240, [https://doi.org/10.1016/S1875-5372\(17\)30143-1](https://doi.org/10.1016/S1875-5372(17)30143-1).
- [603] D. yang Lin, N. nan Zhang, B. He, G. wei Zhang, Y. Zhang, D. yuan Li, Tribological properties of FeCoCrNiAlBx high-entropy alloys coating prepared by laser cladding, *J. Iron Steel Res. Int.* 24 (2017) 184–189, [https://doi.org/10.1016/S1006-706X\(17\)30026-2](https://doi.org/10.1016/S1006-706X(17)30026-2).
- [604] B. Gludovatz, A. Hohenwarter, D. Catoor, E.H. Chang, E.P. George, R.O. Ritchie, A fracture-resistant high-entropy alloy for cryogenic applications, *Science* 345 (2014) 1153–1158, <https://doi.org/10.1126/science.1254581>.
- [605] Q. Chao, T. Guo, T. Jarvis, X. Wu, P. Hodgson, D. Fabijanic, Direct laser deposition cladding of AlxCrFeNi high entropy alloys on a high-temperature stainless steel, *Surf. Coatings. Technol.* 332 (2017) 440–451, <https://doi.org/10.1016/j.surco.2017.09.072>.
- [606] Y. Hu, W. Cong, A review on laser deposition-additive manufacturing of ceramics and ceramic reinforced metal matrix composites, *Ceram. Int.* 44 (2018) 20599–20612, <https://doi.org/10.1016/j.ceramint.2018.08.083>.
- [607] N.P. Bansal, A.R. Boccaccini (Eds.), Ceramics and Composites Processing Methods, John Wiley & Sons, NJ, USA, 2012.
- [608] M.K. Agarwala, A. Bandyopadhyay, R. van Weeren, A. Safari, S.C. Danforth, N. A. Langrana, V.R. Jamalabad, P.J. Whalen, FDC, rapid fabrication of structural components, *Am. Ceram. Soc. Bull.* 75 (1996).
- [609] S. Zhou, Y. Huang, X. Zeng, Q. Hu, Microstructure characteristics of Ni-based WC composite coatings by laser induction hybrid rapid cladding, *Mater. Sci. Eng.* 480 (2008) 564–572, <https://doi.org/10.1016/j.msea.2007.07.058>.
- [610] B. Zheng, N. Yang, J. Yee, K. Gaiser, W.Y. Lu, L. Clemon, Y. Zhou, E.J. Lavernia, J. M. Schoenung, Review on laser powder injection additive manufacturing of novel alloys and composites, *Proc. SPIE* 9738 (2016), 973800, <https://doi.org/10.1117/12.2217909>.
- [611] E. Fereiduni, A. Ghasemi, M. Elbestawi, Selective laser melting of hybrid ex-situ/in-situ reinforced titanium matrix composites: laser/powder interaction, reinforcement formation mechanism, and non-equilibrium microstructural evolutions, *Mater. Des.* 184 (2019), 108185, <https://doi.org/10.1016/j.matedes.2019.108185>.
- [612] M. Das, S. Bysakh, D. Basu, T.S.S. Kumar, V.K. Balla, S. Bose, A. Bandyopadhyay, Microstructure, mechanical and wear properties of laser processed SiC particle reinforced coatings on titanium, *Surf. Coatings. Technol.* 205 (2011) 4366–4373, <https://doi.org/10.1016/j.surco.2011.03.027>.
- [613] M. Das, V.K. Balla, D. Basu, S. Bose, A. Bandyopadhyay, Laser processing of SiC-particle-reinforced coating on titanium, *Scripta Mater.* 63 (2010) 438–441, <https://doi.org/10.1016/j.scriptamat.2010.04.044>.
- [614] P.V. Reddy, G.S. Kumar, D.M. Krishnudu, H.R. Rao, Mechanical and wear performances of aluminium-based metal matrix composites: a review, *J. Bio Tribos. Corros.* 6 (2020) 83, <https://doi.org/10.1007/s40735-020-00379-2>.
- [615] Y. Xu, C. Yu, Q. Miao, S. Yan, G. Ma, Effect of graphite addition on mechanical properties of Al₂O₃ ceramics by directed laser deposition, *Proc. Inst. Mech. Eng. Part B J. Eng. Manuf.* (2020), <https://doi.org/10.1177/0954405420944805>.
- [616] M. Koizumi, M. Niino, Overview of FGM research in Japan, *MRS Bull.* 20 (1995) 19–21, <https://doi.org/10.1557/S0883769400048867>.
- [617] P. Popoola, G. Farotade, O. Fatoba, O. Popoola, Laser engineering net shaping method in the area of development of functionally graded materials (FGMs) for aero engine applications – a review, in: M.C. Paul (Ed.), Fiber Laser, IntechOpen, Croatia, 2016, pp. 383–400, <https://doi.org/10.5772/61711>. Ch. 17.
- [618] S.S. Wang, Fracture mechanics for delamination problems in composite materials, *Stud. Appl. Mech.* 17 (1984) 369–383, <https://doi.org/10.1177/002199838301700302>.
- [619] D.T. Sarathchandra, S.K. Subbu, N. Venkaiah, Functionally graded materials and processing techniques: an art of review, *Mater. Today Proc.* 5 (2018) 21328–21334, <https://doi.org/10.1016/j.matpr.2018.06.536>.
- [620] A. Bandyopadhyay, B. Heer, Additive manufacturing of multi-material structures, *Mater. Sci. Eng. R* 129 (2018) 1–16, <https://doi.org/10.1016/j.mser.2018.04.001>.
- [621] N.K. Sharma, M. Bhandari, A. Dean, Applications of functionally graded materials (FGMs), *Int. J. Eng. Res. Technol.* 2 (2014) 334–339.
- [622] V.K. Balla, S. Banerjee, S. Bose, A. Bandyopadhyay, Direct laser processing of a tantalum coating on titanium for bone replacement structures, *Acta Biomater.* 6 (2010) 2329–2334, <https://doi.org/10.1016/j.actbio.2009.11.021>.
- [623] I. Tomashchuk, D. Grevey, P. Sallamand, Dissimilar laser welding of AISI 316L stainless steel to Ti6-Al4–6V alloy via pure vanadium interlayer, *Mater. Sci. Eng.* 622 (2015) 37–45, <https://doi.org/10.1016/j.msea.2014.10.084>.
- [624] M. Zhong, W. Liu, Laser surface cladding: the state of the art and challenges, *Proc. Inst. Mech. Eng. C: J. Mech. Eng. Sci.* 224 (2010) 1041–1060, <https://doi.org/10.1243/09544062JMES1782>.
- [625] S. Singh, D.K. Goyal, P. Kumar, A. Bansal, Laser cladding technique for erosive wear applications: a review, *Mater. Res. Express* 7 (2020), 12007, <https://doi.org/10.1088/2053-1591/AB6894>.
- [626] J. Edgar, S. Tint, Additive manufacturing technologies: 3D printing, rapid prototyping, and direct digital manufacturing, *Johnson Matthey Technol. Rev.* 59 (2015) 193–198, <https://doi.org/10.1595/205651315x688406>.
- [627] A. Calleja, I. Tabernero, A. Fernández, A. Celaya, A. Lamikiz, L.N.L. De Lacalle, Improvement of strategies and parameters for multi-axis laser cladding operations, *Opt. Laser. Eng.* 56 (2014) 113–120, <https://doi.org/10.1016/j.optlaseng.2013.12.017>.
- [628] Y. Xiong, J.E. Smugeresky, L. Ajdelsztajn, J.M. Schoenung, Fabrication of WC-Co cermets by laser engineered net shaping, *Mater. Sci. Eng.* 493 (2008) 261–266, <https://doi.org/10.1016/j.msea.2007.05.125>.
- [629] G. Muvala, S. Sarkar, A.K. Nath, Laser cladding of Ni-based superalloys, in: P. Cavaliere (Ed.), *Laser Cladding of Metals*, Springer Nature, Switzerland, 2021, pp. 293–331.
- [630] T. Gabriel, D. Rommel, F. Scherm, M. Gorywoda, U. Glatzel, Laser cladding of ultra-thin nickel-based superalloy sheets, *Materials* 10 (2017) 279, <https://doi.org/10.3390/ma10030279>.
- [631] Q. Li, D. Zhang, T. Lei, C. Chen, W. Chen, Comparison of laser-clad and furnace-melted Ni-based alloy microstructures, *Surf. Coatings. Technol.* 137 (2001) 122–135, [https://doi.org/10.1016/S0257-8972\(00\)00732-5](https://doi.org/10.1016/S0257-8972(00)00732-5).
- [632] C. Hu, S. Hou, Effects of rare earth elements on properties of Ni-base superalloy powders and coatings, *Coatings* 7 (2017) 30, <https://doi.org/10.3390/coatings7020030>.
- [633] S. Wulin, J. Echigoya, Z. Beidi, X. Changsheng, H. Wei, C. Kun, Vacuum laser cladding and effect of Hf on the cracking susceptibility and the microstructure of

- Fe–Cr–Ni laser-clad layer, *Surf. Coating. Technol.* 126 (2000) 76–80, [https://doi.org/10.1016/S0257-8972\(00\)00532-6](https://doi.org/10.1016/S0257-8972(00)00532-6).
- [634] G. Bidron, A. Doghri, T. Malot, F. Fournier-dit-Chabert, M. Thomas, P. Peyre, Reduction of the hot cracking sensitivity of CM-247LC superalloy processed by laser cladding using induction preheating, *J. Mater. Process. Technol.* 277 (2020), 116461, <https://doi.org/10.1016/j.jmatprotec.2019.116461>.
- [635] X. Zeng, Z. Tao, B. Zhu, E. Zhou, K. Cui, Investigation of laser cladding ceramic-metal composite coatings: processing modes and mechanisms, *Surf. Coating. Technol.* 79 (1996) 209–217, [https://doi.org/10.1016/0257-8972\(95\)02431-X](https://doi.org/10.1016/0257-8972(95)02431-X).
- [636] J. Przybyłowicz, J. Kusiński, Structure of laser cladded tungsten carbide composite coatings, *J. Mater. Process. Technol.* 109 (2001) 154–160, [https://doi.org/10.1016/S0924-0136\(00\)00790-1](https://doi.org/10.1016/S0924-0136(00)00790-1).
- [637] L.R. Katipelli, A. Agarwal, N.B. Dahotre, Laser surface engineered TiC coating on 6061 Al alloy: microstructure and wear, *Appl. Surf. Sci.* 153 (2000) 65–78, [https://doi.org/10.1016/S0169-4332\(99\)00368-2](https://doi.org/10.1016/S0169-4332(99)00368-2).
- [638] Y.T. Pei, J.H. Ouyang, T.C. Lei, Y. Zhou, Microstructure of laser-clad SiC-(Ni alloy) composite coating, *Mater. Sci. Eng. A* 194 (1995) 219–224, [https://doi.org/10.1016/0921-5093\(94\)09653-8](https://doi.org/10.1016/0921-5093(94)09653-8).
- [639] P. Zhang, Y. Pang, M. Yu, Effects of WC particle types on the microstructures and properties of WC-reinforced Ni60 composite coatings produced by laser cladding, *Materials* 9 (2019) 583, <https://doi.org/10.3390/met9050583>.
- [640] J. Xu, W. Liu, M. Zhong, Microstructure and dry sliding wear behavior of MoS₂/TiC/Ni composite coatings prepared by laser cladding, *Surf. Coating. Technol.* 200 (2006) 4227–4232, <https://doi.org/10.1016/j.surcoat.2005.01.036>.
- [641] G. Lian, C. Zhao, Y. Zhang, M. Feng, J. Jiang, Investigation into micro-hardness and wear resistance of 316L/SiC composite coating in laser cladding, *Appl. Sci.* 10 (2020) 3167, <https://doi.org/10.3390/app10093167>.
- [642] S. Yang, N. Chen, W. Liu, M. Zhong, In situ formation of MoSi₂/SiC composite coating on pure Al by laser cladding, *Mater. Lett.* 57 (2003) 3412–3416, [https://doi.org/10.1016/S0167-577X\(03\)00086-7](https://doi.org/10.1016/S0167-577X(03)00086-7).
- [643] Y. Pu, B. Guo, J. Zhou, S. Zhang, H. Zhou, J. Chen, Microstructure and tribological properties of in situ synthesized TiC, TiN, and SiC reinforced Ti₃Al intermetallic matrix composite coatings on pure Ti by laser cladding, *Appl. Surf. Sci.* 255 (2008) 2697–2703, <https://doi.org/10.1016/j.apsusc.2008.07.180>.
- [644] B.J. Kooi, Y.T. Pei, J.T.M. De Hosson, The evolution of microstructure in a laser clad TiB-Ti composite coating, *Acta Mater.* 51 (2003) 831–845, [https://doi.org/10.1016/S1359-6454\(02\)00475-5](https://doi.org/10.1016/S1359-6454(02)00475-5).
- [645] W. Chen, B. Liu, L. Chen, J. Xu, Y. Zhu, Effect of laser cladding Stellite 6-Cr₃C₂-WS₂ self-lubricating composite coating on wear resistance and microstructure of H13, *Metals* 10 (2020) 785, <https://doi.org/10.3390/met10060785>.
- [646] T. Tolio, A. Bernard, M. Colledani, S. Kara, G. Seliger, J. Duflou, O. Battiaia, S. Takata, Design, management and control of demanufacturing and remanufacturing systems, *CIRP Ann* 66 (2017) 585–609, <https://doi.org/10.1016/j.cirp.2017.05.001>.
- [647] O. Yilmaz, N. Gindy, J. Gao, A repair and overhaul methodology for aeroengine components, *Robot. Comput. Integrated Manuf.* 26 (2010) 190–201, <https://doi.org/10.1016/j.rcim.2009.07.001>.
- [648] C. Bremer, Automated repair and overhaul of aero-engine and industrial gas turbine components, in: Proc. ASME Turbo Expo 2005 vol. 2, Power for Land, Sea, and Air, 2005, pp. 841–846, <https://doi.org/10.1115/GT2005-68193>.
- [649] R. Liu, Z. Wang, T. Sparks, F. Liou, J. Newkirk, Aerospace applications of laser additive manufacturing, in: M. Brandt (Ed.), *Laser Additive Manufacturing: Materials, Design, Technologies, and Applications*, Woodhead Publishing, 2017, pp. 351–371, <https://doi.org/10.1016/B978-0-08-100433-3.00013-0>. Ch. 13.
- [650] M. Hedges, N. Calder, Near net shape rapid manufacture & repair by LENSTM, in: *Cost Effective Manufacture via Net-Shape Processing*, Meeting Proc. RTO-MP-AVT-139, 2006 paper 13.
- [651] M. Balazic, M. Milfeler, J. Kopac, Repair and manufacture of high performance products for medicine and aviation with laser technology, *AJSTPM* 3 (2010) 15–22.
- [652] J.C. Najmon, S. Raeisi, A. Tovar, Review of additive manufacturing technologies and applications in the aerospace industry, in: F. Froes, R. Boyer (Eds.), *Additive Manufacturing for the Aerospace Industry*, Elsevier, Amsterdam, The Netherlands, 2019, pp. 7–31, <https://doi.org/10.1016/B978-0-12-814062-8.00002-9>.
- [653] W. Zhang, *Methodology and Process Innovations in Additive fabrication*, in: *Intell. Energy F. Manuf.*, CRC Press, 2018, pp. 439–466.
- [654] R.P. Mudge, N.R. Wald, Laser engineered net shaping advances additive manufacturing and repair, *Weld. J.* 86 (2007) 44–48.
- [655] Q. Liu, P.K. Sharp, M. Brandt, N. Matthews, S. Sun, R. Djugum, Repair of aircraft components by laser cladding process, *J. Laser. Appl.* 2014 (2014) 308–313, <https://doi.org/10.2351/1.5063074>.
- [656] G. Tapia, A. Elwany, A review on process monitoring and control in metal-based additive manufacturing, *J. Manuf. Sci. Eng.* 136 (2014) 060801, <https://doi.org/10.1115/1.4028540>.
- [657] W. Xi, B. Song, Y. Zhao, T. Yu, J. Wang, Geometry and dilution rate analysis and prediction of laser cladding, *Int. J. Adv. Manuf. Technol.* 103 (2019) 4695–4702, <https://doi.org/10.1007/s00170-019-03932-7>.
- [658] H. Wang, W. Liu, Z. Tang, Y. Wang, X. Mei, K.M. Saleheen, Z. Wang, H. Zhang, Review on adaptive control of laser-directed energy deposition, *Opt. Eng.* 59 (2020), 70901, <https://doi.org/10.1117/1.OE.59.7.070901>.
- [659] P. Kattire, S. Paul, R. Singh, W. Yan, Experimental characterization of laser cladding of CPM 9V on H13 tool steel for die repair applications, *J. Manuf. Process.* 20 (2015) 492–499, <https://doi.org/10.1016/j.jmapro.2015.06.018>.
- [660] L.P. Borrego, J.T.B. Pires, J.M. Costa, J.M. Ferreira, Mould steels repaired by laser welding, *Eng. Fail. Anal.* 16 (2009) 596–607, <https://doi.org/10.1016/j.engfailanal.2008.02.010>.
- [661] J. Leunda, C. Sorianó, C. Sanz, V.G. Navas, Laser cladding of vanadium-carbide tool steels for die repair, *Phys. Procedia* 12 (2011) 345–352, <https://doi.org/10.1016/j.phpro.2011.03.044>.
- [662] A.T. Clare, O. Oyelola, T.E. Abioye, P.K. Farayibi, Laser cladding of rail steel with Co-Cr, *Surf. Eng.* 29 (2013) 731–736, <https://doi.org/10.1179/1743294412Y.0000000075>.
- [663] S.R. Lewis, R. Lewis, D.I. Fletcher, Assessment of Laser Cladding as an Option for Repairing/enhancing Rails, *Wear* 330–331 (2015) 581–591, <https://doi.org/10.1016/j.wear.2015.02.027>.
- [664] H. Koehler, K. Partes, T. Seefeld, F. Vollertsen, Influence of laser reconditioning on fatigue properties of crankshafts, *Phys. Procedia* 12 (2011) 512–518, <https://doi.org/10.1016/j.phpro.2011.03.063>.
- [665] E. Toyserkani, A. Khajepour, S.F. Corbin, *Laser Cladding*, CRC Press, Boca Raton, FL, 2005.
- [666] X. Lei, C. Huajun, L. Hailong, Z. Yubo, Study on laser cladding remanufacturing process with FeCrNiCu alloy powder for thin-wall impeller blade, *Int. J. Adv. Manuf. Technol.* 90 (2017) 1383–1392, <https://doi.org/10.1007/s00170-016-9445-z>.
- [667] B. Rottwinkel, C. Nölke, S. Kaierle, V. Wesling, Crack repair of single crystal turbine blades using laser cladding technology, *Procedia CIRP* 22 (2014) 263–267, <https://doi.org/10.1016/j.procir.2014.06.151>.
- [668] P. Bendicht, N. Alam, M. Brandt, D. Carr, K. Short, R. Blevins, C. Curfs, O. Kirstein, G. Atkinson, T. Holden, R. Rogge, Residual stress measurements in laser clad repaired low pressure turbine blades for the power industry, *Mater. Sci. Eng.* 437 (2006) 70–74, <https://doi.org/10.1016/j.msea.2006.04.065>.
- [669] X. Zhang, W. Li, K.M. Adkison, F. Liou, Damage reconstruction from tri-dexel data for laser-aided repairing of metallic components, *Int. J. Adv. Manuf. Technol.* 96 (2018) 3377–3390, <https://doi.org/10.1007/s00170-018-1830-3>.
- [670] S. Krause, An advanced repair technique: laser powder build-up welding, *Sulzer Tech. Rev.* 83 (2001) 4–6.
- [671] T. Petrat, B. Graf, A. Gumenvyuk, M. Rethmeier, Laser metal deposition as repair technology for a gas turbine burner made of Inconel 718, *Phys. Procedia* 83 (2016) 761–768, <https://doi.org/10.1016/j.phpro.2016.08.078>.
- [672] D. Liu, J.C. Lippold, J. Li, S.R. Rohklin, J. Vollbrecht, R. Grylls, Laser Engineered Net Shape (LENS®) technology for the repair of Ni-base superalloy turbine components, *Metall. Mater. Trans.* 45 (2014) 4454–4469, <https://doi.org/10.1007/s11661-014-2397-8>.
- [673] X. Zhang, W. Cui, W. Li, F. Liou, A hybrid process integrating reverse engineering, pre-repair processing, additive manufacturing, and material testing for component remanufacturing, *Materials* 12 (2019) 1961, <https://doi.org/10.3390/ma12121961>.
- [674] B. Onuike, A. Bandyopadhyay, Additive manufacturing in repair: influence of processing parameters on properties of Inconel 718, *Mater. Lett.* 252 (2019) 256–259, <https://doi.org/10.1016/j.matlet.2019.05.114>.
- [675] K. Lu, W. Wang, A multi-sensor approach for rapid and precise digitization of free-form surface in reverse engineering, *Int. J. Adv. Manuf. Technol.* 79 (2015) 1983–1994, <https://doi.org/10.1007/s00170-015-6960-2>.
- [676] L. Li, C. Li, Y. Tang, Y. Du, An integrated approach of reverse engineering aided remanufacturing process for worn components, *Robot. Comput. Integrated Manuf.* 48 (2017) 39–50, <https://doi.org/10.1016/j.rcim.2017.02.004>.
- [677] T. Yamazaki, Development of a hybrid multi-tasking machine tool: integration of additive manufacturing technology with CNC machining, *Procedia CIRP* 42 (2016) 81–86, <https://doi.org/10.1016/j.procir.2016.02.193>.
- [678] V.T. Le, H. Paris, G. Mandil, Process planning for combined additive and subtractive manufacturing technologies in a remanufacturing context, *J. Manuf. Syst.* 44 (2017) 243–254, <https://doi.org/10.1016/j.jmssy.2017.06.003>.
- [679] A. Bandyopadhyay, K.D. Traxel, M. Lang, M. Juhasz, N. Eliaz, S. Bose, Alloy design via additive manufacturing: advantages, challenges, applications and perspectives, *Mater. Today* (2022), <https://doi.org/10.1016/j.mattod.2021.11.026>.
- [680] M. Korpela, N. Riikonen, H. Piili, A. Salminen, O. Nyrhilä, Additive manufacturing: past, present and future, in: M. Collan, K.E. Michelsen (Eds.), *Technical, Economic and Societal Effects of Manufacturing 4.0*, Palgrave Macmillan, Cham, Switzerland, 2020, pp. 17–42, https://doi.org/10.1007/978-3-030-46103-4_2. Ch.2.
- [681] N. Eliaz, N. Metoki, Calcium phosphate bioceramics: a review of their history, structure, properties, coating technologies and biomedical applications, *Materials* 10 (2017) 334, <https://doi.org/10.3390/ma10040334>.
- [682] O.F. Dippo, K.R. Kaufmann, K.S. Vecchio, High-throughput Rapid Experimental Alloy Development (HT-READ), arXiv preprint (2021). <https://arxiv.org/abs/2102.06180>.
- [683] I. Hemmati, V. Ocelík, J.T.M. De Hosson, Effects of the alloy composition on phase constitution and properties of laser deposited Ni-Cr-B-Si coatings, *Phys. Procedia* 41 (2013) 302–311, <https://doi.org/10.1016/j.phpro.2013.03.082>.
- [684] X. Li, K. Zweicker, D. Grolimund, D. Ferreira Sanchez, A.B. Spierings, C. Leinenbach, K. Wegener, In situ and ex situ characterization of the microstructure formation in Ni-Cr-Si alloys during rapid solidification—toward alloy design for laser additive manufacturing, *Materials* 13 (2020) 2192, <https://doi.org/10.3390/ma13092192>.
- [685] D. Zhang, D. Qiu, M.A. Gibson, Y. Zheng, H.L. Fraser, D.H. StJohn, M.A. Easton, Additive manufacturing of ultrafine-grained high-strength titanium alloys, *Nature* 576 (2019) 91–95, <https://doi.org/10.1038/s41586-019-1783-1>.

- [686] I. Mitra, S. Bose, W.S. Dernell, N. Dasgupta, C. Eckstrand, J. Herrick, M. J. Yaszemski, S.B. Goodman, A. Bandyopadhyay, 3D Printing in alloy design to improve biocompatibility in metallic implants, *Mater. Today* 45 (2021) 20–34, <https://doi.org/10.1016/j.mattod.2020.11.021>.
- [687] A. Bandyopadhyay, I. Mitra, A. Shivaram, N. Dasgupta, S. Bose, Direct comparison of additively manufactured porous titanium and tantalum implants towards *in vivo* osseointegration, *Addit. Manuf.* 28 (2019) 259–266, <https://doi.org/10.1016/j.addma.2019.04.025>.
- [688] B. Datta, F.H. Froes, Additive manufacturing of titanium alloys, *Adv. Mater. Process.* 172 (2014) 18–23.
- [689] <https://www.rpm-innovations.com/>. (Accessed 30 January 2022).
- [690] Directed energy deposition, in: <https://www.ipt.fraunhofer.de/en/Competencies/processes/technology/directed-energy-manufacturing.html>. (Accessed 30 January 2022).
- [691] NASA looks to large-scale DED additive manufacturing for future rocket engines. <https://www.metal-am.com/nasa-looks-to-large-scale-ded-additive-manufacturing-for-future-rocket-engines/>. (Accessed 30 January 2022).
- [692] D. Svetlizky, H. Kazimierczak, B. Ovadia, A. Sharoni, N. Eliaz, Electrochemical processing and thermal properties of functional core/multi-shell ZnAl/Ni/NiP microparticles, *Materials* 14 (4) (2021) 834, <https://doi.org/10.3390/ma14040834>.
- [693] D. Svetlizky, N. Eliaz, Sol-gel encapsulation of ZnAl alloy powder with alumina shell, *Coatings* 11 (11) (2021) 1389, <https://doi.org/10.3390/coatings11111389>.
- [694] O. Tevet, D. Svetlizky, D. Harel, Z. Barkay, D. Geva, N. Eliaz, Measurement of the anisotropic dynamic elastic constants of additive manufactured and wrought Ti6Al4V alloys, *Materials* 15 (2) (2022) 638, <https://doi.org/10.3390/ma15020638>.
- [695] D. Svetlizky, B. Zheng, D.M. Steinberg, J.M. Schoenung, E.J. Lavernia, N. Eliaz, The influence of laser directed energy deposition (DED) processing parameters for Al5083 studied by central composite design, *J. Mater. Res. Technol. – JMR&T* 17 (2022) 3157–3171, <https://doi.org/10.1016/j.jmrt.2022.02.042>.
- [696] Optomec releases pure copper directed energy deposition (DED) additive manufacturing process, in: <https://optomec.com/optomecreleases-pure-copper-directed-energy-deposition-ded-additive-manufacturing-process/>. (Accessed 4 March 2022).
- [697] Lasers Initiate Copper AM Take-Off. <https://www.lasersystemseurope.com/feature/lasers-initiate-copper-am-take>. (Accessed 4 March 2022).
- [698] S. Yadav, C.P. Paul, A.N. Jinoop, A.K. Rai, K.S. Bindra, Laser directed energy deposition based additive manufacturing of copper: process development and material characterizations, *J. Manuf. Process.* 58 (2020) 984–997, <https://doi.org/10.1016/j.jmapro.2020.09.008>.
- [699] S. Landes, T. Suresh, A. Prasad, T. Letcher, P. Gradl, D. Ellis, Investigation of additive manufactured GRCop-42 alloy developed by directed energy deposition methods, in: Proc. ASME 2020 Int. Mechanical Engineering Congress and Exposition, vol. 4, Advances in Aerospace Technology, ASME, 2020, <https://doi.org/10.1115/IMECE2020-24400>, V004T04A026.
- [700] M.M. Aleksandrova, S.A. Urievich, K.A. Andreevich, M.A. Ivanovich, P. A. Vladimirovich, S.A. Romanovich, Application features of laser coaxial melting of powder materials to produce objects from copper alloys, *AIP Conf. Proc.* 2318 (2021), 150018, <https://doi.org/10.1063/5.0035860>.
- [701] D. Maischner, U. Fritsching, A. Kini, A. Weisheit, V. Uhlenwinkel, J. H. Schleifenbaum, T. Biermann, Laser additive manufacturing of copper-chromium-niobium alloys using gas atomized powder, *Int. J. Mater. Res.* 111 (7) (2020) 587–593, <https://doi.org/10.3139/146.111912>.
- [702] H.S. Prasad, F. Brueckner, J. Volpp, A.F.H. Kaplan, Laser metal deposition of copper on diverse metals using green laser sources, *Int. J. Adv. Manuf. Technol.* 107 (2020) 1559–1568, <https://doi.org/10.1007/s00170-020-05117-z>.
- [703] Y. Sato, K. Ono, K. Takenaka, K. Morimoto, Y. Funada, Y. Yamashita, T. Ohkubo, N. Abe, M. Tsukamoto, Fabrication of pure copper rod by multi-beam laser metal deposition with blue diode lasers, *J. Laser Micro/Nanoeng.* 16 (3) (2021) 189–193, <https://doi.org/10.2961/jlmn.2021.03.2007>.
- [704] X. Zhang, T. Pan, Y. Chen, L. Li, Y. Zhang, F. Liou, Additive manufacturing of copper-stainless steel hybrid components using laser-aided directed energy deposition, *J. Mater. Sci. Technol.* 80 (2021) 100–116, <https://doi.org/10.1016/j.jmst.2020.11.048>.
- [705] ASTM F3413-19: Guide for Additive Manufacturing – Design – Directed Energy Deposition, ASTM International, West Conshohocken, PA, 2019.
- [706] P. Gradl, Principles of Directed Energy Deposition for Aerospace Applications, NASA Marshall Space Flight Center, 20 January 2021. https://ntrs.nasa.gov/api/citations/20210000449/downloads/UTEP-Course%20-%20Principles%20of%20DED_Gradl_Jan2021.pdf. (Accessed 4 March 2022).
- [707] P.R. Gradl, C.S. Protz, Technology advancements for channel wall nozzle manufacturing in liquid rocket engines, *Acta Astronaut.* 174 (2020) 148–158, <https://doi.org/10.1016/j.actaastro.2020.04.067>.
- [708] From aerospace engineering to AM: melanie lang on FormAlloy and the future of directed energy deposition (DED), *Metal AM* 6 (3) (2020) 145–152.
- [709] D.G. Ahn, Directed energy deposition (DED) process: state of the art, *Int. J. Precis. Eng. Manuf.-Green Tech.* 8 (2021) 703–742, <https://doi.org/10.1007/s40684-020-00302-7>.
- [710] Freeform, RPM Innovations, Inc. <https://www.rpm-innovations.com/freeform-directed-energy-deposition.html>. (Accessed 4 March 2022).
- [711] B. Blakey-Milner, P. Gradl, G. Snedden, M. Brooks, J. Pitot, E. Lopez, M. Leary, F. Berto, A. Plessis, Metal additive manufacturing in aerospace: a review, *Mater. Des.* 209 (2021), 110008, <https://doi.org/10.1016/j.matdes.2021.110008>.
- [712] P. Gradl, S.E. Greene, C. Protz, B. Bullard, J. Buzzell, C. Garcia, J. Wood, K. Cooper, J. Hulka, R. Osborne, Additive manufacturing of liquid rocket engine combustion devices: a summary of process developments and hot-fire testing results, in: 54th AIAA/SAE/ASEE Joint Propulsion Conference, 2018 article AIAA-2018-4625.
- [713] BeAM and PFW Aerospace Work Together to Qualify 3D Printed Aerospace Component. <https://3dprint.com/229935/beam-and-pfw-aerospace-work-together/>. (Accessed 4 March 2022).
- [714] BeAM Machines – How DED achieves greater fuel efficiency in aerospace. <https://blogs.autodesk.com/advanced-manufacturing/2018/11/29/greater-fuel-efficiency-in-aerospace/>. (Accessed 4 March 2022).
- [715] A. Bandyopadhyay, Y. Zhang, B. Onuike, Additive Manufacturing of Bimetallic Structures, *Virtuual Phys. Prototyp.* 17 (2) (2022) 256–294, <https://doi.org/10.1080/17452759.2022.2040738>.
- [716] B. Zheng, Y. Zhou, J.E. Smugeresky, E.J. Lavernia, Processing and behavior of Fe-based metallic glass components via Laser-Engineered Net Shaping, *Metall. Mater. Trans. A* 40 (2009) 1235–1245, <https://doi.org/10.1007/s11661-009-9828-y>.